

Skin Lesion Analysis: A State-of-the-Art Survey, Systematic Review, and Future Trends

Md. Kamrul Hasan^{a,b,*}, Md. Asif Ahamad^b, Choon Hwai Yap^{a,**}, Guang Yang^{c,d,**}

^a*Department of Bioengineering, Imperial College London, UK*

^b*Department of Electrical and Electronic Engineering (EEE), Khulna University of Engineering & Technology (KUET), Khulna-9203, Bangladesh*

^c*National Heart and Lung Institute, Imperial College London, UK*

^d*Cardiovascular Research Centre, Royal Brompton Hospital, UK*

Abstract

The Computer-aided Diagnosis or Detection (CAD) approach for skin lesion analysis is an emerging field of research that has the potential to alleviate the burden and cost of skin cancer screening. Researchers have recently indicated increasing interest in developing such CAD systems, with the intention of providing a user-friendly tool to dermatologists in order to reduce the challenges that are raised by manual inspection. The purpose of this article is to provide a comprehensive literature review of cutting-edge CAD techniques published between 2011 and 2020. The Preferred Reporting Items for Systematic Reviews and Meta-Analyses (PRISMA) method was used to identify a total of 365 publications, 221 for skin lesion segmentation and 144 for skin lesion classification. These articles are analyzed and summarized in a number of different ways so that we can contribute vital information regarding the methods for the development of CAD systems. These ways include: relevant and essential definitions and theories, input data (datasets utilization, preprocessing, augmentations, and fixing imbalance problems), method configuration (techniques, architectures, module frameworks, and losses), training tactics (hyperparameter settings), and evaluation criteria (metrics). We also intend to investigate a variety of performance-enhancing approaches, including ensemble and post-processing. In addition, in this survey, we highlight the primary difficulties associated with evaluating skin lesion segmentation and classification systems using minimal datasets, as well as the potential solutions to these difficulties. In conclusion, enlightening findings, recommendations, and trends are discussed for the pur-

pose of future research surveillance in related fields of interest. It is anticipated that it will guide researchers of all levels, from beginners to experts, in the process of developing an automated and robust CAD system for skin lesion analysis.

Keywords: Computer-aided diagnosis, Deep learning, Machine learning, Skin lesion segmentation, Skin lesion classification, Skin lesion datasets.

Nomenclature

Acronym	Full Form
ACC	Accuracy
AdB	AdaBoost
AI	Artificial Intelligence
AK	Actinic Keratosis
ANN	Artificial Neural Network
AUC	Area Under Curve
BACC	Balanced Accuracy
BCC	Basal Cell Carcinoma
BEMD	Bi-dimensional Empirical Mode Decomposition
CAD	Computer-aided Diagnosis
CC	Correlation Coefficient
DF	Dermatofibroma
DL	Deep Learning
DSC	Dice Similarity Coefficient
DT	Decision Tree
EBC	Ensemble Binary Classifier
ENN	Elman Neural Network
F1S	F1-score
FFBPNN	Feed Forward Back Propagation Neural Network
FNR	False Negative Rate

*Corresponding author

**Co-senior last author

Email addresses: k.hasan22@imperial.ac.uk OR m.k.hasan@eee.kuet.ac.bd (Md. Kamrul Hasan), asif.fx@live.com (Md. Asif Ahamad), c.yap@imperial.ac.uk (Choon Hwai Yap), g.yang@imperial.ac.uk (Guang Yang)

Preprint submitted to Medical Image Analysis

August 26, 2022

Acronym	Full Form
FOM	Figure of Merit
FPR	False Positive Rate
FCN	Fully Convolutional Network
GAN	Generative Adversarial Network
GLCM	Gray Level Co-occurrence Matrix
GLDM	Gray Level Difference Method
HcCNN	Hyper-Connected CNN
HD	Hausdorff Distance
HMD	Hammoude Distance
IAD	Interactive Atlas of Dermoscopy
IRMA	Image Retrieval in Medical Applications
ISIC	International Skin Imaging Collaboration
JI	Jaccard Index
KMC	K-Means Clustering
KNN	K-Nearest Neighbors
LBP	Local Binary Patterns
LDA	Linear Discriminant Analysis
LR	Learning Rate
MCC	Matthew Correlation Coefficient
Mel	Melanoma
ML	Machine Learning
MPNN	Multilayer Perceptron Neural Network
MSM-CNN	Multi-Scale Multi-CNN
NB	Naive Bayes
Nev	Nevus
NPV	Negative Predictive Value
PNN	Probabilistic Neural Network
PRE	Precision
PRISMA	Preferred Reporting Items for Systematic Reviews and Meta-Analyses
PSNR	Peak to Signal Ratio
QDA	Quadratic Discriminant Analysis
RF	Random Forest
SCC	Squamous Cell Carcinoma

Acronym	Full Form
SE	Segmentation Error
SEN	Sensitivity
SENet	Squeeze-and-Excitation Networks
SGD	Stochastic Gradient Descent
SIFT	Scale-Invariant Feature Transform
SK	Seborrheic Keratosis
SLA	Skin Lesion Analysis
SLC	Skin Lesion Classification
SLS	Skin Lesion Segmentation
SPE	Specificity
SSIM	Structural Similarity Indices
SVM	Support Vector Machine
TDS	Total Dermatoscopy Score
VL	Vascular Lesion

1. Introduction

Malignant melanoma is the deadliest cancer type among all skin cancers [1] that can be cured at the beginning stage by an imperative early diagnosis. Traditionally, doctors and radiologists utilize dermatoscopy as a gold-standard technique to diagnose various pigmented skin lesions, employing hand-held devices and computer vision methods to contribute worthy insights scenario. Recently, medical image processing has been growing for decades with increasingly effective tools to assist dermatologists in recognizing and classifying skin lesions [2]. Therefore, a Computer-aided Diagnosis (CAD) system is an unavoidable tool for clinicians and/or dermatologists in decision making, especially in investigating an excessive number of patients in shorter time duration [3]. However, the computational schemes in a CAD system essentially consist of several fundamental steps: image acquisition, preprocessing, segmentation, feature extraction, and classification [4]. It is noteworthy that some researchers consider segmentation a preprocessing for the subsequent feature extraction and then classification. Additionally, the segmented lesion masks and classification outcome can be employed for concurrent lesion detection and recognition [3, 5]. Examples of such simul-

taneous lesion detection and recognition by Hasan et al. [3] can be watched on YouTube¹. However, in the last decade, from 2011 to 2020, numerous researches have been carried out on Skin Lesion Analysis (SLA), especially lesion segmentation and classification, practicing computer vision algorithms, handcrafted feature engineering, and automated Artificial Intelligence (AI). Fig. 1 displays the number of articles for each year from 2011 to 2020 on lesion segmentation and classification. From Fig. 1, it can be undoubtedly remarked that the

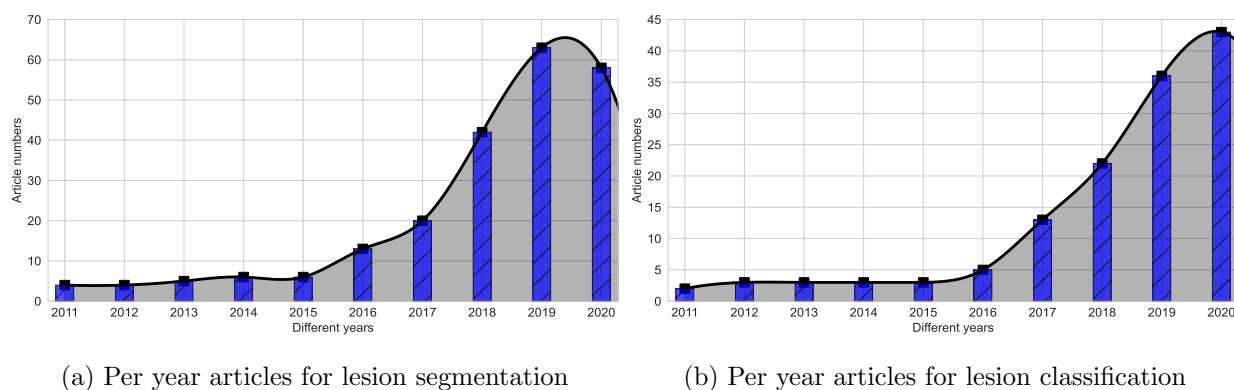


Figure 1: The number of publications (in blue bars) in the last decade on lesion segmentation (left) and lesion classification (right), collected from Google scholar (see details in section 2) by searching for “skin lesion segmentation” and “skin lesion classification”. The trendlines are also delivered in black color with continuous curves, exhibiting the sudden rise in the number of SLA articles for both tasks. The publication numbers in 2020 (left figure) have probably decreased due to the COVID-19 pandemic.

SLAs have become an exciting and fast-growing area of research. Moreover, the publication numbers have increased continuously per year, as explicated in both Fig. 1 (a) and Fig. 1 (b), especially after 2016. Therefore, these enormous articles demand systematic survey and insight discussions of utilized datasets, preprocessing methodologies, segmentation strategies, feature engineering procedures, classification techniques, and evaluation benchmarks for an automated SLA procedure(s), leading to open-door directions for beginners to expert-level researchers.

This aimed article provides a rigorous survey, review, and analysis of the SLA methods

¹https://youtu.be/nlfr_NCPy4U [Access date: 12-Mar-2022]

in the last decade's published literature from 2011 to 2020. To conduct the aspired process, we primarily focus on Skin Lesion Segmentation (SLS) and Skin Lesion Classification (SLC), where the employed preprocessing is a prerequisite step for both tasks. The former scheme, SLS, can be accomplished by applying various image analysis (and/or computer vision) algorithms [4, 6] and end-to-end Deep Learning (DL) methods [7]. The latter task, SLC, can be succeeded by involving different Machine Learning (ML) [8] and end-to-end DL algorithms [8, 9]. It necessitates mentioning that the employment of ML-based SLC requires comprehensive feature engineering [4]. Therefore, we discuss SLA's feature extraction steps in the SLC task. Again, it is also noteworthy that the end-to-end DL models often do not demand preprocessing steps due to their powerful automated learning capability [10]. However, this article explores different SLS and SLC papers from 2011 to 2020 for summarizing their input data (datasets utilization, preprocessing, augmentations, and solving imbalance problems), method configuration (techniques, architectures, module frameworks, and losses), training tactics (hyperparameters settings), and evaluation criteria (metrics). Their straightforward technical concepts and utilization tendencies with recommendations are systematically provided to assist the researchers in getting that information in a single article. However, the essential contributions of this survey article on the SLS and SLC will be supportive for the research community in the following contexts:

- Provide essential knowledge regarding SLA tasks by compiling articles published over the past decade (2011-2020), covering SLS and SLC mechanisms with a variety of integral strategies and insightful back-and-forth exchanges.
- Investigate the perspicuity scenario of a variety of datasets with potential future trends and their existing requirements in the field of survey analysis that is being addressed.
- Analyze the many different preprocessing and augmentation procedures that are used in SLA in order to reveal their effectiveness, trends, and necessity. For instance, augmentations can be employed to construct an authentic and robust supervised SLA model, handle class imbalance issues, and so on.

- Summarize the many SLS and SLC strategies used over the past ten years, such as automated DL algorithms, handcrafted feature engineering, ML models, and SLS post-processing, to gather enough useful knowledge for the scientific community.
- Examine the trends in employment over a range of training conditions, as well as the hyperparameters such as batch size, learning rate, loss function, optimizer, and epoch.
- Accumulate a variety of assessment benchmarks along with adequate explanation details to disclose the tendencies in the SLS and/or SLC tasks.
- Finally, categorize all the necessary actions, such as preprocessing, augmentation, SLS & SLC methods, and evaluation metrics, in the SLA frameworks into three types: *first-tier* (highly effective), *second-tier* (moderately effective), and *third-tier* (less effective), according to the last decade’s employment frequencies that will deliver crucial guidelines for the future SLA process developments. In the end, uncover the prospective essentials in the SLA tasks that will be an open challenge for researchers interested in this field.

The remains of the paper are organized as follows: Section 2 clarifies the inclusion and exclusion criteria for SLA article selection. Section 3 describes various available skin lesion datasets and scrutinizes their utilization trends. The employment of various preprocessing and augmentations for the automated SLA task are explored in Section 4 with the class imbalance problem solution analysis. Section 5 reports different SLS techniques along with the last decade’s tendencies. This section also highlights different post-processing schemes in the SLS task. Various SLC elements like lesion features and ML- and DL-based classifiers are investigated in Section 6. The training schemes with different hyperparameter settings and evaluation benchmarks are described in Section 7. Lastly, Section 8 provides informative observations, recommendations, and trends for future research directions in related fields of interest, with the article’s conclusion in Section 9.

2. Article Selection

This review’s article searching methodology makes adoption of the well-known Preferred Reporting Items for Systematic Reviews and Meta-Analyses (PRISMA) strategy [11], which is depicted in Fig. 2, along with the inclusion and exclusion benchmarks [12] for the reviewed articles. Total numbers of $SLS = 423$ and $SLC = 338$ articles were obtained for the SLS and

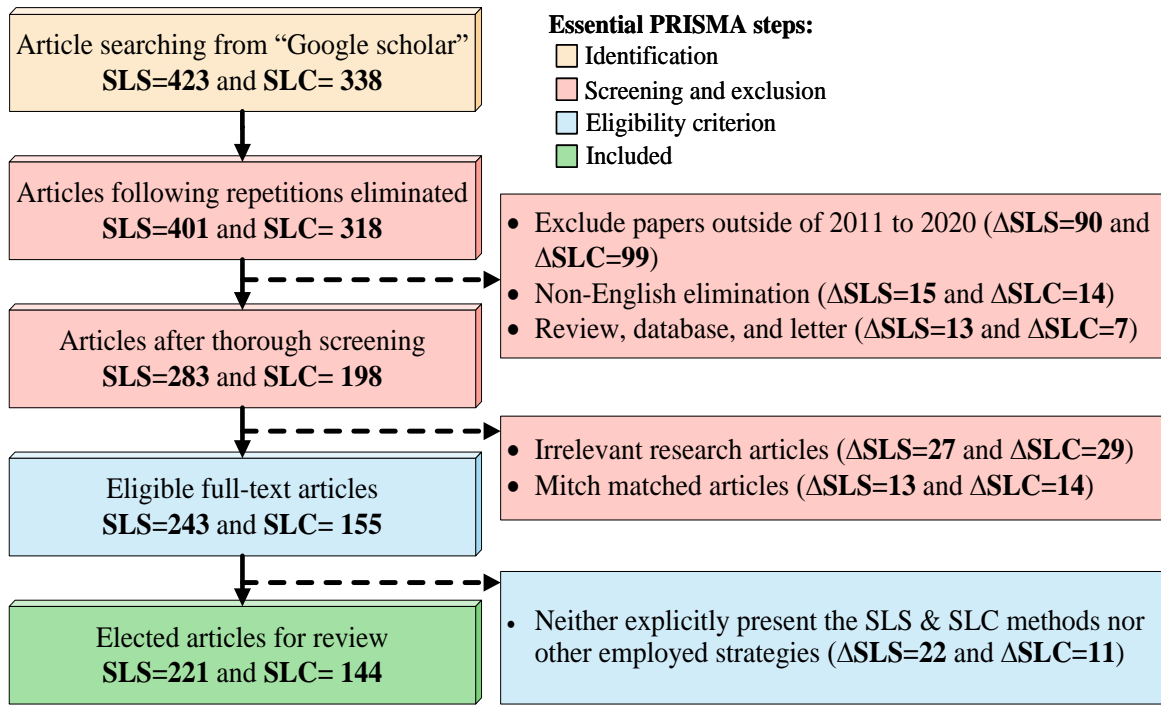


Figure 2: The employed PRISMA process for articles exploring approach, where we describe the evidence for the article’s inclusion and exclusion standards.

SLC methods with the keywords “skin lesion segmentation” and “skin lesion classification”, respectively, from “Google scholar”. Some duplications in the literature are eliminated afterwards, providing $SLS = 401$ and $SLC = 318$ articles, respectively, for SLS and SLC. Then, in the first screening round (first-level exclusion), the articles of non-English language ($\Delta SLS = 15$ and $\Delta SLC = 14$) and the review, database, or letter-type articles ($\Delta SLS = 13$ and $\Delta SLC = 7$) are excluded. Additionally, only the articles in the year range 2011 ~ 2020 are preserved in this round. This exclusion provides $SLS = 283$ and $SLC = 198$ literature

in total (see Fig. 2). After that, scrutinizing is carried out on all the picked articles from the previous steps, showing that $\Delta SLS = 27$ and $\Delta SLC = 29$ articles have unnecessary research purposes, and $\Delta SLS = 13$ and $\Delta SLC = 14$ articles' schemes are not suited. This second exclusion gives $SLS = 243$ and $SLC = 155$ articles (see Fig. 2). Finally, $\Delta SLS = 22$ and $\Delta SLC = 11$ articles are eliminated, as they neither explicitly exhibit the SLS and SLC systems nor other exercised strategies. Through the succeeding identification, screening, and eligibility experimentation, $SLS = 221$ and $SLC = 144$ articles are ultimately included to conduct this intended review method. Fig. 1 displays the per year distribution of those included papers from 2011 to 2020 on the SLS (= 221) and SLC (= 144), indicating that the publications have massively increased, predominantly after 2016.

3. Image Acquisition

The first stage of a computerized SLA system is image acquisition, with numerous available non-invasive imaging techniques such as dermoscopy, photography, confocal scanning laser microscopy, optical coherence tomography, ultrasound imaging, magnetic resonance imaging, and spectroscopic imaging to assist dermatologists [13]. Macroscopic and dermoscopic images are examples of images acquired from such systems that have been extensively adopted for SLA purposes [4]. However, accumulating those acquired images in a dataset is at the heart of any automated system development, either for the segmentation or classification of skin lesions. Many public datasets for SLS and/or SLC have been utilized for a long time. Some of these datasets are International Skin Imaging Collaboration (ISIC) [14–19], PH2 [20], Interactive Atlas of Dermoscopy (IAD) [21], Image Retrieval in Medical Applications (IRMA) [22], Dermaquest [23], etc. The former ISIC datasets include five distinct open versions with various image numbers and classes for five consecutive years, such as ISIC-16 [14], ISIC-17 [15], ISIC-18 [16, 17], ISIC-19 [18], and ISIC-20 [19] respectively for the years from 2016 to 2020. The next section 3.1 briefly summarizes those datasets.

3.1. Different Datasets

The **ISIC-16**² is a dataset for binary SLS and SLC, having 900 training and 379 testing images, without validation images (see Table 2). It is intended to distinguish the lesions as either Nevus (Nev) or Melanoma (Mel), where the images have resolutions of 556×679 to 2848×4828 pixels. The **ISIC-17**³ is a binary SLS and multi-class SLC task. The latter SLC contains three classes: Nev, Seborrheic Keratosis (SK), and Mel (see Table 2). This dataset has 2750 images for training, validation, and testing, with image resolutions of 453×679 to 4499×6748 pixels. The **ISIC-18**⁴ images are derived from the HAM10000 dataset [17], including 10015 images for multi-class SLC and 12500 images for binary SLS, with the resolutions of 450×600 pixels. This dataset does not publish validation or test images and comprises seven classes: Nev, SK, Basal Cell Carcinoma (BCC), Actinic Keratosis (AK), Dermatofibroma (DF), Vascular Lesion (VL), and Mel (see Table 2). The **ISIC-19**⁵ is an extension of one more class, i.e., Squamous Cell Carcinoma (SCC), in ISIC-18 with almost double sample images. It has 25331 images from multiple sites (HAM10000, BCN20000 [18], and MSK) applying different preprocessing methods. The images of ISIC-19 have resolutions of 600×450 to 1024×1024 pixels, without explicit validation and test images like ISIC-18 (see Table 2). The **ISIC-20**⁶ contains 33126 dermoscopic images with the resolutions of 1024×1024 pixels (see Table 2). Similar to ISIC-16, this dataset also contains binary SLC images from over 2000 patients, aiming to be classified as Nev and Mel.

The **PH2**⁷ is a database acquired at the Dermatology Service of Hospital Pedro Hispano, Portugal. This dataset contains 200 images of melanocytic lesions, including 160 in Nev class and 40 in Mel class, with a 768×560 pixels resolution. The **IAD**⁸ dataset has 700×447 RGB pixels images, without constituting segmentation masks. However, Celebi et al. [24]

²<https://challenge.isic-archive.com/landing/2016> [Access date: 21-Jun-2022]

³<https://challenge.isic-archive.com/landing/2017> [Access date: 21-Jun-2022]

⁴<https://challenge.isic-archive.com/landing/2018> [Access date: 21-Jun-2022]

⁵<https://challenge.isic-archive.com/landing/2019> [Access date: 21-Jun-2022]

⁶<https://www.kaggle.com/c/siim-isic-melanoma-classification/overview> [Access date: 21-Jun-2022]

⁷<https://www.fc.up.pt/addi/ph2%20database.html> [Access date: 21-Jun-2022]

⁸<https://espace.library.uq.edu.au/view/UQ:229410> [Access date: 21-Jun-2022]

Table 2: Image distribution of various publicly available datasets for the SLS and SLC tasks, having different numbers of classes and image samples.

Datasets		Number of images for various tasks and classes									
		SLS task		Class-wise images for SLC task							
		Images	Masks	Nev	SK	BCC	AK	DF	VL	Mel	SCC
ISIC-16	Training	900	900	727	–	–	–	–	–	173	–
	Testing	379	379	304	–	–	–	–	–	75	–
ISIC-17	Training	2000	2000	1372	254	–	–	–	–	374	–
	Validation	150	150	78	42	–	–	–	–	30	–
	Testing	600	600	393	90	–	–	–	–	117	–
ISIC-18	Training	12500	12500	6705	1099	514	327	115	142	1113	–
ISIC-19	Training	–	–	12875	2624	3323	867	239	253	4522	624
ISIC-20	Training	–	–	32542	–	–	–	–	–	548	–
PH2	–	200	200	160	–	–	–	–	–	40	–
IAD	–	100	100	70	–	–	–	–	–	30	–
Dermaquest	–	137	137	61	–	–	–	–	–	76	–
IRMA	–	–	–	560	–	–	–	–	–	187	–

provides ground truth masks to continue the research study. The **Dermaquest** dataset has 137 images for the binary SLS. The SLC is a binary classification task with 76 samples in Mel class and 61 in Nev class. The **IRMA** dataset is unlisted but available under special request to the authors and was created by the Department of Medical Informatics, RWTH Aachen University. It comprises 747 dermoscopic images with a resolution of 512×512 pixels, of which 187 images are in Mel class, and 560 are in Nev class.

An overview of these datasets with their sample distribution for SLS and SLC tasks is manifested in Table 2. An observation of this table reveals that the SLC class varies from binary to eight classes, where most of the SLC tasks are binary. The per-class sample numbers tell us that the classes are massively imbalanced, especially for the ISIC-19 and ISIC-20. Such an imbalanced class distribution forces a supervised SLC system to be biased towards the overrepresented class if it is not considered during the training [25]. In some datasets, the samples are significantly smaller, which is also a limitation for developing automated SLS and SLC systems. However, section 4.2 explores the employed solutions for such problems in the SLS and SLC in the last decade from 2011 to 2020. The next

section 3.2 explores those datasets’ employment frequencies in various SLA literature from 2011 to 2020, dispensing their appliances’ crazes in the last decade.

3.2. Datasets’ Utilization and Trends

Table 3 confers the distribution of different datasets in the selected 221 SLS articles (see Fig. 2) for each year between 2011 and 2020. It necessitates remarking that some articles utilized multiple datasets for their SLS model, which are assigned to all those datasets’ columns. However, it is glimpsed from Table 3 that researchers utilized publicly available IAD datasets to validate their SLS algorithms mostly between 2011 and 2015, prior to the applications of automated DL models in SLS (see Fig. 1). In contrast, most published work

Table 3: The number of articles each year from 2011 to 2020 for SLS on different publicly available datasets in Table 2.

Year	ISIC-16	ISIC-17	ISIC-18	PH2	IAD	Dermaquest	Others
2020	[3, 5, 26–42]	[3, 5, 13, 27, 31, 34, 36, 37, 39, 41–61]	[5, 31, 33, 34, 36, 39, 46, 54, 55, 61–67]	[2, 13, 26, 29, 31, 33, 34, 36, 40, 42, 44, 47, 48, 51, 52, 55–58, 60, 64, 68–72]	[2]	[69, 73–75]	[76–79]
2019	[80–91]	[81, 84, 85, 88–117]	[84, 88, 94, 100, 107, 110, 115, 118–127]	[58, 81, 82, 90, 91, 94, 95, 99, 102, 113–115, 119, 128–133]	[134]	[135]	[136–138]
2018	[139–148]	[141, 145–163]	[164–170]	[139, 143–145, 147, 149, 155, 159, 160, 162, 171–173]		[174, 175]	[176, 177]
2017	[154, 178–183]	[154, 181, 184–189]		[154, 190]		[191–194]	[195]
2016	[196–199]				[196, 200–203]	[7, 202, 202, 204]	[205–207]
2015				[208]			[209–213]
2014							[214–219]
2013					[220]		[221–223]
2012					[224, 225]		[226, 227]
2011					[228, 229]		[230, 231]
Total	52	91	40	61	12	14	31

applied datasets with fewer samples that were not publicly accessible during that period (2011-2015). It is remarkable that the number of articles that were published on the SLS prior to 2016 was significantly lower than the number of articles published after 2016, which indicates that the paper numbers increased significantly after 2016 following the launch of ISIC datasets, which are the fundamental requirements of supervised DL models. Although ISIC-16, ISIC-17, ISIC-18, and PH2 datasets were introduced after the IAD and Dermaquest,

they were devoted to many articles, such as 52, 91, 40, and 61, respectively. Comparing three versions of the ISIC datasets, the ISIC-18, having more examples, are applied in fewer articles since it does not contain separate validation and test sets, requiring time-consuming cross-validation to describe the outcomes. Additionally, a random selection of validation and test sets is not guaranteed to provide a robustly trained SLS model. On the other hand, the ISIC-16 also does not provide validation images and has fewer training samples. Therefore, the choice of ISIC-17 to build a robust SLS model is appropriate, as this mania is reflected in the last decade’s scenario. Surprisingly, the PH2 dataset was practiced more than ISIC-16 and ISIC-18, although it has fewer samples and only training images. The discernible reason is that some authors trained and evaluated their model on ISIC [13, 232], where they further evaluated their SLS model on the PH2 dataset to uncover guaranteed robustness, as PH2 was neither utilized during the training nor validation phases.

Likewise, the inspection in Table 4 displays the allocation of the nominated 144 articles (see Fig. 2) of the SLC for each year between 2011 and 2020, where the articles with multiple datasets are assigned to all those datasets’ columns. Again, the utilization of datasets before

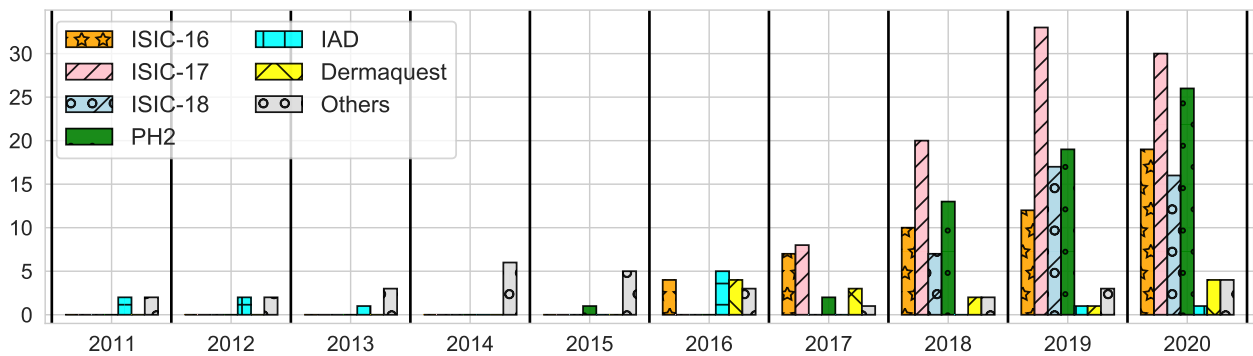
Table 4: The number of articles each year from 2011 to 2020 for the SLC on different publicly available datasets in Table 2.

Year	ISIC-16	ISIC-17	ISIC-18	ISIC-19	PH2	IAD	Dermaquest	Others
2020	[63, 233–236]	[46, 58, 59, 59, 63, 233, 234, 237–241]	[46, 63, 234, 237, 242–256]	[46, 257–262]	[58, 235, 239, 240, 246, 263]	[264, 265]	[266]	[267–270]
2019	[1, 82, 88, 271–273]	[1, 88, 97, 100, 115, 116, 273–282]	[1, 88, 100, 115, 124, 273, 279, 283–290]	[291, 292]	[1, 82, 128, 286]	[1, 134]	[286]	[286, 293, 294]
2018	[145, 295–297]	[145, 157, 298–301]	[170, 299, 302–307]		[173, 298, 308]		[309]	[310–313]
2017	[178, 314–316]	[317–321]			[315]	[315]	[316, 322, 323]	[324, 325]
2016	[326]				[327]	[328]	[328, 329]	[328, 330]
2015								[331–333]
2014						[334]		[335, 336]
2013								[337–339]
2012						[340]	[341]	[342]
2011								[343, 344]
Total	20	39	42	9	15	8	9	26

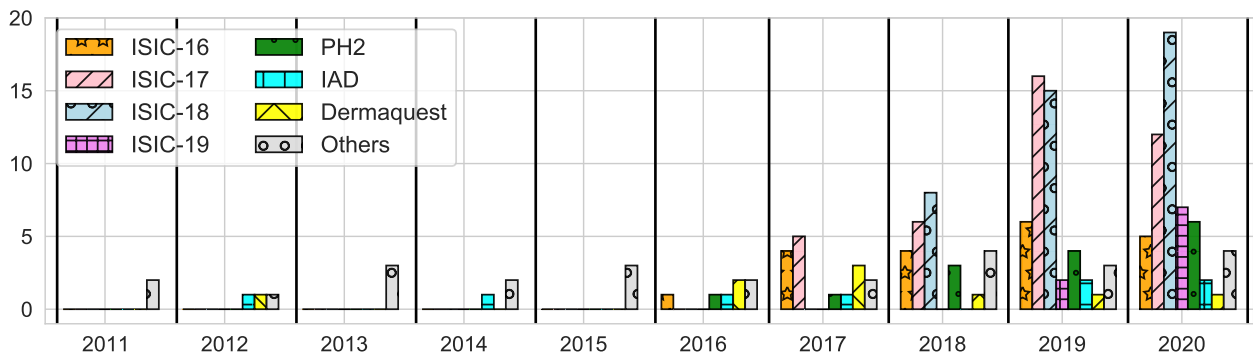
2016 obeys the same pattern as in Table 3 for the SLS task. After 2016, the observations in Table 4 revealed that the authors preferred datasets with more class numbers to build

an SLC model that results in greater utilization of the ISIC-18 dataset. The increased class number with imbalanced class sample distribution is challenging to the SLC models, whose solutions are desirable to build a robust SLC model [3, 5] without any particular class bias. Similar to the SLS task, the PH2 dataset was also devoted as an external dataset to validate the SLC algorithms further, giving assured robustness.

A further summary of various dataset utilization in the specified 365 articles (221 for SLS and 144 for SLC) is displayed in Fig. 3, revealing the trends of datasets’ appliances in the last decade from 2011 to 2020. As demonstrated in both the figures, the earlier articles



(a) Number of articles per year using a specific dataset for the SLS task



(b) Number of articles per year using a specific dataset for the SLC task

Figure 3: The summary of the dataset’s utilization from 2011 to 2020 for the SLS (top) and SLC (bottom) on different publicly available datasets, demonstrating the most valuable datasets in the last decade.

applied relatively tiny datasets to their SLA system, which were not even publicly available, restricting the research community’s reproducibility. As obtaining annotated medical images

is extremely expensive [5, 300], few researchers were interested in working on the SLA during that period, roughly from 2011 to 2015. However, this obstacle was overcome after introducing the ISIC datasets in 2016, as Fig. 3 (a) and Fig. 3 (b) disclose that the study on the SLS and SLC tasks has increased massively. It is noteworthy to quote from Fig. 3 that after 2016, the utilization of IAD, Dermaquest, and private datasets either reduced or stagnated for most of the years. Therefore, ISIC datasets can be marked as representative datasets for the SLA. The additional examination determines that the ISIC-17 dataset can be deemed a delegate SLS dataset according to our review of the 221 articles for SLS. A similar claim for the SLC task is that the ISIC-18 is a representational SLC dataset. Again, the one-by-one scrutinization of the chosen literature and Fig. 3 demonstrate that PH2 is commonly employed as an external dataset to validate the results obtained from the ISIC training for both SLS and SLC tasks. Such a conclusion on the SLA datasets over the last decade will afford solid ground for beginners and expert-level researchers to determine a suitable dataset for their intended SLS and SLC schemes.

4. Preprocessing and Augmentations

Preprocessing aims to improve image data quality, suppress unwilling distortions, or enhance essential features for further processing. On the other hand, image augmentation assembles new training examples from existing training data; that is often impossible to truly capture an image that accounts for every real-world scenario a supervised model may encompass. However, identifying the correct preprocessing and augmentation actions most helpful in expanding model performance demands a vital insight into the problem, data collection, and production environment, which may function satisfactorily in one circumstance and is inappropriate in others. Therefore, this article aspires to summarize the applied preprocessing (in section 4.1) and augmentations (in section 4.2) techniques in the last decade (2011-2020) for the SLA task, which will expose a general guideline to future researchers. The procedures to mitigate the class bias problem are also surveyed in section 4.2.

4.1. Preprocessing

Image preprocessing is an essential step in any decision-making pipeline to remove noise and enhance the quality of the original image by removing unrelated and surplus parts in the image’s background for further processing. A suitable selection of preprocessing techniques can significantly improve the accuracy of the aimed system [3, 5, 345]. The scrutinization of selected articles exposes that the skin lesion images contain many different types of noise and artifacts: markers, body hairs & veins, body fibers, air bubbles, reflections, non-uniform lighting, rolling lines, shadows, non-uniform vignetting, artificial landmarks, and patient-specific effects like lesion textures, colors, diverse shape & size of lesion area [13]. However, the most commonly applied preprocessing in the selected 365 literature from 2011 to 2020 is presented in Table 5, conferring their corresponding articles for more detailed descriptions and employment outcomes.

Table 5: Commonly employed preprocessing for SLA from 2011 to 2020, scrutinizing a total of 365 articles (221 for segmentation and 144 for classification).

Methods	Remarks	Employed articles
Hair removal	The lesion’s boundary and texture information are often occluded due to the presence of hair, leading to over-segmentation and weak pattern analysis [346]. Therefore, an automatic hair removal method [346] is necessitated, preserving all the lesion features.	[1, 7, 27, 29, 56, 63, 70, 76, 93, 114, 126, 130, 133, 136, 139, 143–145, 155, 159, 161, 173, 173, 178, 185, 187, 197, 198, 200, 203, 204, 215, 216, 225, 244, 256, 264, 297, 301, 304, 314, 319, 325, 330, 332, 339]
Normalization	Subtraction of mean RGB values computed over each image or whole training dataset to exclude poor contrast issues, which also deals with the various lighting conditions in the skin images [249, 278].	[1, 56, 97, 99, 111, 154, 155, 159, 185, 204, 210, 225, 228, 241, 249, 255, 262, 264, 277, 278, 289, 291–293, 312, 316, 320, 329]
Standardization	Appliances of the mean and standard deviation of RGB values to scale all images to the same range to decrease biasing from different sources [255].	[1, 56, 79, 125, 255, 278, 289]
Median filter	Filtering an image by placing the median value in the input window at the center of that window to lessen impulsive, salt-and-pepper, or sudden random noise.	[27, 29, 147, 209, 214, 215, 217, 223, 255, 264, 267, 319, 325, 332]
Remove light reflections	Devices’ light reflections are eliminated by applying morphological closing and erosion. A non-linear median filter is also helpful for removing light reflection and other tiny dots in the background outside the lesion area [215].	[7, 126, 185, 203, 204, 215, 223, 325]

Table 5 Continued from previous page

Methods	Remarks	Employed articles
Sharpening filter	The sharpening spatial filter removes blurring, improving the definition of fine detail and sharpening edges that are not clearly defined in the original given image.	[330]
Wiener filter	It is a low pass linear filter, usually applied in the frequency domain, for images degraded by additive noise, blurring, and constant power additive noise.	[332]
Gabor filter	A Gabor filter is a bandpass filter and can be defined as a sinusoidal plane of particular frequency and orientation, modulated by a Gaussian envelope.	[332]
Histogram equalization	It improves the contrast of an image by utilizing its histogram, spreading out the most frequent pixel intensity values, or stretching out the image's intensity range.	[203, 332]
Elimination of shading	It is induced by imaging non-flat skin surface and light-intensity falloff towards the edges of the skin image, causing color degradation and poor segmentation results [225].	[99, 225, 262, 339]
Mean filter	It is a smoothing method to overcome the noise effect by reducing the intensity variation between neighboring pixels, a circular or square neighbor.	[136, 192, 194, 208, 225, 338]
Automatic color equalization	This method enhances both color information and contrast by applying two main stages, including chromatic or spatial adjustment and dynamic tone reproduction scaling [228].	[59, 185, 225, 228, 241, 267, 291, 292, 338]
Contrast enhancement	It adjusts the relative brightness and darkness of lesions to improve their visibility. The contrast or tone of the skin image can be modified by mapping the gray levels in the image to new values through a gray-level transform.	[2, 59, 76, 82, 82, 88, 126, 136, 143, 145, 145, 155, 159, 161, 172, 173, 173, 194, 198, 200, 208, 212, 214, 228, 239, 252, 256, 273, 301]
Dark region removal	The black corners having nearly the same lesion's intensity due to a round circular lens can be excluded by applying binary masks of the dark corners obtained from the OTSU's thresholding [200].	[93, 130, 133, 145, 200, 223, 283]
Gamma correction	It controls the overall brightness that is not adequately corrected, seeming either bleached out or too dark.	[204, 282]
Color space transformation	It is the translation of the representation of a color from one basis to another. In general, CIE L*a*b*, CIE L*u*v*, YCrCb (Y color component has most of the image details), and HSV are remarkably practiced in literature [198].	[2, 29, 51, 57, 111, 143, 154, 169, 176, 189, 190, 194, 198, 204, 208, 210, 218, 241, 256, 273]
Bias field correction	It adjusts the bias field signal before the subsequent processing, reducing intensity heterogeneity.	[208]
Gaussian filter	A Gaussian filter blurs an image using a Gaussian function to decrease noise and detail, similar to a mean filter.	[2, 174, 198, 208, 252, 256]

Table 5 Continued from previous page

Methods	Remarks	Employed articles
CLAHE [†]	CLAHE is a variant of adaptive histogram equalization and applied to enhance foggy skin images' perceptibility level.	[187]

[†]CLAHE: Contrast Limited Adaptive Histogram Equalization

It requires citing that explaining the to-the-point theories of all the preprocessing procedures is not the primary focus of this article. We, therefore, provide the citations in Table 5 for the corresponding processes so that the scholars can explore them to achieve complete theoretical information. However, the inspection in Table 5 reveals that hair removal, normalization, median filter, contrast enhancement, and color space transformation are the most widely applied preprocessing employed in the last decade. They can be recognized as the representative preprocessing for the SLA for future research in this field. This finding will contribute a primary estimation to the beginner to expert-level researchers to determine a suitable preprocessing algorithm for their lesion analysis's framework. Furthermore, it is noted from the scrutinization of those selected 365 articles that many authors utilized grayscale images rather than the given RGB images. Such a conversion can be obtained in many ways, for instance, by averaging RGB channels and taking a single channel from different color spaces. However, the most commonly exercised technique for such grayscale conversion is given in Eq. 1.

$$Y = 0.299 \times R + 0.587 \times G + 0.114 \times B, \quad (1)$$

where R, G, and B are the weighted summations of red, green, and blue pixels, respectively, and Y is the grayscale luminance value. Furthermore, Fig. 4 displays the utilization frequencies of various preprocessing techniques in a bar plot in the last decade from the decided 365 SLA articles, revealing that hair removal, contrast enhancement, normalization, color space transformation, and median filtering are massively accepted top-5 preprocessing methods respectively employed in 23.83%, 15.03%, 14.51%, 10.36%, and 7.25% articles for the SLA. Due to their massive utilization frequency, those five preprocessing methods can be grouped as *first-tier* techniques (highly effective). Other preprocessing methods like

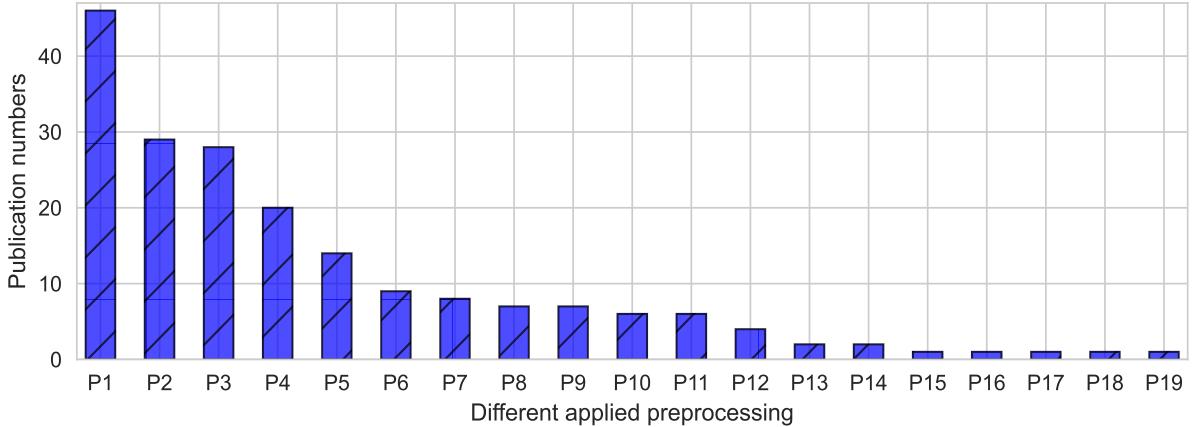


Figure 4: The number of articles employing different preprocessing in the last decade for the SLS and SLC tasks, where the preprocessing P1 to P19, respectively, indicate Hair removal, Contrast enhancement, Normalization, Color space transformation, Median filter, Automatic color equalization, Remove light reflections, Standardization, Dark region removal, Mean filter, Gaussian filter, Elimination of shading, Histogram equalization, Gamma correction, Sharpening filter, Wiener filter, Gabor filter, Bias field correction, Contrast Limited Adaptive Histogram Equalization.

automatic color equalization, removal of light reflections, standardization, dark region removal, mean filter, and Gaussian filtering are employed in the same number of SLA articles, approximately 4.7% of articles. They are categorized as *second-tier* preprocessing strategies in the SLA. The remaining elimination of shading, histogram equalization, gamma correction, sharpening filter, wiener filter, Gabor filter, bias field correction, and contrast limited adaptive histogram equalization are organized as *third-tier* preprocessing strategies (less effective) due to their less engagement commonness in the last decade from 2011 to 2020. Such preprocessing tiers from the last decade’s SLA publications will provide a concrete foundation for beginners and expert-level researchers to determine an appropriate preprocessing strategy in this domain.

4.2. Augmentation and Imbalance Problem

Data augmentation is a pathway to lessen overfitting in models, increasing the training data samples in many ways. Firstly, the most popular practice for data augmentation is to perform affine image transformations and color modification. Secondly, the texture

transformation is to synthesize a texture from a texture-source image, preserving the visual characteristics of the actual image like contour, shading, lines, strokes, and regions [347]. Thirdly, Generative Adversarial Network (GAN) is a relatively new and powerful tool to perform unsupervised new images using the min-max strategy. It is advantageous in many image generation and manipulation problems such as text-to-image synthesis, superresolution, image-to-image translation, image blending, and image inpainting [347]. However, the one-by-one scrutinization of the selected 365 articles returns the following augmentations in the last decade from 2011 to 2020 for the SLA task: Rotation [1, 13, 30, 34, 36, 40, 42, 46, 46, 48, 52, 54, 58–61, 64, 67, 79, 83, 91, 94, 97, 98, 103, 111, 116, 116, 117, 119, 122, 124, 125, 131, 141, 148, 148, 150, 151, 153, 154, 154, 156, 157, 161, 165, 166, 169, 180, 188, 191, 235–237, 241, 242, 250, 253, 254, 257, 259, 261, 263, 268, 272, 277, 278, 280, 281, 283, 289, 293, 295, 300, 304, 305, 316, 317, 319, 320], Horizontal flipping [13, 30, 34, 36, 41, 42, 48, 51, 52, 54, 58–61, 64, 66, 67, 79, 83, 85, 90, 91, 94, 97, 98, 103, 105, 107, 108, 111, 116, 116, 117, 119, 124, 125, 131, 148, 150, 151, 153, 154, 156, 157, 160, 161, 165, 169, 179, 183, 184, 188, 191, 235, 236, 238, 242, 250, 253, 254, 257, 259, 260, 263, 268, 272, 277, 278, 283, 289, 293, 295, 300, 304, 305, 316, 317, 319], Vertical flipping [13, 34, 36, 41, 42, 48, 51, 52, 54, 58–61, 66, 67, 79, 83, 85, 90, 91, 94, 97, 103, 105, 107, 108, 111, 116, 116, 117, 119, 124, 125, 148, 151, 153, 154, 154, 157, 160, 161, 165, 169, 179, 183, 184, 188, 191, 235, 236, 238, 242, 250, 253, 254, 259, 260, 263, 268, 272, 283, 289, 293, 295, 300, 304, 305, 316, 317, 319], Scaling [34, 40, 52, 54, 58–60, 67, 79, 85, 122, 124, 148, 150, 151, 153, 154, 157, 165, 166, 180, 237, 246, 250, 254, 263, 265, 268, 278, 283, 316], Region cropping [54, 58, 61, 64, 90, 94, 108, 148, 157, 169, 179, 183, 188, 242, 246, 249, 253, 265, 285, 293, 305, 307, 319], Shifting [1, 13, 58, 67, 91, 103, 119, 122, 124, 125, 151, 153, 154, 166, 236, 237, 254, 259, 268, 293, 316, 320], Contrast adjustment [39, 40, 54, 59, 79, 94, 103, 105, 117, 165, 175, 184, 235, 263, 283], Shearing [34, 58, 58, 67, 94, 122, 169, 250, 272, 278, 283, 317], Horizontal and vertical or both flipping [13, 40, 51, 67, 148, 157, 257, 261, 265], Adaptive histogram equalization [40, 54, 59, 94, 107, 123, 237, 246, 329], Gaussian noises [39, 40, 154, 157, 160, 285, 329], RGB to HSV transformation [51, 103, 117, 184], Elastic distortion [40, 91, 170, 329], Adding noises (salt or pepper noises) [54, 285, 329], Color jittering [108, 117, 238], Gamma correc-

tion [107, 235], GAN [251, 285], Whitening [58], and Dihedral transformation [165]. These typically applied augmentations are briefly discussed and explained in Table 6.

Table 6: Commonly employed augmentations for SLA from 2011 to 2020, scrutinizing a total of 365 articles (221 for segmentation and 144 for classification).

Method	Details descriptions
Rotation (A1)	Rotate the image coordinates of (x_1, y_1) by an angle of θ around (x_0, y_0) , resulting the coordinates of (x_2, y_2) where $x_2 = \cos(\theta) \times (x_1 - x_0) + \sin(\theta) \times (y_1 - y_0)$ and $y_2 = -\sin(\theta) \times (x_1 - x_0) + \cos(\theta) \times (y_1 - y_0)$.
Horizontal flipping (A2)	Change the image by a mirror-reversal of an original across a vertical axis, where the left side switches to the right side and vice versa.
Vertical flipping (A3)	Modify an image with a mirror-reversal of the original across a horizontal axis, where the top side switches to the bottom side and vice versa.
Scaling (A4)	Enlarge or reduces the image’s physical size by changing the number of pixels it contains, changing the size of the contents of the image and resizing the canvas accordingly.
Region cropping (A5)	A data augmentation technique that picks a random subset of the original image containing more salient information about the region of interest.
Shifting (A6)	Translation of an image in up, down, left, or right, along with any combination of the above direction, where every point of the object must be moved in the same direction and for the same distance.
Contrast adjustment (A7)	Remap image intensity values to the full display range of the data type, sharpening differences between black and white. It can either make an image more vivid or mute the tones for a more subdued feel.
Shearing (A8)	Shift one part of an image, a layer, a selection, or a path to a direction and the other part to the opposite direction; for example, a horizontal shearing will shift the upper part to the right and the lower part to the left, resulting in a diamond from a given rectangle.
Both flipping (A9)	Modify an image with a mirror-reversal of the original across both the vertical and horizontal axes, where the top side switches to the bottom side and then the left side switches to the right side and vice versa.
Histogram Equalization (A10)	Adjust the contrast of an image by using its histogram, spreading out the most frequent pixel intensity values, or stretching out the image’s intensity range. It allows the image’s areas with lower contrast to gain a higher contrast.
Gaussian noises (A11)	A type of mean spatial filtering that produces a new image by altering the structural details of an input image.
HSV (A12)	Provide a numerical readout of the image corresponding to the color names contained therein, abstracting the color (hue) by separating it from saturation and pseudo-illumination.
Elastic distortion (A13)	Generate a coarse displacement grid with a random displacement for each grid point that is then interpolated to compute a displacement for each pixel. Finally, the input image is then deformed using displacement vectors and spline interpolation.
Adding noises (A14)	An impulse noise caused by sharp and sudden disturbances in the image signal that presents as sparsely occurring white and black pixels.
Color jittering (A15)	A type of image data augmentation that randomly changes the brightness, contrast, and saturation of the image. It also adds random noise to the image.

Table 6 Continued from previous page

Method	Details descriptions
Gamma correction (A16)	A nonlinear operation that encodes and decodes luminance or tristimulus values in video or still image as $V_{in} = A \times V_{out}^\gamma$, where γ and A are the raised power and multiplied factors, respectively.
Whitening (A17)	A whitening transformation converts a vector of random variables with a known covariance matrix into a set of new variables whose covariance is the identity matrix, which has widely been adopted to remove redundancy by making adjacent pixels less correlated.
Dihedral transformation (A18)	A linear transformation that includes rotations and reflections of the images in the eight possible directions or angles of a dihedron.
GAN (A19)	Produce new data samples from a given random noise from a latent space and deliver unique images that mimic the feature distribution of the original dataset.

The employment of these augmentations in the last decade’s articles is displayed in the bar plot as a utilization frequency, as illustrated in Fig. 5. It reveals that the rotation, horizontal flipping, vertical flipping, scaling, region of interest cropping, and shifting are the top-6 augmentations employed for the SLA tasks, respectively in 21.22 %, 20.95 %, 18.30 %, 8.75 %, 6.10 %, and 6.0 % of the total articles. It is also noteworthy that those six most

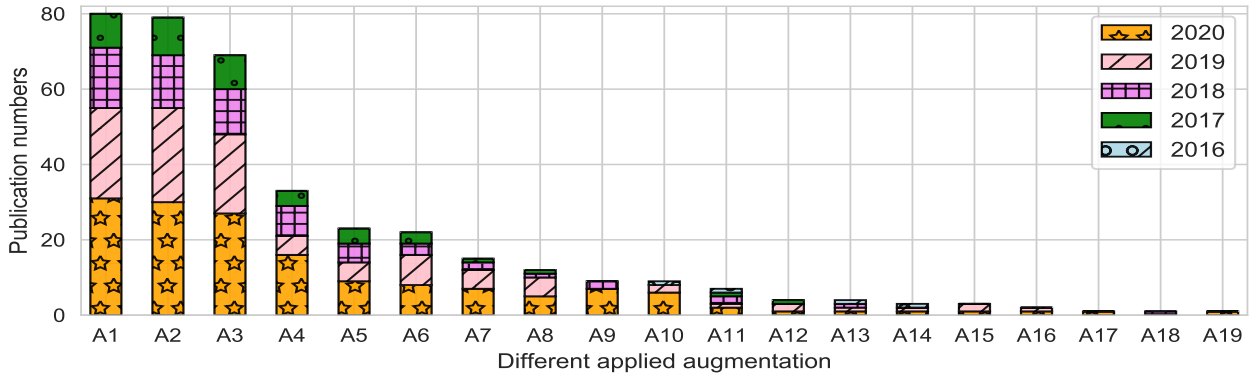


Figure 5: The number of articles employing different augmentations in the last decade for the SLS and SLC tasks, where the augmentations A1 to A19 are defined in Table 6.

essential augmentations (*first-tier*) are more operated in 2020, and their deployments have decreased from 2020 to 2016. Like preprocessing methods, contrast adjustment, shearing, both axis flipping, histogram equalization, and adding Gaussian noises can be classified as the *second-tier* augmentation methods due to their medium utilization. Due to the insignificant applications in the selected literature, the remaining augmentation techniques are termed

third-tier. Furthermore, the close inspection of Fig. 5 demonstrates that none of the top-10 augmentations is applied before 2016. It is also remarkable that the number of articles with the appliance of augmentation rises day by day from 2016 to 2020. Recalling Fig. 1 shows that the number of SLA articles after 2016 has enormously increased after DL’s engagement, especially CNN methods. Such an advancement in CNN models for SLA tasks reinforces the appliance of different augmentations as CNNs rely heavily on big data to be a generic model. However, an example of insight visualization of the top-5 augmentations with their original image has been displayed in Fig. 6. These example images demonstrate a high level

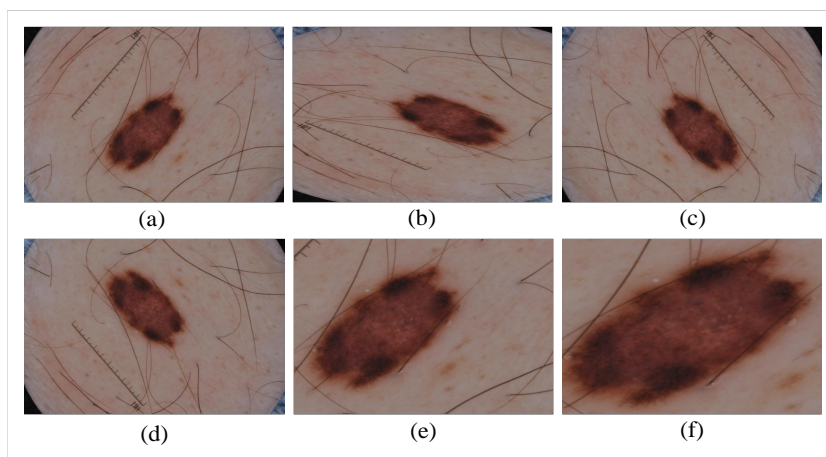


Figure 6: Examples of top-5 augmentations utilized in the last decade (2011-2020) for the SLA task, where (a) original image, (b) 90° rotation, (c) horizontal flipping, (d) vertical flipping, (e) scaling, and (f) random cropping.

of distinctions in shape, orientation, and spatial information, making them more reliable augmentation, viz. synthetic image composition techniques in supervised learning systems. Again, Table 6, Fig. 5, and Fig. 1 also point out that geometric augmentations viz. spatial information alteration are more prevalent in CNN-based learning systems. In contrast, the color or texture augmentations are more dominant in handcrafted feature-based ML and computer vision algorithms. Although GAN is a recent trend in other fields, it has not been massively employed in the SLA task in the last decade (see Fig. 5). A good synchronization is required between the generator and the discriminator stages of GAN. Sometimes, the learning process of GANs may have a missing pattern, the generator begins to degenerate,

the same sample points are continuously generated, and the learning cannot be continued.

Again, the class distribution of all datasets (see Table 2) confirms that the class sample images are imbalanced, which could induce the classifier to be biased towards the particular class that holds more samples [25]. This situation is noticeable in computerized medical diagnosis domains due to the scarcity of massive manually annotated training samples, especially in skin lesion datasets. However, the authors of SLA articles applied many techniques to mitigate that class bias problem. The authors in [59, 249, 259, 261–263, 270, 278, 282, 283, 289, 295] rewarded more extra consideration to the class with minority samples, estimating the class weight using a portion of $W_n = N_n/N$, where W_n , N , and N_n separately indicate the n^{th} -class weight, the total number of samples, and the sample in the n^{th} -class. Bisla et al. [115], Aldwgeri and Abubacker [290], DeVries and Ramachandram [320] collected additional images and merged with the minority class to balance with the majority class. Sometimes, the augmentations in Table 6 are also applied to the minority class to increase its sample numbers, as in [1, 46, 115, 148, 241, 246, 251, 254, 268, 279, 280, 289, 291]. Almaraz-Damian et al. [256] applied the SMOTE oversampling technique, demonstrating an improvement in the differentiation of melanoma and benign lesion images. To handle imbalanced classes, Molina-Molina et al. [258] employed the ensemble method using three classifiers with a linear plurality vote, where the other two models can overcome the bias from any candidate model. Lastly, the authors in [250, 257, 260, 264, 286, 304, 313, 316, 317, 327] employed random oversampling and undersampling. The former method randomly selects examples from the minority class with replacements and adds them to the training dataset. In contrast, the latter undersampling chooses examples from the majority class and deletes them from the training dataset. The one-by-one scrutinization of the selected 365 SLA papers and these discussions reveal that the most common methods for solving the class imbalance in the SLA tasks are class weighting, augmentations in the minority class, oversampling, and undersampling. These techniques can be a primary preference for forthcoming researchers to materialize a generic SLA framework.

5. Segmentation Techniques

There has been a notable improvement in research for developing segmentation algorithms and techniques for SLA in the recent past [8]. SLS algorithms can be broadly grouped into edge-, region-, threshold-, and soft computing or AI-based segmentation. The following sections (5.1~5.5) briefly familiarize those clusters of SLSs, and the insightful discussions on the nominated 221 SLS articles from 2011 to 2020 are delivered in section 5.6.

5.1. Edge-based SLS

They depend on the edges by searching for edge pixels and connecting them to form image contours and can be categorized into manual and automatic. The former manual method employs the mouse to trace lines representing image boundaries among regions. In contrast, the latter automatic method uses edge detection algorithms like watershed algorithm [174], active contours [139, 173, 218, 226, 339], canny edge detector [209, 212], and multi-direction gradient vector flow snake model [339]. In this type of segmentation, an edge filter is dedicated to the image, pixels are categorized as edge or non-edge, relying on the filter output, and pixels that are not isolated by an edge are allocated to the identical class. It is observed and concretely revealed that active contours are the most popular edge-based SLS method in the last decade's 221 papers.

5.2. Region-based SLS

In these algorithms, images are partitioned into regions or groups of similar pixels depending on their various properties, assuming that neighboring pixels within the same region have a similar value. Each pixel is compared with its neighbors in a particular region, and according to some specific conditions, it is clustered. This variety of SLS includes iterative region-based [171, 228], iterative stochastic region-merging [230], mean shift-based gradient vector flow [229], K-means & fuzzy C-means clustering [155, 163, 178, 185, 187, 189, 193–195, 206, 206, 211, 217, 219, 221, 224, 227], and Eikonal-based region growing clustering [216]. Conclusively, the one-by-one article scrutinization discloses that K-means & fuzzy C-means clustering are massively devoted in seventeen articles to region-based SLS methods

in the last decade; hence, it can be supposed as the representation of the region-based SLS approach.

5.3. *Threshold-based SLS*

This cluster can be described as point-based or pixel-based segmentation, depending on the threshold estimation algorithms, and often suffers from inappropriate threshold estimation due to different artifacts in the dermoscopic images [13]. OTSU [43, 48, 49, 73, 74, 76, 95, 133, 136, 176, 190, 198, 201, 204, 222, 225, 339], histogram estimation [187, 193, 210], morphological operations [144, 176, 223], optimal color channel-based empirical threshold estimation [214], and mean pixel intensity level-based threshold estimation [215] are the examples of this cluster. Notably, the OTSU thresholding technique is the most common threshold-based SLS approach in approximately seventeen articles of the selected 221 SLS articles, turning it into a metaphorical instance of this category. The conceivable rationale for choosing this technique is that it operates on an automatic and faster threshold estimation methodology.

5.4. *AI-based SLS*

AI models, especially CNNs, currently permit building an end-to-end supervised model without requiring manual feature extraction [348, 349] and exhibit tremendous success in many domains of medical imaging: arrhythmia detection [350–352], skin lesion segmentation and classification [3, 5, 13, 353, 354], breast cancer detection [355–357], brain disease classification [358], pneumonia detection from CXR images [359], fundus image segmentation [360, 361], minimally invasive surgery [362], lung segmentation [363] and *etc.* This category applies soft computing techniques in the segmentation process, including genetic algorithms [71, 220], fully convolutional neural networks [7, 83, 84, 91, 98, 102, 111, 121, 125, 138, 140–142, 146, 149, 150, 152–154, 156–161, 164–170, 175, 179–182, 184, 186, 188, 189, 191, 296], expectation-maximization [197], rule-based algorithms [196], Co-operative neural network [228], and artificial bee colony [147]. Again, the individual scrutinization of the selected 221 SLS articles indicates that fully convolutional neural networks are massively applied for the

SLS task, approximately forty-three articles in the last decade from 2011 to 2020, which can be deemed as the last decade’s representative SLS method.

5.5. Other SLS methods

In addition to those above-discussed four SLS varieties, the remaining applied SLS approaches in the last decade are probabilistic maximum-a-posteriori [145, 231], Markov random field [177, 208, 213], Delaunay Triangulation [203], Grap-cut [155], Cellular Automata [202], Wavelet transform [172, 200], and optimized color feature [88, 143]. Like four other categories of segmentation strategies, they are also categorized as other methods of the SLS task in the last decade from 2011 to 2020.

5.6. Insight Investigation on SLS Methods

Fig. 7 dispenses the SLS article numbers in the last decade, conferring the frequencies of various SLS procedures as discussed in the previous five subsections. It is observed from

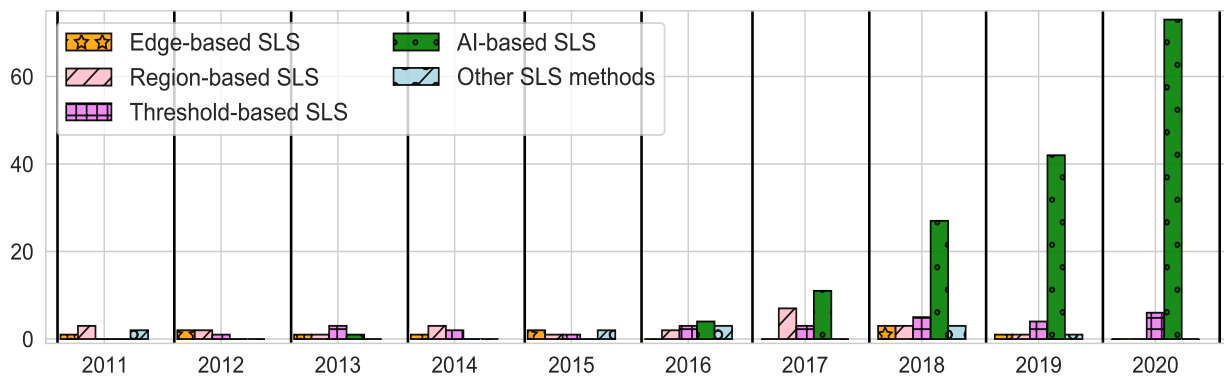


Figure 7: The number of articles employed different SLS methods in the last decade, consulting the commonly applied techniques.

the figure that the AI-based SLS processes have been most commonly employed in the last decade, especially after 2016. The appliance of the five earlier mentioned SLS categories is compared in the donut chart in Fig. 8, bestowing that a total of 64.8% of articles have employed AI-based SLS. In conclusion, Fig. 1, Fig. 7, and Fig. 8 combinedly demonstrate that the employment of AI-based SLS models has become crucial in the SLS task as the

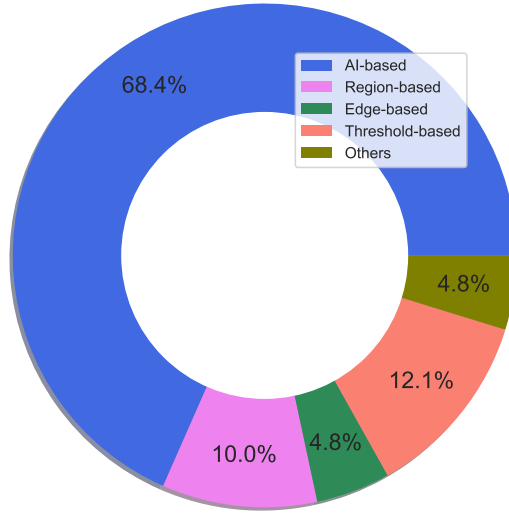


Figure 8: The donut chart of the percentage of SLS articles in the last decade from 2011 to 2020 for the five categories, as mentioned earlier.

number of SLS articles has been expanding massively since 2016. This SLS category can be considered as a *first-tier* SLS method, while the threshold-based and region-based SLS can be designated *second-tier* and *third-tier* SLS techniques, respectively. It requires mentioning that explaining the to-the-point theories of these SLS techniques is not the principal focus of this article; instead, we have concentrated on the overall SLS scenario in the last decade to highlight the trends in the aimed field of interest. The detailed point-to-point discussion of DL-based SLS methods is available in a review article of Kassem et al. [8]. However, the insight scrutinization of the AI-based SLS articles reveals that 51.2% of articles have employed DL methods, particularly deep CNNs. Therefore, the following paragraph focuses on the insightful discussion of the CNN architecture employed for the SLS task.

In order to build an end-to-end CNN-based SLS system, a model consists of two essential components: the encoder and the decoder [13]. The former component, the encoder, comprises convolutional and subsampling layers and is responsible for the automatic feature extraction. The convolutional layers are applied to construct the feature maps, whereas the subsampling layers are employed to achieve spatial invariance by decreasing those maps' resolution. This reduction in resolution heads to an extension of

the field of view of the feature map, which in turn makes the extraction of more salient features and minimizes the computational cost [362]. This is notably observed from the chosen 221 SLS article that many authors have employed different variants of pre-trained (on ImageNet, PASCAL-VOC, MS-COCO, etc) CNN models in the encoders like AlexNet [88, 179], Xception [55, 91], VGG [37, 79, 86, 88, 89, 98, 121, 125, 140, 157, 184, 186], ResNet [28, 46, 50, 56, 63, 66, 68, 79, 97, 98, 105, 115, 116, 141, 165, 175], LeNet [63], Inception [47, 99, 123], InceptionResNet [37], and DenseNet [13, 47, 60, 61, 117, 150, 156]. Remarkably, it is revealed that 36.36 %, 27.28 %, and 15.91 % articles of the transfer learning-based SLS articles employed ResNet, VGG, and DenseNet. Again, the latter component in the CNN-based SLS system, the decoder, semantically projects the distinctive lower resolution features learned by the encoder onto the pixel space of higher resolution to achieve a dense pixel-wise classification. The semantic segmentation networks have similar encoder designs, but they vary mainly in their decoder mechanism concerning how the discriminating features are projected onto the pixel space. However, the significantly decreased feature maps due to subsampling often undergo spatial resolution loss, which introduces coarseness, less edge information, checkerboard artifacts, and over-segmentation in semantically segmented masks [13]. To defeat these problems, Ronneberger et al. [364] proposed to skip connections in a U-Net, which provided the decoder to recover the relevant features learned at each stage of the dropped encoder due to pooling. Similarly, Long et al. [365] fused features at various coarseness levels of the encoder in Fully Convolutional Network (FCN) to refine the segmentation. However, when the deconvolution kernel size is not divisible by the up-scaling factor, a deconvolution overlap occurs as the number of low-resolution features that contribute to a single high-resolution feature is not constant across the high-resolution feature map [366]. Due to this deconvolution overlap, checkerboard artifacts may appear in the segmented mask. Therefore, Al-Masni et al. [232] proposed a full resolution convolution network, excluding subsampling layers in the encoder to conserve the spatial information of the feature maps. However, the subsampling of feature maps is exceptionally desirable to be employed on CNN due to the several positive perspectives, as previously mentioned. A complete survey and review on those decoder mechanisms and skip (shortcut) connection

can be discovered in [367].

In some articles, the authors ensembled multiple SLS models or outputs to produce a refined lesion segmentation [46, 47, 52, 61, 65, 99, 111, 127, 154, 157, 165, 168–170, 185]. For example, a bagging-type ensemble approach was executed in [154] to combine outputs of various FCNs with improving the image segmentation performance on the testing images. Liu et al. [111], Chen et al. [157], Qian et al. [169] ensembled different outputs in the post-processing to increase the segmentation results. Firstly, they segmented an input image by augmenting it to generate different outputs. Then reverse operations were performed on the results that were finally averaged to get a lesion mask. Goyal et al. [99] employed DeeplabV3 and Mask R-CNN to propose three ensemble model variants. Ensemble-ADD combines the results from both models, Ensemble-Comparison-Large picks the larger segmented area by comparing the number of pixels in the output of both methods, and Ensemble-Comparison-Small picks the smaller area from the output. Lastly, a pixel-wise majority voting ensemble for lesion segmentation was proposed and implemented in [52]. Additionally, many scholars in many articles have incorporated different post-processing methods to refine the segmented lesion masks, as explained in Table 7.

Table 7: Commonly employed post-processing for SLS from 2011 to 2020, scrutinizing a total of 221 for lesion segmentation.

Details post-processing method	Articles
Conditional random fields, as a statistical modeling method for structured prediction, considering neighboring pixels' information in the new pixel prediction.	[52, 90, 103, 116, 123, 175]
The binary lesion masks are followed by morphological dilation operations. The region closer to the image center is picked, followed by unwanted components like corner effect removal and filling of the small holes.	[41]
The best cluster from all the predicted clusters is determined by calculating the mean value for each cluster and selecting the maximum mean value. Then morphology operations, for example, opening, closing, and filling holes are applied to enhance the segmented lesion masks.	[71]
Subtraction of smaller or misclassified areas and sharp fragments from the mask's borders.	[27, 159]
Iterative self-organizing data analysis technique was employed to threshold the output probability map from the sigmoid activator of their DSNet to retrieve the lesion mask.	[13]
Simply morphological smoothing and extracting the largest connected component from the predicted binary lesion mask.	[7, 65, 86, 188, 193, 228]

Table 7 Continued from previous page

Details post-processing method	Articles
Watershed-based postprocessing feeds high-confidence pixel classifications as seeds into the watershed algorithm.	[79]
Several consecutive morphological filtering, such as dilation, erosion, closing, and opening, for enhancing the predicted lesion boundary.	[72, 81, 93, 99, 114, 125, 133, 154, 158, 185, 192, 214, 217]
A convex hull operation follows the morphological opening process of the predicted binary mask for lesion shape approximation.	[39]
Region merging and morphological operations are applied to obtain the final lesion mask.	[35]
Fill in the small holes in the predicted binary lesion mask.	[7, 91, 170, 185, 188, 189, 193]
The output probability map is subjected to three consecutive post-processing actions constructing the final mask: thresholding the probability map at 0.5, choosing the largest connected component, and finally, filling the small holes.	[121, 139]
k-means clustering and flood-fill algorithms are combined to obtain the final lesion region. Then, holes are sealed by applying a hole-filling algorithm.	[155]
The lesion region close to the center of the image is picked and followed by the hole filling and morphological closing operations to refill the small holes and isolated islands. Finally, a Gaussian mask weighs the closeness of connected regions against the center of the image, and then the largest area is nominated as the final segmented mask.	[172]
A dual-threshold method to generate a binary mask, where a relatively high threshold (= 0.8) is devoted to determining the lesion center, and a lower threshold (= 0.5) is applied to the output map. After filling small holes with morphological dilation, the final lesion mask is decided.	[154, 166]
The largest connected binary objects are stored and joined with adjacent regions. Then, morphological operations are applied to fill holes and remove any extra elements other than the skin. Lastly, a convolution filter with a smoothing operation is performed to get the final lesion masks.	[200]
A graph-cut algorithm is applied to the output score maps to fine-tune the predicted masks.	[180]

The above table reveals that morphological operations, such as dilation, erosion, closing, and opening, have been played a horsepower and massively employed for post-processing segmented lesion masks, as many articles have applied [41, 71, 72, 81, 93, 99, 114, 125, 133, 154, 158, 172, 185, 192, 214, 217]. Small holes and disconnected island regions in the segmented lesion masks were often resolved in many ways in the selected 221 SLS articles. For example, hole-filling algorithms can fill tiny holes [7, 91, 170, 185, 188, 189, 193], and the island regions can be abolished by keeping the more significant regions from the region properties techniques [7, 65, 86, 188, 193, 228]. In some articles [52, 90, 103, 116, 123, 175], the authors have involved Conditional random fields techniques to refine the segmented

masks. These discussions on different post-processing methods reveal that they can be a preparatory choice for forthcoming researchers to assemble a generic SLA framework.

6. Classification Techniques

Computational SLC methods related to the lesion features are founded on the ABCD(E) rule, pattern analysis, seven-point checklist, and Menzies’ method. Those methods are illustrations of clinical techniques operated for the prognosis and diagnosis of image-based skin cancer [4], color, diameter (or differential structures in the case of dermoscopic images), and evolution (or elevation) features, according to the standards delivered in Table 8. The

Table 8: Standards of the ABCD(E) rule for diagnosing skin cancer from clinical and dermoscopy examination.

Features	Dermoscopic investigation with detailed description	Score
Asymmetry (A)	One-half of the lesion does not match the other, meaning that the border, colors, or structures are asymmetric in 0, 1, or 2 perpendicular axes. For example, the shape is symmetric for Nev lesion and asymmetric for Mel lesion.	0 – 2
Border (B)	The lesion edges are irregular, ragged, notched, or blurred, where the border is regular or well-defined for Nev lesion and irregular or ill-defined for Mel lesion.	0 – 8
Color (C)	There are six possible primary colors: white, red, light brown, dark brown, blue-grey, and black. The color is not uniform for Mel lesion and uniform for Nev’s lesion.	1 – 6
Diameter (D)	Presence of five differential structural components such as network, structureless areas, branched streaks, dots, and globules, where the spot is greater than a quarter of an inch.	1 – 5
Evolution (E)	Changes in size, shape, or shades of color features for Mel lesion.	–

Total Dermatoscopy Score (TDS) is then estimated using Eq. 2, following Table 8 to decide the types of lesions as Nev or Mel.

$$TDS = A_{score} \times W_A + B_{score} \times W_B + C_{score} \times W_C + D_{score} \times W_D \quad (2)$$

where W_A , W_A , W_A , and W_A are the weight factors for the feature types, which are 1.3, 0.1, 0.5, and 0.5, respectively. The lesions are considered to be Nev, suspicious, and Mel if the TDS has the values of < 4.75 , $4.75 - 5.45$, and > 5.45 from the Eq. 2. The other traditional methods of the SLC have been reviewed in detail by Oliveira et al. [4]. However, those SLC methods require a dermatologist for the naked-eye assessment that may include a

fault-prone recognition, as it endures from the comparability between the lesions and healthy tissues. Dermatologists' manual examination is usually monotonous, time-consuming, and impressionistic, directing them to different distinction accurateness relying on their knowledge and workload [3, 5]. Hence, we mainly focus on reviewing automated CAD systems to mitigate the above-mentioned limitations. There has been a significant advancement in developing automated lesion classification algorithms and approaches for SLA in the recent past [8]. Some methods were based on handcrafted feature engineering with ML models, while DL-based automatic feature learning schemes are most popularly applied nowadays [8]. Therefore, this section has been partitioned into two parts for carrying out the SLC review analysis according to ML- and DL-based SLCs.

6.1. ML-based SLC

As noted previously, ML-based SLC strategies depend on successfully engineering the handcrafted lesion features that are firstly described and reviewed in section 6.1.1. Then, the employed classifiers are inspected in section 6.1.2.

6.1.1. Lesion Features

Lesion attributes (or features) can be extracted either globally or locally to acquire category information. Most of the works explore the global features of the lesion, for instance, extracting features from all segmented regions [59, 87, 145, 173, 314, 324, 327]. Some examinations have employed local characteristics, allowing the characterization of a diverse lesion region. However, lesion features are organized into different types: shape, color variation, texture analysis, and other miscellaneous. The applied and extracted lesion features in the last decade from 2011 to 2020 are summarized in Table 9 and clustered into those four categories as mentioned earlier. They are again discussed in the following paragraphs to investigate their utilization frequencies.

Table 9: Different pigmented skin lesion features from macroscopic and dermoscopic images in the last decade from 2011 to 2020.

Different lesion attributes	Articles
Shape-based lesion attributes	
Convex hull to estimate notched and ragged edges	[344]
Circularity Index $((4\pi A)/P^2)$ for border's irregularity, where A and P are the lesion contour's area and perimeter, respectively.	[256, 339, 344]
Hull/Contour Ratio to measure the raggedness or spikiness of the lesion border	[339, 344]
The lesion boundary comes from a snake-based edge detection technique, segmenting the image into skin area A_s and lesion area A_l . The average skin pattern isotropies in the skin (m_s) and lesion (m_l) areas are calculated as $m_s = \frac{1}{N_s} \sum_{(i,j) \in A_s} I(i,j)$ and $m_l = \frac{1}{N_l} \sum_{(i,j) \in A_l} I(i,j)$, where N_s and N_l are the number of sub-images in the skin and lesion areas.	[337, 343]
Clinical border irregularity features, delineating a skin lesion into eight segments.	[341]
Morphologically fine irregularities feature from the image I, as $f^B = \frac{I_c - I_l}{I_l} + \frac{I_l - I_o}{I_l}$, where I_l , I_c , and I_o respectively denote the original lesion area, ROI's closing, and ROI's opening.	[341]
Coarse irregularities from the perimeters of the low-frequency border and the original border as $f^B = \frac{ P_{lesion} - P_{low} }{P_{lesion}}$, where P_{lesion} and P_{low} are the lengths of the perimeter of the original and low-frequency border (details in [341]).	[341]
Structural irregularities from the Fourier descriptors as $f^B = \sum_{u=0}^{N-1} (C(u) - \bar{C}(u))^2$, where C is the Fourier coefficient (details in [341]).	[341]
Asymmetry features were extracted by a shrinking active contour model to find major and minor axes, vertical and horizontal dash lines, of the lesion boundary.	[340]
The asymmetry feature by computing the principal and secondary axes of inertia, where the axes of the image were aligned with the axes of inertia, allowing a better assessment of the lesion symmetry in terms of geometry and internal structures.	[338]
The border feature for finding the abrupt ending of pigment pattern in two peripheral regions: inside and outside the lesion, using the Euclidian Distance Transform.	[338]
The asymmetry characterization features such as the ratio between the lesion area and its bounding box area, equivalent diameter $(4A/(L_1\pi))$, the ratio between the principal axes (L_2/L_1) , the ratio between sides of the lesion bounding box, the ratio between the lesion perimeter (p) and its area (A), $(B_1 - B_2)/A$ [B_1 and B_2 are the areas in each side of axis L_1 or L_2], and B_1/B_2 ratios concerning the axis L_1 or L_2 .	[178, 256, 293, 297, 330, 339]
Boundary Irregularity description features like average and variance gradient magnitudes of the pixels in the extended lesion rim in each of the three channels ($i = 1, 2, 3$); average and variance of the $R (= 1, 2, \dots, 8)$ $\mu_{R,i}$ values in each of the three channels. $\mu_{R,i}$ is the mean of 8 different symmetric regions, obtained by rotating orthogonal axes by 45 degrees.	[178, 339]
Ulnar variance measures the relative length of articular surfaces of some particular radius and image asymmetry.	[330]
Solidity, asymmetry index, extent, diameter, circularity, eccentricity, aspect ratio, structural similarity, and the ratio of the major to the minor axis as structural features.	[1, 237, 267, 327]
2D and 3D shape features (details in [315]).	[315]
Color-based lesion attributes	

Table 9 Continued from previous page

Different lesion attributes	Articles
R, G, B colors means ($\mu = (\mu_R, \mu_G, \mu_B)$) and their covariance matrices (Σ) (details in [342]).	[342, 344]
Six color features from two-stage detection algorithms: color clustering using a mean-shift algorithm and color supervised classification based on a dataset of reference RGB codes.	[338]
Maximum, minimum, mean, and variance of the intensities of the pixels inside the lesion segment in the color variation channel and each of the three original channels; ratios between the mean values of the original three channels, for example, μ_R/μ_G , assuming only pixels inside the lesion segment.	[87, 145, 173, 178, 241, 256, 264, 297, 315, 339]
The variance, skewness, and entropy as color-related features.	[87, 145, 237, 241, 256, 330]
Boundary color value differences for each channel as $f = \frac{1}{N} \sum_{i=1}^N (V_i - V_m)^2$, where V_i , V_m , and N are the value of i^{th} boundary pixel, the mean value of the boundary pixel, and the number of boundary pixels.	[322]
Boundary color clustering features, clustering a lesion with different k groupings (details in [322]).	[322]
Color features of six different colors like white, red, light brown, dark brown, blue-gray, and black (estimation details in [301]).	[134, 301]
Histogram-based features (color distribution)	[368–370]
Color asymmetry	[370]
Kullback-Leibler divergence of the color distribution (each channel separately) from the two halves along each axis.	[327]
Texture-based lesion attributes	
Twelve generalized cooccurrence matrices features like energy, contrast, correlation, entropy, homogeneity, inverse difference moment, cluster shade, cluster prominence, max probability, autocorrelation, dissimilarity and variance.	[342]
Five differential structures based on texture relevant for the detection of melanoma: homogeneous areas, streaks, dots, globules, and pigment network.	[338]
Textural variation in the channel as maximum, minimum, mean, and variance of the intensities of the pixels inside the lesion segment.	[178, 339]
Texture-base Gray Level Co-occurrence Matrix (GLCM) features that include mean, correlation, homogeneity, contrast, energy, dissimilarity, kurtosis, variance, entropy, maximum probability, inverse difference, angular second moment, and standard deviation.	[1, 134, 256, 264, 294, 301, 310, 321, 324, 330, 371]
Haralick texture features using gray-tone spatial-dependence matrices (details in [315]).	[315]
SFTA features (details in [173]).	[173]
SURF, SIFT, and ORB features	[241]
Texture-based RSurf features	[326]
Bi-dimensional Empirical Mode Decomposition (BEMD), BEMD-Riesz, Gray-level Difference Method (GLDM), and combined BEMD-Riesz with GLDM.	[314]
Fractal dimensions and GLDM features (details in [297]).	[1, 297]
Histogram of oriented gradients features (details in [173]).	[87, 134, 145, 173]

Table 9 Continued from previous page

Different lesion attributes	Articles
Gabor wavelets features (details in [134]).	[87, 134]
Fractal-based regional texture analysis-based texture features (details in [1]).	[1]
Edge and local edge Histogram features (details in [87]).	[87]
Texture feature-based on fractional Poisson to estimate the structure of regions in an image (details in [325]).	[325]
Coarseness features that measure of different angle of texture representation.	[330]
Other (miscellaneous) lesion attributes	
Local Binary Patterns (LBP) features	[87, 134, 241, 266, 294, 326]
Manual information	[372]
Model-based features.	[4, 373]

Shape features (see list of names in Table 9) consider the lesion’s asymmetry or border’s irregularity, dividing the lesion region into two sub-regions by an axis of symmetry to analyze the area’s similarity by overlapping the two sub-regions of the lesion along the axis. Then, the asymmetry index is estimated by the difference between the two sub-regions of the lesion, for example, the XOR operation between them [4]. Sometimes, geometrical measurements from the segmented lesion area have been commonly computed to assess the lesion’s asymmetry and border irregularity, which include the area of the lesion, aspect ratio, compactness, perimeter, greatest diameter, shortest diameter, equivalent, convex hull, eccentricity, solidity, rectangularity, entropy measures, circularity index, and irregularity index (see details in Table 9) [1, 237, 267, 327]. Out of the 144 SLC articles, twenty-nine articles (20.1%) employed lesion shape features in the last decade for the SLC task.

The RGB color space is commonly employed to represent the colors of skin lesions. Other color spaces have also been applied in order to acquire more specific information about a lesion’s colors, such as normalized RGB, HSV, HVC, CMY, YUV, I1/2/3, Opp, IiN, JCh, L*C*H, CIEXYZ, CIELAB, and CIELUV (see details in [4]). Several statistical measures such as minimum, maximum, average, standard deviation, skewness, and variance are widely applied to feature extraction from skin lesion images, computing each color channel of the lesion region using one or several color models [87, 145, 173, 178, 237, 241, 256, 264, 297, 315, 330, 339, 342, 344, 374]. Furthermore, these measures may also be applied to other regions

associated with the lesion’s border to identify a sharp transition, indicating malignancy. Skin lesion features based on relative colors have been proposed to assess color features from different regions associated with the lesion. The relative color consists of comparing each pixel value of the lesion to the average color value of the surrounding skin. Likewise, this feature may present advantages such as compensating for the variation of the image’s color caused by illumination and equalizing variations in skin color among individuals. The occurrence of the possible primary colors present in the skin lesions has also been analyzed, and the number or percentage of pixels within the segmented area for each of the primary colors [375]. However, out of the 144 SLC articles, twenty-eight SLC articles (19.4%) employed lesion color features in the last decade for the SLC task.

Texture analysis is generally regarded as discriminating between benign and malignant lesions by estimating their structure’s roughness, encompassing descriptors like statistical-, model-, and filter-based methods [4]. Among the various statistical-based texture descriptors applied in the literature, the GLCM has been one of the most commonly utilized [1, 134, 256, 264, 294, 301, 310, 321, 324, 330, 371]. GLCM is a statistical measure that computes the joint probability of occurrence of gray levels considering two pixels spatially separated by a fixed vector. Several measures may be computed based on the GLCM, such as mean, correlation, homogeneity, contrast, energy, dissimilarity, kurtosis, variance, entropy, maximum probability, inverse difference, angular second moment, and standard deviation [1, 134, 256, 264, 294, 301, 310, 321, 324, 330, 371]. Model-based texture descriptors have also been proposed to assess the skin lesion’s texture, such as fractal dimensional [1, 297], auto-regression, and Markov random fields. Among these, fractal dimension has been applied with the box-counting method, one of the most commonly used methods since it is simple and effective [1, 297]. Wavelet, Fourier, and Gabor transform [87, 134], and scale-invariant feature transform (SIFT) [173, 241], which are filter-based texture descriptors, have also been proposed for feature extraction of skin lesion images. Such descriptors allow the decomposition of the input image into parts in order to extract features from the structures of interest. Sobel, Hessian, Gaussian, and difference of Gaussians features have also been extracted based on the bank of Gaussian filters [87, 134, 145, 173]. However, thirty-two

articles (22.2%) out of 144 SLC articles utilized lesion texture characteristics in the last decade for the SLC task.

The authors combined the color and texture features in some articles [294, 342, 372, 376] to construct a distance measure between a test image and a database image, using color covariance-based features and the Bhattacharyya distance metric [342]. Although texture-based lesion features are slightly more used, most articles applied all three types of features to represent the feature vector with all categories of lesion characteristics, as various feature types expose various properties of the skin lesion. Fig. 9 displays the most generally applied (at least in two articles) lesion characteristics from Table 9 in the last decade from 2011 to 2020 for the SLC task. A close observation in Fig. 9 indicates a wide range of attributes from

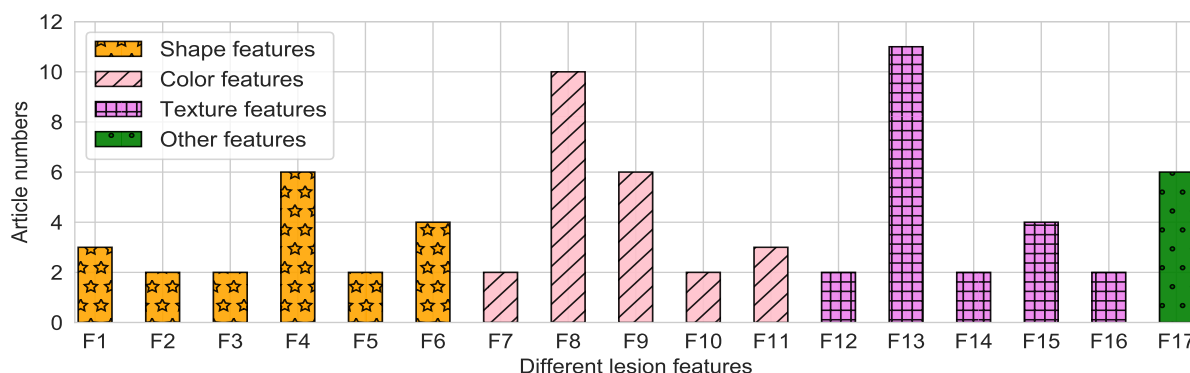


Figure 9: The frequency of utilization of various skin lesion attributes with their complementary number of employed articles for the SLC task. F1→ Circularity index, F2→ Contour ratio, F3→ Average skin pattern isotropies, F4→ Asymmetry characterization, F5→ Boundary irregularity description, F6→ Structural features, F7→ RGB colors means and covariances, F8→ Maximum, minimum, mean, and variance of the intensities, F9→ Variance, skewness, and entropy as color-related features, F10→ White, red, light brown, dark brown, blue-gray, and black color features, F11→ Color histogram-based features, F12→ Textural variation in the channels, F13→ Gray level co-occurrence matrix, F14→ Fractal dimension, F15→ Histogram of oriented gradients, F16→ Gabor wavelets features, and F17→ Local binary patterns.

each type of feature category, revealing that Asymmetry characterization (F4), Maximum, minimum, mean, and variance of the intensities (F8), Gray level co-occurrence matrix (F13), and Local binary patterns (F17) are most common shape, color, texture, and other types lesion attributes, respectively. These lesion features can be deemed as the representative le-

sion characteristics of those attribute categories (first-tier). Additionally, structural features, skewness, and entropy as color-related features and histograms of oriented gradients are the second instances (second-tier) of lesion characteristics of shape-, color-, and texture-based lesion attributes. In contrast, the other remaining lesion attributes in Fig. 9 are viewed as the less significant attributes (third-tier). In the remarks, Fig. 9 helps the researchers to make an attribute's ranking according to the times of appliance in the SLC article in the last decade from 2011 to 2020, which will subsequently equip them with an initial lesion attribute selection policy for further automated SLC tasks.

6.1.2. Lesion Classifiers

After feature extraction, a feature selection step is crucial [377, 378], and has been employed for the SLC task to determine the most relevant features and reduce the dimensionality of the feature space [1, 241, 264, 266, 297, 379]. Moreover, such features may influence the performance of the classification process, i.e., render it a slower process. Several benefits are associated with the application of feature selection schemes [4] such as reducing the feature extraction time, decreasing the classification complexity, improving the classification accuracy rate, lowering training-testing time, simplifying the understanding, and visualizing the data. The feature selection process has the following steps: feature subset selection, feature subset evaluation, stopping criterion, and validation procedure [4], which is then headed by lesion classification step(s).

The classification phase consists of recognizing and interpreting the information about the skin lesions based on extracted and selected lesion features. The classification process is generally accomplished by randomly dividing (or K-folding) the available image samples into training and testing sets. The training step consists of developing a classification model to be employed by one or more classifiers based on the samples of the training set. Each sample comprises features extracted from a provided image and its corresponding class value, which are applied as input data to the classifier for the learning process. The testing step measures the model's accuracy learned by the training step over the test set. In the last decade, from 2011 to 2020, the most generally engaged SLC models are Support Vector

Machine (SVM) [1, 81, 82, 134, 145, 173, 178, 252, 264, 297, 310, 314, 315, 321, 324, 325, 327, 330, 333, 340, 341, 371, 380–382], K-nearest Neighbors (KNN) [178, 239, 264, 293, 325, 327, 331, 339, 342, 344, 380, 381], AdaBoost (AdB) [244, 315, 325, 327], Decision Tree (DT) [237, 327, 381], Random Forest (RF) [237, 244, 338], Artificial Neural Network (ANN) [330, 381], Multilayer Perceptron Neural Network (MPNN) [264], Linear Discriminant Analysis (LDA) [82], Quadratic Discriminant Analysis (QDA) [82], Naive Bayes (NB) [327], K-means Clustering (KMC) [334], Probabilistic Neural Network (PNN) [383], Feed Forward Back Propagation Neural Network (FFBPNN) [380], Ensemble Binary Classifiers (EBC) [336], and Elman Neural Network (ENN) [264].

The synopsis of the ML models utilized in the last decade from 2011 to 2020 from the designated SLC papers has been displayed in the pie plot in Fig. 10. After carefully

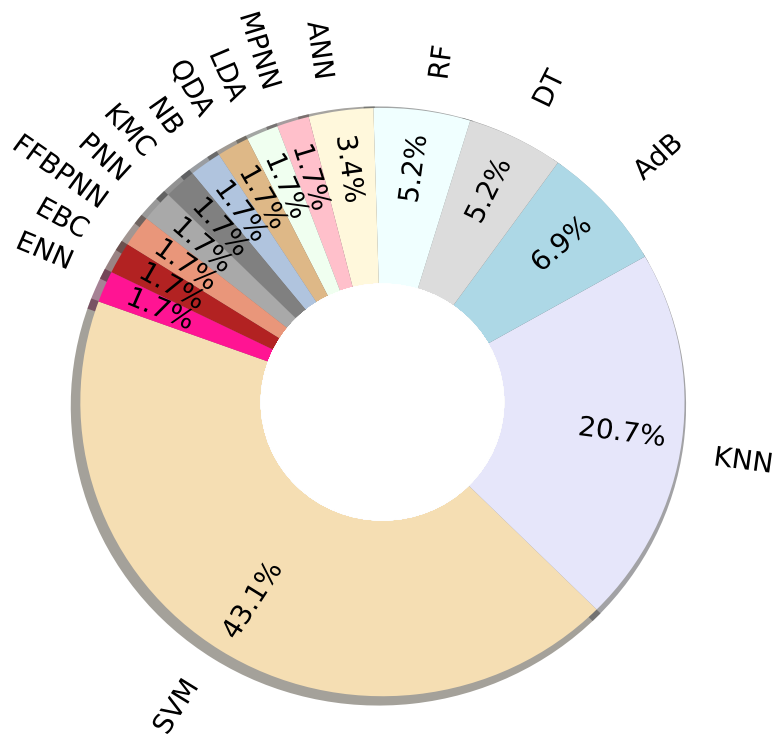


Figure 10: The pie chart of the percentage of SLC articles employing various ML models on handcrafted lesion features in the last decade from 2011 to 2020.

scrutinizing those chosen SLC papers, this figure reveals the top operating ML models

and the percentage of various ML algorithm utilization for the SLC task. This figure also demonstrates that SVM and KNN are the topmost skin lesion classification methods in those 144 SLC articles, which are 43.1% and 20.7% of the total SLC article, respectively. Undoubtedly, those two ML models can be regarded as the representative ML classification models (*first-tier*) for the SLC task. Again, it is also observed from Fig. 10 that SVM, KNN, AdB, DT, RF, and ANN are the most applied methods, populating 84.7% of the total SLC articles. Therefore, AdB, DT, RF, and ANN can be categorized as the *second-tier* ML models for the SLC task. In contrast, the other nine ML models such as MPNN, LDA, QDA, NB, KMC, PNN, FFBPNN, EBC, and ENN are applied in the remaining 15.3% of articles, where each of them is applied in 1.7% of the total 144 articles. For the SLC task, they can be organized as the *third-tier* ML models (less significant). However, quick calculation time, simple algorithm to interpret, versatile usefulness for regression and classification, and evolution with new data are the potential reasons for the massive employment of the SVM and KNN model in the SLC literature. These results sufficiently claim the insight scenario of selecting ML models for the SLC task that helps the researchers initialize the related field investigations. In the expositions, those discussions enable the researchers to tag the ML models in the last decade from 2011 to 2020 and will provide an idea for classifier preference for automated SLC task(s).

6.2. DL-based SLC

As discussed in the earlier section, ML-based SLC requires extensive feature engineering with comprehensive parameter tuning to achieve better and more robust performance, which is often challenging due to the appearance of various intrinsic and extrinsic noises in dermoscopic images (see details in [3, 13]). On the other hand, the CNN-based DL-SLC approaches provide excellent SLC results and boost diagnostic procedure rates while being end-to-end systems. Nowadays, CNN-based segmentation networks have been widely applied for medical images, outperforming traditional image processing methods relying on handcrafted features [361]. However, the one-by-one scrutinization of the 144 SLC articles demonstrates that most authors employed pre-trained (on ImageNet, PASCAL-VOC, MS-

COCO, etc.) CNN models and fine-tuned with the skin lesion datasets. The most commonly employed pre-trained CNN models found in the SLC literature from 2011 to 2020 are: MobileNet [235, 246, 248, 256, 292, 308], variants of EfficientNet [59, 248, 249, 257, 263, 283], DenseNet [148, 235, 240, 242, 243, 250, 254–256, 258, 283, 285, 292, 304], SeReNeXt-50 [249], variants of VGGNet like VGG16 [63, 88, 157, 170, 235, 236, 246, 252, 255, 256, 261, 262, 268, 269, 277, 278, 292, 300, 316, 319] and VGG19 [236, 269, 308], LeNet-5 [63, 282, 306], GoogleNet [234, 253, 262, 269, 300], PNASNet-5-Large [257, 284], Squeeze-and-Excitation Networks (SENet) [257, 263, 284, 305], AlexNet [88, 157, 234, 262, 277, 278, 300, 326, 328], Xception [235, 250, 256, 257, 259], different versions of Inception model like Inception-V3 [235, 253, 256, 257, 269, 279, 283, 292, 318, 320] and Inception-V4 [257, 284, 298], variants of ResNet like ResNet101 [46, 235, 242, 250, 255, 257, 269, 270, 273, 275, 278, 287], ResNet152 [257], Resnet50 [63, 97, 115, 116, 148, 157, 234, 251, 255, 256, 260–262, 273, 277, 278, 280, 283, 285, 286, 293, 295, 299, 300, 307–309, 311, 323], ResNeXt with weakly supervised learning [263, 283, 313], and SE-ResNeXt101 [257, 283], NASNet-A-Large [235, 257, 259], and mixture of Inception and ResNet (InceptionResNet-V2. [235, 240, 252, 257, 259, 284]). In contrast, a few authors have proposed new networks, a modification of the current models, or hybrid methods dedicated to the SLC task, for example, in [3, 5, 233, 245, 249, 265] etc., which are briefly illustrated in the next paragraph.

Hasan et al. [5] designed an end-to-end hybrid-CNN classifier with a two-level ensembling. A channel-wise concatenated 2D feature map was proposed to enhance the first-level ensembling’s depth information. In contrast, the authors also proposed aggregating the various outputs from different fully connected layers in the second-level ensemble, learning more discriminating features with limited training samples. Wu et al. [233] proposed a densely connected convolutional network with an Attention and Residual learning method for the SLC task, where each ARDT block consists of dense blocks, transition blocks, and attention and residual modules. Compared to a residual network with the same number of convolutional layers, the size of the parameters of the densely connected network proposed was reduced by half. The improved densely connected network added an attention mechanism and residual learning after each dense and transition block without additional

parameters. Bi et al. [265] presented a hyper-connected CNN (HcCNN) to classify skin lesions having an additional hyper-branch that hierarchically integrates intermediary image features, unlike existing multi-modality CNNs. The hyper-branch enabled the network to learn more complex combinations between the images at early and late stages. They also coupled the HcCNN with a multi-scale attention block to prioritize semantically meaningful subtle regions in the two modalities across various image scales. Hasan et al. [3] proposed a CNN-based framework for simultaneous detection and recognition of skin lesions, named Dermo-DOCTOR, consisting of two encoders. The feature maps from the two encoders were fused channel-wise, called the fused feature map. This fused feature map was utilized for decoding in the detection sub-network, concatenating each stage of two encoders' outputs with corresponding decoder layers to retrieve the lost spatial information due to pooling in the encoders. For the recognition sub-network, the outputs of three fully connected layers, utilizing feature maps of two encoders and fused feature map, were aggregated to obtain a final SLC class. Mahbod et al. [249] developed a three-level fusion scheme named multi-scale multi-CNN (MSM-CNN). They trained CNN models with cropped images at a fixed size at level one. At level two, they also fused the results from the individual networks trained on the six different image sizes (i.e., 224×224 , 240×240 , 260×260 , 300×300 , 380×380 , and 450×450). At the third and final fusion level, the authors fused the predicted probability vectors of the various architectures to yield the final classification result. The final MSM-CNN classification was thus derived from 90 ($5 \times 6 \times 3$) sub-models. Sun et al. [245] constructed a CNN-based SLC model that is loosely based on a baseline vanilla CNN network. The basic structure was two convolutional layers followed by a max-pooling layer containing fewer filters to reduce the training time. Additionally, their network included more dropout layers and less fully connected neurons to combat the overfitting present when replicating the original network.

The one-by-one scrutinization of the selected 144 SLC articles demonstrates that some authors in [87, 88, 124, 148, 235, 238, 241, 242, 252, 256, 258, 261, 273, 279, 287, 296, 326] combined the CNN's automated lesion features and handcrafted manual features (described in Table 9) for the SLC task to enhance the classification results in the last decade. They

either extracted CNN attributes and merged them with manual features and then categorized them using a typical ML model(s) (as mentioned in 6.1.2) or manually extracted lesion features and stacked them in a particular CNN layer and then classified them using a Fully-connected layer. Furthermore, single CNN models are often indirectly limited when trained with highly variable and distinctive image datasets with limited samples. The authors of many SLC articles [59, 249, 250, 253, 259, 262, 277, 278, 284, 300] mitigated this difficulty by applying the ensemble techniques. There are many analyses on designing those ensemble techniques; for instance, should the individual ensemble’s candidate model train first and then perform aggregation like in [99, 249, 263, 300, 304, 384–386]? Despite their approaches’ satisfactory results, such an ensemble is tedious and time-consuming, driving colossal time and resources for training and testing, as each model is independently trained and tested. Therefore, Hasan et al. [5] proposed an end-to-end ensemble strategy that mitigated those weaknesses in [99, 249, 263, 300, 304, 384–386] without compromising state-of-the-art SLC results.

Again, the synopsis of the DL models employed in the last decade (2011-2020) from the specified 144 SLC articles has been portrayed in the pyramid plot in Fig. 11. A close inspection of the figure reveals the top working DL architecture with their utilization percentage for the SLC task. It is also observed from Fig. 10 that ResNet, VGG, DenseNet, InceptionNet, and AlexNet are the top-5 most SLC methods in those 144 SLC articles, which are 31.4%, 15.0%, 12.4%, 8.5%, and 5.9% of the total SLC article, respectively. They can be clustered as the SLC’s most significant (first-tier) CNN models. The other architectures are employed in 0.7% ~ 3.9% of the SLC articles, where the InceptionResNet, MobileNet, EfficientNet, GoogleNet, and Xception are separately used in 3.3% ~ 3.9% articles and thought of as the second-tier CNN models for the SLC task. In contrast, the other CNN models in Fig. 10 are assumed to be the less significant, i.e., third-tier CNN models for the same mission. The further insight inspection of those architectures exposes that out of 31.4% ResNet models, the ResNet-50 and ResNet-101 applied in 19.6% and 7.8% articles in the last decade. Similarly, for 15.0% VGG architectures, the VGG-16 and VGG-19 applied in 13.1% and 1.9% articles. Again, the Inception-V3 is more commonly employed

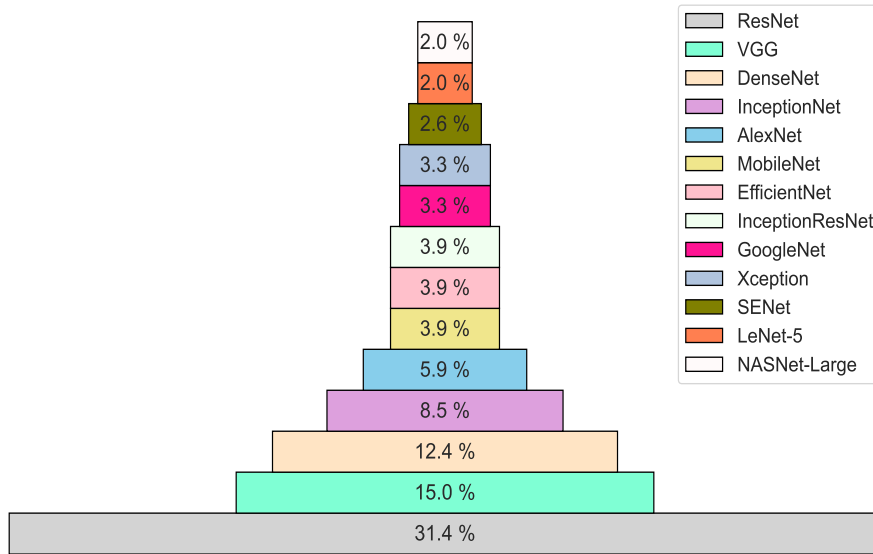


Figure 11: A pyramid chart of the percentage of SLC articles employing different DL models on automated lesion feature learning through convolution in the last decade from 2011 to 2020.

than Inception-V4 in 8.5 % SLC articles. Similar patterns are also visible in all other networks; that is, the smaller network of each type of architecture is most commonly used, for example, EfficientNetB0 than other EfficientNets, DenseNet121 than other DenseNets, and MobileNet-V2 than MobileNets. This scenario can be explained insightfully using Fig. 12. This figure illustrates different CNN architectures with their corresponding number of learning parameters. The more the parameter numbers, the more the necessary samples in the training set, as DLs are extensively hungry for big data. The prior discussions for Fig. 11 have coincided with Fig. 12, as the smaller networks, meaning models with fewer parameters, have been admirably employed for the SLC task in the last decade from 2011 to 2020. This is because they require fewer training samples, and getting more samples is challenging in the medical imaging domain [3, 5, 13, 300], especially SLA datasets. It is also pointed out that some authors from [59, 249, 250, 253, 259, 262, 277, 278, 284, 300] have selected the smallest networks from Fig. 12 and combined them for ensemble designing that performed very well even with fewer training samples.

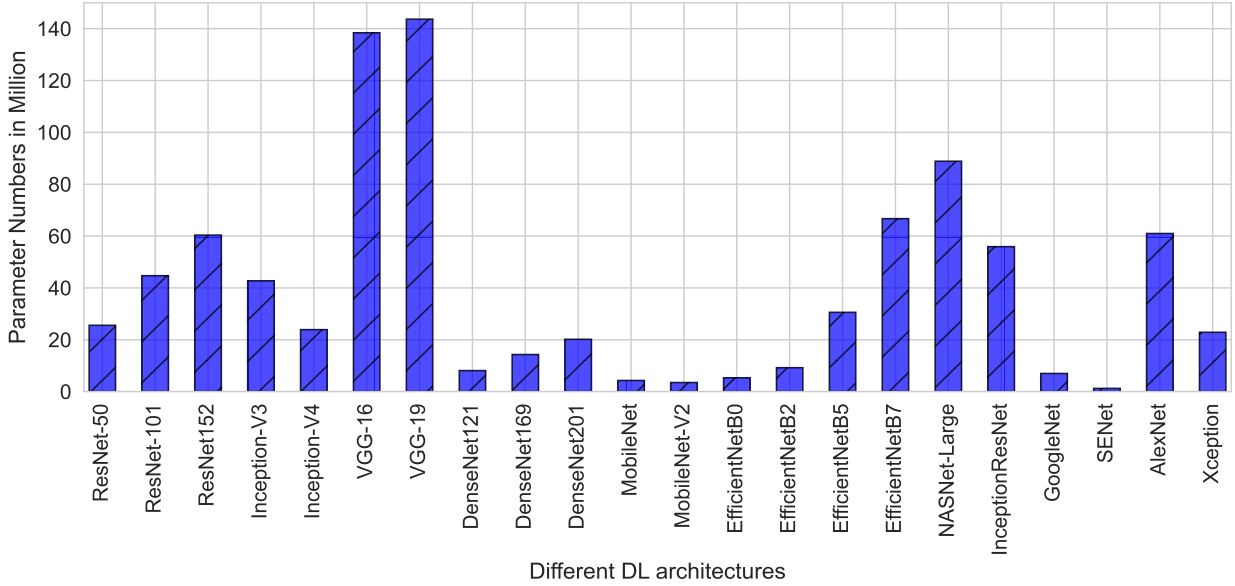


Figure 12: The bar plot of diverse CNN architectures with their complementary number of learning parameters employed for the SLC task in the last decade from 2011 to 2020.

7. Training and Evaluation

This section surveys and explores the training protocol and trained model’s evaluation engaged for the SLA tasks in the last decade from 2011 to 2020. We investigate the hyperparameter settings and training environments from many separate articles in sections 7.1 and 7.2, respectively. Lastly, section 7.3 analyzes the evaluation strategies for the aimed task and year range. It is noteworthy that the articles that have explicitly specified those issues are considered to furnish the information in this section.

7.1. Hyperparameter Settings

Hyperparameters cannot be directly learned from the regular training process in learning algorithms. The CNN models’ performance depends critically on identifying a good set of hyperparameters that must be tuned for a robust CNN model [377]. The one-by-one scrutinization of the selected 365 SLA articles (221 for segmentation and 144 for classification) yields several explicitly mentioned hyperparameters in the aimed SLA task, which are explained with a survey analysis in the following paragraphs.

Batch size is the number of images utilized to train a single forward and backward pass and one of the essential hyperparameters. A larger or smaller batch size does not usually guarantee a better outcome, as there is a tradeoff between achieved results and computational resource availability [387]. Kandel and Castelli [387] experimented on different batch sizes with fixed data and CNN architecture and revealed that it significantly impacted the network’s performance. However, the one-by-one scrutinization of the selected 365 articles exposes that the utilized batch sizes are 100 [253], 96 [312], 64 [114, 248], 36 [50], 32 [26, 238, 257, 286, 290, 302], 26 [388], 24 [242], 20 [89, 141, 146, 148, 270, 309, 323], 18 [47], 16 [32, 36, 46, 54, 65, 111, 121, 157, 159, 170], 12 [66, 279], 10 [150, 233], 8 [42, 57, 79, 103, 123, 164, 166, 169, 389], 6 [186], 4 [34, 67], 2 [84], and 1 [53, 86, 108]. Fig. 13 indicates that the most commonly employed (78.0%) batch sizes lie between 8 to

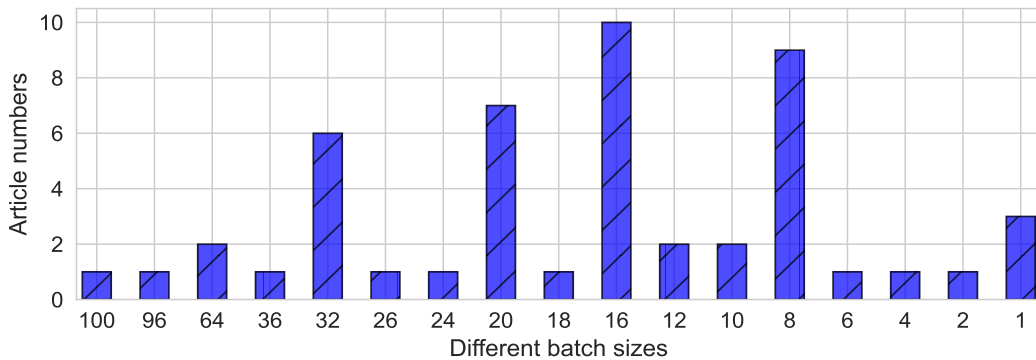


Figure 13: The number of articles that utilized various batch sizes in the last decade for the SLA.

32, where the batch sizes of 8, 16, 20, and 32 are applied in the 18.0%, 20.0%, 14.0%, and 12.0% articles, respectively. It is also observed that the higher batch sizes like 100, 96, and 64 are used in merely 4.0% of the articles, as they are associated with high computational resources. On the other hand, fewer batch sizes are very time-consuming for the converging during training of the models. Therefore, the batch sizes of 1, 2, 4, and 6 are applied in 12.0% of the articles. Fig. 13 and those discussions help future researchers to determine the proper batch size for the SLA or other similar task(s) from the past utilization regularities.

Learning Rate (LR) (η) is a hyperparameter that controls how much the network’s weights (W) are adjusted ($W_{new} = W_{old} - \eta \times \nabla$) concerning the loss gradient (∇). Too

small of an LR functions a slowly converging training, while too large of an LR creates the training model diverge [5]. However, the one-after-another review of the chosen 365 SLA articles exposes that the last decade’s employed LR are 0.1 [13, 51, 122], 0.01 [64, 66, 68, 96, 150, 259, 306, 320, 321, 381], 0.001 [26, 34, 41, 42, 46, 47, 56, 78, 131, 149, 153, 156, 169, 175, 184, 186, 238, 245, 248, 251, 254, 257, 260, 302, 304, 307, 309, 310, 323, 389], 0.0001 [31, 32, 36, 44, 53, 58, 65, 67, 83, 89, 90, 102, 103, 111, 115, 116, 123, 127, 151, 161, 164, 166, 179, 188, 191, 233, 242, 249, 253, 270, 275, 279, 284–286, 289–291, 312, 317], 0.00001 [94, 141, 146, 148, 157, 159, 295], 0.000001 [140, 388], 0.0000000001 [180], 0.0002 [50, 54, 84, 105, 108, 113, 117, 189], 0.003 [39], 0.00003 [60], 0.005 [57, 236], 0.0005 [265], 0.00005 [121], 0.007 [61, 120]. Fig. 14 displays that the LR between $1e-2$ and $1e-5$ were massively applied in the last decade from 2011 to 2020 for the aimed SLA task, approximately 79.6 % of the total candidate articles. More specifically, the last decade’s LR of $1e-3$ (27.8 %)

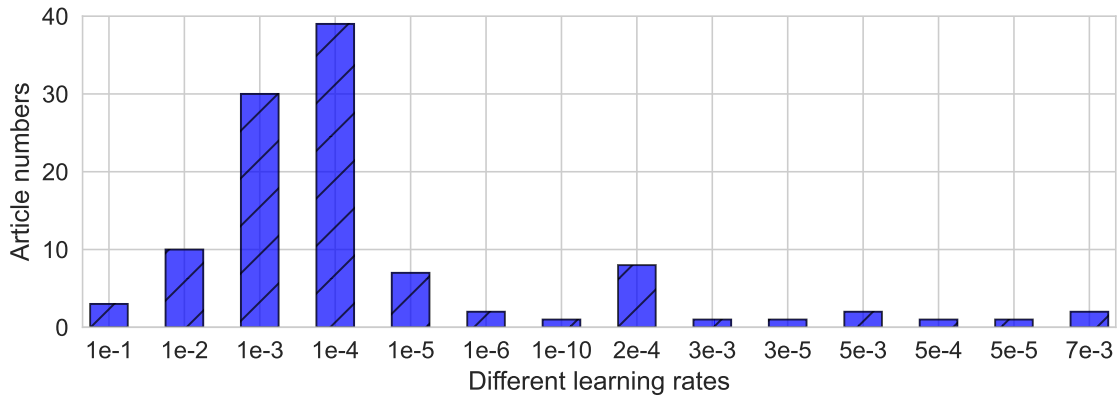


Figure 14: The number of articles that employed various LR in the last decade for the SLA task.

and $1e-4$ (36.1 %) are the best choices for developing the supervised SLA model. Again, it is also noteworthy from the bar plot in Fig. 14 that the LR of scales $e-2$ to $e-5$ are employed in 94.4 % of the total articles while the remaining 5.6 % applied to other scales of LR like $e-1$, $e-6$, and $e-10$. These discussions reveal that too small and too large LR were not employed in the last decade for the SLA; instead, the authors picked an LR value between them that will also be forthcoming guidance for the beginner to expert level of researchers.

Loss function, also known as cost function or error function, is an objective function or

criterion for minimizing during the supervised DL model’s training. The scrutinization of the selected articles reveals that the most commonly employed loss function is cross-entropy for both the SLS and SLC tasks that are employed in [30, 42, 45, 51, 56, 58, 60, 63, 89–91, 94, 98, 102, 111, 115, 127, 140, 148, 150, 154, 157, 161, 164, 165, 168, 175, 184, 189, 236, 238, 253–255, 262, 263, 265, 283, 295, 298, 308, 317, 318]. Other loss functions in the last decade are Softmax [122, 180, 186, 323, 328], Square error [60, 324], Logistic loss function [242]. Although binary or categorical cross-entropy functions are widely employed as loss functions in SLS, they may lead to bias effects as the size of a lesion is drastically smaller than the size of the background [362]. Therefore, some authors employed Dice Similarity Coefficient (DSC) (as in Eq. 3) or Jaccard Index (JI) (as in Eq. 4), which are applied in [2, 33, 40, 48, 50, 60, 64, 83–85, 99, 107, 109, 113, 121, 123, 138, 141, 142, 149, 151, 154, 169, 176, 191, 299].

$$L_{DSC}(y, \hat{y}) = -1 + \frac{2 \times \sum_{i=1}^N y_i \times \hat{y}_i}{\sum_{i=1}^N y_i + \sum_{i=1}^N \hat{y}_i} \quad (3)$$

$$L_{JI}(y, \hat{y}) = -1 + \frac{\sum_{i=1}^N y_i \times \hat{y}_i}{\sum_{i=1}^N y_i + \sum_{i=1}^N \hat{y}_i - \sum_{i=1}^N y_i \times \hat{y}_i} \quad (4)$$

where, y , \hat{y} and N are the true label, predicted label and the total number of pixels respectively. $\log \hat{y}_i$ and $\log(1 - \hat{y}_i)$ are the measure of log-likelihood of pixel being lesion or not respectively. The product of y and \hat{y} in those two equations is the measure of similarity (intersection) between true and predicted mask. Again, some authors in [13, 32, 34, 39, 54, 58–60, 65, 66, 79, 103, 107, 116, 117, 153, 170] have been combined BCC and Eq. 3 or Eq. 4 for further enhancing the lesion segmentation results, as mentioned in Eq. 5.

$$L_{SLS}(y, \hat{y}) = 1 - \frac{\sum_{i=1}^N y_i \times \hat{y}_i}{\sum_{i=1}^N y_i + \sum_{i=1}^N \hat{y}_i - \sum_{i=1}^N y_i \times \hat{y}_i} - \frac{1}{N} \sum_{i=1}^N [y_i \log \hat{y}_i + (1 - y_i) \log(1 - \hat{y}_i)] \quad (5)$$

In summary, observing those loss functions demonstrates that the BCC is widely applied for the SLC and SLS tasks, whereas Eq. 3 or Eq. 4 or Eq. 5 are commonly applied for the SLS job in the last decade from 2011 to 2020, which, in turn, will be an upcoming recommendation for the beginner to expert level of experimenters.

Optimizer discovers the value of the model’s parameters (weights), minimizing the error (cost function as described in the previous paragraph) and maximizing the predefined metric (see Table 13) when mapping inputs to outputs. It widely affects the CNN models’ accuracy and training speed [5]. In the last decade (2011-2020), the most commonly applied optimizers (with their corresponding articles) for the SLA models are Adam, also known as an adaptive optimizer, [32, 34, 36, 39, 41, 42, 45, 50, 54, 56, 58, 58, 60, 61, 67, 68, 83, 84, 90, 94, 98, 102, 103, 111, 113, 115–117, 121, 123, 127, 146, 149, 151, 153, 154, 159, 161, 166, 169, 170, 175, 184, 189, 191, 242, 245, 249, 255, 260, 263, 278, 279, 284, 286, 289, 291, 312, 320], Stochastic Gradient Descent (SGD) [26, 31, 41, 47, 51, 57, 66, 86, 89, 98, 101, 105, 120, 131, 140, 141, 148, 150, 152, 154, 156, 157, 164, 170, 179–181, 186, 188, 233, 238, 257, 275, 278, 302, 304, 306, 309, 313, 323, 388, 390], Adadelta [13], and Nadam [79]. Indeed, 98.1 % of the articles applied Adam (57.3 %) and SGD (40.8 %) optimizers. However, it has also appeared from the aimed review that the authors had fine-tuned those optimizers’ control parameters like the momentum in SGD, decay rate in Adadelta, and the exponential decay rate for the first and second moments (β_1 and β_2) in Adam and Nadam. The variations of these parameters in the selected 365 articles are scanned to provide survey information and noted in Table 10. The momentum accelerates gradient descent in the appropriate direction and dampens oscillations while the decay rate continuously changes the LR values to construct an adaptive optimizer. On the other hand, β_1 and β_2 are the initial decay rates utilized when estimating the first and second moments of the gradient, which are multiplied by themselves (exponentially) at the end of each training step (batch). However, it is noteworthy from the table that the most commonly applied momentum, decay rate, β_1 , and β_2 in the last decade (2011 to 2020) for the SLA are 0.90, 0.0001, 0.50 (or 0.90), and 0.999, respectively. Expectedly, these discussions and Table 10 will be an appropriate recommendation for beginner to expert level experimenters to determine an optimizer with

Table 10: The variations of different parameters in optimizer(s) like momentum, decay rates, β_1 , and β_2 in the selected 365 articles.

Parameters	Values	Corresponding articles
Momentum	0.25	[321]
	0.90	[31, 47, 51, 53, 57, 61, 66, 89, 101, 114, 115, 120, 140, 141, 148, 150, 156, 170, 179–181, 186, 233, 238, 257, 265, 304, 306, 313, 317, 323, 381, 388]
	0.95	[28]
	0.99	[41, 86, 152]
Decay rates	0.001	[114, 141, 286]
	0.0001	[28, 66, 101, 148, 181, 186, 233, 275, 290, 309, 323],
	0.00001	[28, 260]
	0.000001	[53]
	0.00158	[79]
	0.5	[117]
	0.005	[42, 156, 306]
	0.0005	[41, 47, 86, 152, 179]
0.00005	[265]	
β_1	0.50	[45, 50, 84, 115, 117]
	0.60	[289]
	0.90	[41, 115, 146, 278, 312]
β_2	0.990	[115, 278, 312]
	0.995	[289]
	0.999	[41, 45, 50, 84, 117, 146]

suitable parameters.

Epoch implies one pass over the entire dataset. The initial weights will be subjected to transformations during the next cycle of the same training dataset. The epoch optimization mainly consists of two significant problems: underfitting and overfitting. A few epochs lead to the underfitting of the data during the network’s training, which indicates that the network cannot capture the underlying tendency of the data. Again, increasing the epoch numbers will find an optimal solution for maximum accuracy. Regardless, beyond this stage, a further increase in the epoch numbers will lead to the overfitting of the data, which means the network does not reflect the reality of the data because it captures the noise in the data. Unfortunately, there is no absolute answer to choosing the best epoch. However, this article scrutinizes the appointed 365 SLA articles to find the last decade’s utilized epoch numbers to discover the general crazes. In the last decade (2011-2020), the most commonly involved

epochs (with their corresponding articles) for the SLA models are 500 [44, 58, 60, 302], 300 [46, 146, 148, 181], 360 [96], 200 [50, 51, 99, 108, 121, 159, 236], 250 [54, 188], 192 [312], 165 [79], 150 [32, 105], 100 [26, 34, 39, 47, 56, 170, 233, 238, 242, 245, 263, 265, 282, 304], 90 [94], 80 [64, 103, 157], 60 [290, 388], 50 [116, 248, 251], 40 [279], 24 [285], 35 [57], 15 [127], 13 [65], 3 [111]. Those epoch values and their appliance frequencies demonstrate that the fewer epochs (< 50) are applied in solely one article, whereas the high number of epochs (> 200) are also employed in fewer articles for the SLA in the last decade. Additionally, a close inspection reveals that epochs of 100 and 200 are most generally employed in the last decade to train the SLA models, respectively, in 27.45% and 13.73% of 51 articles that specifically documented the epoch numbers; in succession to these back-and-forth, the researchers will find a new pathway to decide the epoch number in their experimentations.

7.2. Training Environments

In order to train different ML and DL algorithms and architectures, there are numerous frameworks and libraries to provide a convenient training protocol. These frameworks assemble complex mathematical functions, training algorithms, and statistical modeling available without programming from scratch. Some equip distributed and parallel processing abilities and fortunate development and deployment attributes. However, Table 11 displays the commonly devoted DL and/or ML frameworks in the selected 365 SLA articles that have been applied in the last decade from 2011 to 2020. The articles that have explicitly prescribed training protocol(s) are assessed to deliver the facts in this section. It is noticeable from Table 11 that Keras, TensorFlow, and Pytorch with Python and/or MATLAB programming languages (massively Python) have been most popularly devoted in the last decade to training automated SLA models. However, the adaptation of those DL frameworks depends on many factors, for example, the level of API, computational speed, architecture, and debugging facilities, which are briefly characterized in the following paragraph.

Keras is a high-level API with comparatively slower performance, capable of running on top of TensorFlow, CNTK, and Theano. TensorFlow, with relatively faster interpretation, is a framework that provides both high-and low-level APIs. Pytorch, on the other hand, is

Table 11: Widespread ML and/or DL frameworks and libraries applied for SLA tasks in the last decade (2011 to 2020).

Framework (Year)	Institution	Corresponding articles
Caffe (2015)	UC, Berkeley	[41, 86, 179, 180, 191]
Keras (2015)	Individual author	[13, 32, 58, 60, 63, 65, 79, 83, 98, 111, 118, 126, 131, 138, 140, 142, 150, 153, 159, 166, 188, 388]
TensorFlow (2015)	Google brain	[63, 65, 79, 83, 90, 99, 103, 105, 111, 138, 156, 158, 161, 164, 166, 167, 175, 184, 188]
Theano (2008)	University of Montreal	[154]
Pytorch (2016)	Facebook	[31, 39, 42, 44, 45, 50, 51, 54, 84, 96, 99–102, 105, 113, 116, 117, 121, 152, 169, 170]

a lower-level and faster API focused on direct work with array expressions. Additionally, Keras is usually employed for small datasets as it is remarkably slower. In opposition, TensorFlow and PyTorch are utilized for high-performance models and large datasets that demand fast execution. Again, Keras has a straightforward architecture, turning it more readable and concise. Tensorflow, on the contrary, is not very easy to operate even though it furnishes Keras as a framework that constructs assignments more comfortably. In contrast, PyTorch has a complicated architecture, and the readability is smallish, corresponding to Keras. Lastly, in Keras, there is usually a less frequent necessity to debug simple networks. Nevertheless, in the case of TensorFlow, it is pretty challenging to accomplish debugging. Pytorch, contrastingly, has better debugging credentials than the other two. In conclusion, these contractive conversations will open opportunities for the research community to pick a DL framework according to users' preferences.

7.3. Model Evaluation

Once the SLS and SLC are accomplished, the next step is the assessment of those two methods. The successes of SLS and SLC are typically reported in a confusion matrix that includes the statistics about actual and predicted pixels or classes, as described in Table 12. Each column indicates anticipated events in such a matrix, while each row represents actual samples. The correct forecasts, such as TP and TN, respectively designate that the target with a positive condition has favorably been recognized, while the objective with a negative

Table 12: Description of TP, TN, FN, and FP in a confusion matrix for evaluating segmentation and classification methods.

		Predicted conditions	
		Predicted positive condition (PP)	Predicted negative condition (PN)
Total population = P + N			
Actual conditions	Actual positive condition (P)	True Positive (TP) (Correct detection)	False Negative (FN) (Type-II error)
	Actual negative condition (N)	False Positive (FP) (Type-I error)	True Negative (TN) (Correct rejection)

condition has successfully been rejected. An FN or false-negative error is a test result that incorrectly shows that a positive condition does not hold, revealing the underestimation by the methods. In contrast, an FP or false-positive error is a judgment that exhibits the overestimation of positive samples. However, the most commonly employed metrics for the SLS and SLC evaluations in the last decade from 365 selected articles are Accuracy (ACC), Sensitivity (SEN), Precision (PRE), Specificity (SPE), Figure of Merit (FOM), Segmentation Error (SE), False Positive Rate (FPR), F1-score (F1S), Negative Predictive Value (NPV), DSC, Hausdorff Distance (HD), Area Under Curve (AUC), JI, False Negative Rate (FNR), XOR [367], Correlation Coefficient (CC), Hammoude Distance (HMD), Matthew Correlation Coefficient (MCC), Peak to Signal Ratio (PSNR), Structural Similarity Indices (SSIM), and Balanced Accuracy (BACC). These metrics are summarized in Table 13 communicating their employed articles from the last decade.

Table 13: A list of SLS and SLC evaluation metrics with their corresponding articles applied in the last decade (2011 to 2020), examining a total of 365 articles (221 for segmentation and 144 for classification).

Metrics	SLS articles	SLC articles
ACC	[7, 27, 29–33, 36–38, 40–48, 50–55, 57–64, 66, 68, 70, 72, 74–76, 79, 81–85, 87–89, 91, 94, 95, 97–101, 103, 105, 106, 111, 113–115, 117–120, 126–128, 131, 132, 134, 135, 138, 140–157, 159, 160, 162, 163, 168, 173–176, 178, 179, 181, 183, 184, 186, 188, 191, 192, 195, 202–204, 206, 208, 209, 211, 214, 215, 217, 221, 223, 296, 339, 382, 388, 389, 391–397]	[1, 46, 58, 63, 80–82, 87, 88, 97, 115, 128, 134, 145, 157, 173, 178, 233–241, 243, 244, 246, 247, 249–253, 256, 258, 259, 261, 264–267, 269–273, 276, 278, 282, 287, 289–291, 293, 295–299, 301, 304, 306, 310, 311, 313, 314, 316–318, 320–322, 326–331, 333–337, 339, 341, 344, 371, 380, 381, 390, 398]

Table 13 Continued from previous page

Metrics	SLS articles	SLC articles
SEN	[2, 7, 13, 27–29, 31, 32, 34, 37, 42–46, 48, 50, 51, 54, 55, 57, 58, 60–62, 64, 65, 72, 74–76, 81–84, 86–89, 91, 94, 97–99, 103, 105–107, 111, 114, 115, 117–121, 128, 131, 134, 135, 138, 140, 142–147, 149–156, 159, 160, 162, 168, 171–176, 178, 179, 183, 184, 186, 188, 191, 195, 198, 200, 202, 203, 206, 208, 209, 214, 215, 217, 221–225, 225, 227, 229–231, 296, 339, 382, 382, 388, 389, 391–397, 399]	[1, 46, 58, 81, 87, 88, 97, 115, 128, 134, 145, 148, 173, 178, 233, 235, 237, 239–241, 243, 247, 250, 251, 253–259, 261, 263–271, 273, 276, 282, 283, 285, 289–291, 296–299, 301, 314–316, 322, 324–327, 329, 334, 336, 337, 339, 341, 344, 371, 381, 398]
PRE	[28, 46, 62, 64, 76, 81, 82, 86–88, 131, 140, 143–145, 171, 172, 196, 198, 209, 221, 225, 382]	[46, 81, 87, 88, 128, 145, 148, 235, 240, 247, 250, 251, 253–256, 258, 259, 265, 268, 270, 272, 273, 276, 285, 290, 291, 295, 298, 309, 311, 316, 317, 322, 323, 326, 327, 336, 344, 381]
SPE	[7, 13, 29, 31, 32, 34, 37, 42, 43, 45, 48, 50, 51, 54, 55, 57, 58, 60–62, 65, 72, 74–76, 81, 83, 84, 86, 88, 89, 91, 94, 97–99, 103, 105–107, 111, 114, 115, 117–121, 128, 134, 135, 138, 142, 144–147, 149–156, 159, 160, 162, 168, 173–175, 178, 179, 183, 184, 186, 188, 191, 192, 195, 198, 202, 203, 206, 208, 209, 214, 215, 217, 221–225, 227, 229, 231, 296, 339, 382, 388, 389, 391–394, 396, 397]	[1, 58, 81, 88, 97, 115, 128, 134, 145, 173, 178, 233, 237, 239, 241, 243, 250, 251, 253, 256–258, 261, 263–271, 273, 276, 282, 283, 289, 290, 296–299, 301, 314, 315, 322, 324–327, 329, 334, 336, 337, 339, 341, 371, 381, 398]
FOM	[231]	
SE	[2, 68, 102, 191, 192, 200, 219, 230, 382, 399]	
FPR	[2, 76, 82, 88, 144, 145, 200, 206, 230, 399, 400]	[88, 145, 239, 240, 273, 336]
F1S	[46, 55, 63, 76, 86, 87, 102, 160, 162, 173, 203, 225, 395]	[46, 63, 87, 148, 173, 235, 246, 247, 250, 254–256, 261, 269, 283, 285, 291, 297, 299, 314, 327, 336, 381]
NPV	[76, 144, 209, 221]	[128, 268, 290]
DSC	[27, 29–37, 40, 42–45, 48–54, 56–58, 60–62, 64–66, 70–72, 74, 75, 83–85, 89–92, 94, 96–101, 103, 105–109, 111–114, 116–123, 129, 131, 132, 136, 138, 139, 141–143, 146–149, 151–157, 159, 163, 168, 171, 172, 178–183, 186, 188, 189, 191, 194, 219, 389, 393]	[1, 97, 116, 178, 330]
HD	[2, 206]	
AUC	[13, 59, 81, 88, 140, 196, 388]	[58, 59, 81, 88, 233, 236, 238, 239, 241–243, 246, 248, 250, 253, 256, 262, 263, 265, 270, 272, 273, 276–278, 280–282, 295, 297–299, 302, 311, 317, 319, 320, 327]
JI	[2, 13, 30–34, 36–38, 40, 42–45, 47–54, 54–58, 60–62, 64–66, 70–72, 74, 75, 79, 83–85, 89–94, 96–101, 103, 105–109, 111–114, 116–123, 125, 132, 138, 141, 142, 146, 147, 149–153, 155–158, 161, 163–165, 165, 167–169, 177, 178, 180, 182, 194, 196, 197, 219, 389, 393, 401]	[1, 82, 97, 116, 157, 178, 330]
FNR	[76, 81, 82, 144, 145, 176, 200]	[81, 82, 145, 239, 240]
XOR	[86, 129, 133, 139, 172, 198, 199, 214, 227, 228, 231]	
CC	[71, 193, 194]	

Table 13 Continued from previous page

Metrics	SLS articles	SLC articles
HMD	[129, 139, 172]	
MCC	[51, 62, 76]	[256, 269]
PSNR	[71]	
SSIM	[71]	
BACC	[202]	[250, 251, 256, 305, 308, 336, 381]

Sometimes, qualitative evaluations are also reported in many articles in addition to the quantitative SLS evaluation [3, 5, 7, 13, 26, 32, 35, 36, 42, 43, 45, 51, 59, 61, 62, 65, 71, 74, 78, 83–85, 90, 94, 110, 135, 137, 143, 152, 156, 160, 164, 165, 175, 180, 182, 186, 188, 191, 195, 200, 203, 213, 224, 227, 396, 402]. Overlaying the segmented masks onto the ground truth masks is performed as qualitative evaluations. The intersected region(s) indicates true positive, and the remaining two regions are false-positive and false-negative. However, in some cases, the multi-class evaluation metrics are required for the SLS and SLC tasks, which are the expansions of the binary metrics in Table 13. These metrics are averaged to achieve a multi-class metric across all the classes in many possible ways, such as micro, macro, etc. The former averaging method (micro) believes class imbalance, calculating the metrics globally by counting the number of times each class was correctly and incorrectly predicted. In contrast, the latter approach (macro) does not assume imbalance, measuring each class’s metrics independently and attaining their unweighted mean. Sometimes, scholars employ k-fold cross-validation to verify the robustness of the trained model. In such a case, the obtained metrics from each fold are expressed as an average value with a standard deviation [357], which can be expressed as Eq. 6. If the standard deviation has a higher value, it symbolizes higher inter-fold variation, consequently poor robustness and vice-versa.

$$M = \frac{1}{K} \times \sum_{i=1}^K M_i \pm \sqrt{\frac{\sum_{i=1}^K (M_i - \mu)^2}{K}}, \quad (6)$$

where $M_i \in \mathbb{R}$, $i \forall K$, denotes an estimated metric with a mean value of μ and K is the fold numbers. Additionally, the authors in [39, 230, 256] exploit the statistical validation test, i.e., Analysis of Variance (ANOVA), to evaluate the SLS and SLC techniques for revealing the significance of the experimentations with a suitable p -value. Moreover, Total

Computation Time (TCT) is occasionally employed to judge the SLS and SLC methods for determining the time the algorithms need. The smaller the required time, the better the SLS and SLC methods for the real-time application in the CAD systems. However, among the reviewed articles, a few papers considered the TCT for the evaluation strategy-which are: SLS [79, 88, 101, 141, 144, 145, 193, 194, 203, 226] and SLC [81, 88, 145, 239, 240].

Fig. 15 summarizes the employment frequencies of all the applied metrics from the selected 365 SLA articles in the last decade. A close inspection and observation of the lit-

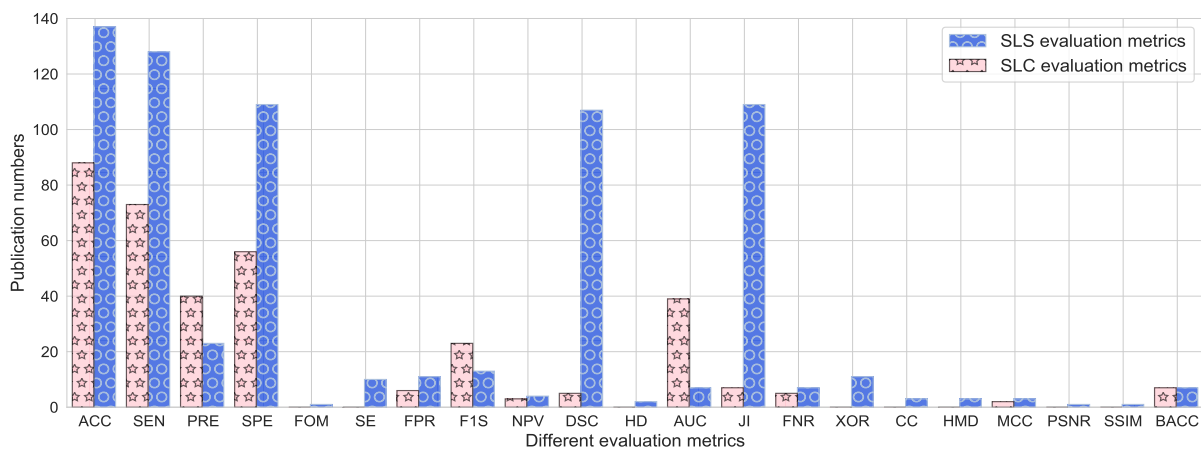


Figure 15: The number of articles employing different evaluation metrics, conferring the commonly applied metrics.

erature expose that accuracy, sensitivity, specificity, dice similarity coefficient, and Jaccard index are the most-5 frequently used metrics for the SLS evaluation respectively employed in 61.99%, 57.92%, 49.32%, 48.42%, and 49.32% articles. Therefore, they can be treated as the *first-tier* SLS evaluation metrics. In contrast, accuracy, sensitivity, precision, specificity, and AUC are the most-5 regularly applied metrics for the SLC evaluation respectively practiced in 61.11%, 50.69%, 27.78%, 38.89%, and 27.08% articles, leading to the *first-tier* SLC evaluation metrics. The other metrics, rather than the top-5 in both SLS and SLC tasks, are negligibly employed in the last decade’s literature. Therefore, we have omitted to assign them to a *second-tier*; instead, we have considered them as the *third-tier* metrics (less significant). Again, although dice similarity coefficient and Jaccard index are massively practiced in SLS evaluation, they are negligibly employed for SLC evaluation. Some metrics

like accuracy, sensitivity, specificity, precision, F1-score, balance accuracy, false-positive, and false-negative rates are almost similarly employed for the SLS and SLC evaluation. Moreover, although many articles practice accuracy as SLS and SLC metrics, they do not consider the class imbalance measurement. If there are considerable samples in one particular class, the trained models tend to learn that class more correctly, increasing the false-positive or false-negative rates. The conventional metrics dispense very high values if there is no penalization of class imbalance, which is accounted for in some metrics, for instance, ROC and AUC estimation [3, 5, 13, 361]. Nevertheless, barely 3.17% for SLS and 27.08% for SLC articles acknowledge this issue by determining the AUC values for their assessment. Expectedly, these conversations and Fig. 15 will, in turn, be forthcoming advice for the beginner to expert level researchers to determine the appropriate evaluation metrics for the SLA task(s).

8. Observations and Recommendations

This section thoroughly reveals our important observations from point-to-point scrutinization of the chosen 365 articles (221 for segmentation and 144 for classification). Consequently, we have suggested several recommendations for the SLA tasks, including input data (datasets utilization, preprocessing, augmentation, and solving imbalance problems), approach configuration (techniques, architectures, module frameworks, and loss function), training protocol (hyperparameter settings), and evaluation criteria (metrics). This will act as future guidance for beginner-to-expert-level scholars to build their own decision-making SLA framework from the given datasets. The notable observations and recommendations are as follows:

- Currently, ISIC datasets have been most commonly applied to the SLS and SLC tasks, especially after 2016, which can be deemed the symbolic dataset in this problem domain (see Fig. 3). However, it is undeniable that there is a necessity for larger, more diverse, and more representative skin lesion datasets (with more inter-class diversity) to train data-hungry DL models to drive them more accurate and robust. The most popular

ISIC Archive contains over 69,900 publicly available skin lesion images, but many cases lack manual segmentations as the proper ground truth. Experts in the same field could improve these initial annotations by using crowdsourcing techniques to collect annotations from people who are not experts and then running their ensemble based on the annotations that come up most often.

- From the review analysis of this article, it can be revealed that there is no solid specific clarification to the question: is preprocessing essential, or which preprocessing approach is the best for the skin lesion images in the SLA task? To disclose the first answer, two considerations have been discovered in the last decade’s SLA articles: if handcrafted features engineering with ML models or other computer vision-based models is employed, preprocessing is strongly suggested, and/or if DL-based automated models are applied, preprocessing is poorly advised. Although the selection of the preprocessing method depends on the algorithm types, they can be initially appointed from the last decade’s history of the utilization frequencies (see details in section 4.1, especially in Fig. 4).
- The appliances of the augmentations are highly recommended only for the data-craving DL-based computerized SLA techniques, as they were negligibly involved in the other SLA techniques in the literature from 2011 to 2020 (see Fig 5). The typical baseline augmentation strategies can also be discovered from the discussions in section 4.2, leading to the construction of an information desk on SLA’s augmentation(s) preference. Although augmentations are involved in the minority class to increase its sample numbers and class weighting that rewards extra consideration to the class with minority samples is most commonly suggested in the last decade’s SLA articles (see details in section 4.2).
- The insight overlooked in the last decade’s SLS articles reveals that DL-based procedures, especially CNN models to learn lesion’s spatial information, are the recent manias, especially after 2016 (see Fig. 1, Fig. 7, and Fig. 8). Therefore, CNN-based

encoder-decoder networks are the most prioritized procedures for the SLS task. Again, the investigation of the encoder structure reveals that ResNet, VGG, and DenseNet family networks are the top-most applied encoder architectures in the last decade and are the standard crazes for the SLSs. In contrast, U-Net-like structures are the trends in the decoder mechanism in the CNN-based SLS job. Additionally, segmented lesion masks are generally improved by employing several post-processing techniques (see Table 7), where the various morphological operations are the trendy operations in the last decade from 2011 to 2020 (see back-and-forth in section 5.6, particularly in Table 7).

- Although this survey article discloses the most commonly employed lesion’s attributes (see Fig. 9) and ML-based classifiers (see Fig. 10) for the handcrafted SLC strategies, the DL-based automated approaches are the last few years’ tendencies (see Fig. 11). Further scrutinization also reveals the most frequent CNN architectures like ResNet, VGG, DenseNet, InceptionNet, and AlexNet for lesion’s attribute learning, which are extensively discussed in section 6.2. Using lightweight pre-trained architectures that are appropriate for the smaller training set is also observed and recommended as they have been massively applied in the last decade from 2011 to 2020 with fewer training examples. According to previous research, it is advantageous to engage in ensemble learning and/or combine handcrafted and automated CNN’s lesion features to capture the discernment lesion characteristics, thereby improving the SLC outcome(s).
- The previous 365 SLA literature also enabled the beginners and expert-level researchers to determine the best experimental settings that are most typically operated for both SLS and SLC tasks. Although it is tough to decide the values of the proper hyperparameters, recent trends support the initial estimation. For illustration, the synopsis in Fig. 13 and Fig. 14 aid in understanding the last decade’s history of batch size and LR employment, respectively, revealing that their shallow and/or very high values are rarely exploited. Cross-entropy (binary or multi-class) is the most suggested loss function for the SLS and SLC tasks. However, many authors have enforced extra care

in the SLS's loss function, considering DSC (or JI) function as in Eq. 3 and Eq. 4 (see details reflection in Eq. 5). Again, optimizers and epoch numbers are also very crucial components in the training process, which are also recommended by this survey article. For example, adaptive and SGD optimizers have been massively engaged in the earlier decade, as well as mid-range epoch numbers, for instance, near about 100 & 200, are highly suggested. Various numerical values of the optimizers' parameters are organized in Table 10 to supply an idea to the forthcoming researcher. Moreover, Keras, TensorFlow, and Pytorch are highly advised for ML and/or DL frameworks (explained in the second paragraph of section 7.2) with python programming language for future SLA strategies development, as they are the standard trends in the SLA implementation in the last decade from 2011 to 2020 (see Table 11).

- There is no universally appropriate evaluation criterion [367], as different evaluation benchmarks grasp different characteristics of an SLS and/or SLC algorithm's performance on a provided dataset. The presented Fig. 15 will lead to deciding the most commonly applied metrics that have been employed in the last decade from 2011 to 2020. Direct quantitative assessment system using the metrics (see Table 13), qualitative evaluation, and reflection of TCT are the three most standard approaches to estimating the SLA method(s). In order to thoroughly explain the performance of the SLA technique(s) insightfully, all three of these evaluation techniques should be involved. Unfortunately, it has infrequently been applied in related assessment studies in the last decade, especially the TCT (SLS: [79, 88, 101, 141, 144, 145, 193, 194, 203, 226] and SLC: [81, 88, 145, 239, 240]). This is one of the shortcomings of the current practice in the SLA articles, and the researchers should consider them together in future experimentation.
- Although an enormous number of SLA articles have been published in the past, none of the articles have considered developing user-friendly clinical applications in practical settings, and only a few studies have developed toy applications. The researchers should concentrate on real-time application products in conjunction with SLA tech-

nique improvement.

9. Conclusion

The survey recapitulates the last decade’s (2011–2020) 365 SLA articles, primarily focusing on dataset utilization, preprocessing, augmentations, solving imbalance problems, SLS & SLC techniques, training tactics (frameworks and hyperparameters settings), and evaluation benchmarks (metrics). The SLA’s survey analysis exposes the ISIC as this domain’s representative dataset(s). Preprocessing is strongly suggested for handcrafted feature engineering with ML models, whereas it is poorly recommended for DL-based automated models. Additionally, DL-based computerized SLA techniques are the standard crazes in the skin lesion domain as they perform better than the other SLA methods and require minimal parameter tuning while being end-to-end. This survey also suggested that qualitative and quantitative evaluations with SLA’s TCT should be applied to assess the method(s) insightfully from diverse aspects. Furthermore, prospective researchers should consolidate real-time application products with SLA’s technique improvement(s). Expectedly, the outcomes of this article will be helpful to the related research community for recovering those challenges, selecting a suitable SLA method, and its evaluation metric. The recommendations may also be an excellent starting point for future researchers to develop an effective SLA decision-making system for real-life applications in clinical settings.

Acknowledgement

Guang Yang was supported in part by the BHF (TG/18/5/34111, PG/16/78/32402), the ERC IMI (101005122), the H2020 (952172), the MRC (MC/PC/21013), the Royal Society (IEC/NS-FC/211235), the NVIDIA Academic Hardware Grant Program, the SABER project supported by Boehringer Ingelheim Ltd, NIHR Imperial Biomedical Research Centre (RDA01), and the UKRI Future Leaders Fellowship (MR/V023799/1).

References

- [1] S. Chatterjee, D. Dey, S. Munshi, Integration of morphological preprocessing and fractal based feature extraction with recursive feature elimination for skin lesion types classification, *Computer methods and programs in biomedicine* 178 (2019) 201–218.
- [2] P. M. Pereira, R. Fonseca-Pinto, R. P. Paiva, P. A. Assuncao, L. M. Tavora, L. A. Thomaz, S. M. Faria, Dermoscopic skin lesion image segmentation based on local binary pattern clustering: comparative study, *Biomedical Signal Processing and Control* 59 (2020) 101924.
- [3] M. K. Hasan, S. Roy, C. Mondal, M. A. Alam, M. T. E. Elahi, A. Dutta, S. T. U. Raju, M. T. Jawad, M. Ahmad, Dermo-doctor: A framework for concurrent skin lesion detection and recognition using a deep convolutional neural network with end-to-end dual encoders, *Biomedical Signal Processing and Control* 68 (2021) 102661.
- [4] R. B. Oliveira, J. P. Papa, A. S. Pereira, J. M. R. Tavares, Computational methods for pigmented skin lesion classification in images: review and future trends, *Neural Computing and Applications* 29 (2018) 613–636.
- [5] M. K. Hasan, M. T. E. Elahi, M. A. Alam, M. T. Jawad, R. Martí, Dermoexpert: Skin lesion classification using a hybrid convolutional neural network through segmentation, transfer learning, and augmentation, *Informatics in Medicine Unlocked* (2022) 100819.
- [6] K. Korotkov, R. Garcia, Computerized analysis of pigmented skin lesions: a review, *Artificial intelligence in medicine* 56 (2012) 69–90.
- [7] M. H. Jafari, N. Karimi, E. Nasr-Esfahani, S. Samavi, S. M. R. Soroushmehr, K. Ward, K. Najarian, Skin lesion segmentation in clinical images using deep learning, in: 2016 23rd International conference on pattern recognition (ICPR), IEEE, pp. 337–342.
- [8] M. A. Kassem, K. M. Hosny, R. Damaševičius, M. M. Eltoukhy, Machine learning and deep learning methods for skin lesion classification and diagnosis: A systematic review, *Diagnostics* 11 (2021) 1390.
- [9] M. Dildar, S. Akram, M. Irfan, H. U. Khan, M. Ramzan, A. R. Mahmood, S. A. Alsaiani, A. H. M. Saeed, M. O. Alraddadi, M. H. Mahnashi, Skin cancer detection: a review using deep learning techniques, *International journal of environmental research and public health* 18 (2021) 5479.
- [10] G. Ososkov, P. Goncharov, Shallow and deep learning for image classification, *Optical Memory and Neural Networks* 26 (2017) 221–248.
- [11] M. R. Islam, M. A. Moni, M. M. Islam, M. Rashed-Al-Mahfuz, M. S. Islam, M. K. Hasan, M. S. Hossain, M. Ahmad, S. Uddin, A. Azad, et al., Emotion recognition from eeg signal focusing on deep learning and shallow learning techniques, *IEEE Access* 9 (2021) 94601–94624.
- [12] M. K. Hasan, M. A. Alam, S. Roy, A. Dutta, M. T. Jawad, S. Das, Missing value imputation affects the performance of machine learning: A review and analysis of the literature (2010–2021), *Informatics*

- in *Medicine Unlocked* 27 (2021) 100799.
- [13] M. K. Hasan, L. Dahal, P. N. Samarakoon, F. I. Tushar, R. Martí, Dsnet: Automatic dermoscopic skin lesion segmentation, *Computers in Biology and Medicine* 120 (2020) 103738.
 - [14] D. Gutman, N. C. Codella, E. Celebi, B. Helba, M. Marchetti, N. Mishra, A. Halpern, Skin lesion analysis toward melanoma detection: A challenge at the international symposium on biomedical imaging (isbi) 2016, hosted by the international skin imaging collaboration (isic), arXiv:1605.01397 (2016).
 - [15] N. C. Codella, D. Gutman, M. E. Celebi, B. Helba, M. A. Marchetti, S. W. Dusza, A. Kalloo, K. Liopyris, N. Mishra, H. Kittler, et al., Skin lesion analysis toward melanoma detection: A challenge at the 2017 international symposium on biomedical imaging (isbi), hosted by the international skin imaging collaboration (isic), in: 2018 IEEE 15th international symposium on biomedical imaging (ISBI 2018), IEEE, pp. 168–172.
 - [16] N. Codella, V. Rotemberg, P. Tschandl, M. E. Celebi, S. Dusza, D. Gutman, B. Helba, A. Kalloo, K. Liopyris, M. Marchetti, et al., Skin lesion analysis toward melanoma detection 2018: A challenge hosted by the international skin imaging collaboration (isic), arXiv:1902.03368 (2019).
 - [17] P. Tschandl, C. Rosendahl, H. Kittler, The ham10000 dataset, a large collection of multi-source dermatoscopic images of common pigmented skin lesions, *Scientific data* 5 (2018) 1–9.
 - [18] M. Combalia, N. C. Codella, V. Rotemberg, B. Helba, V. Vilaplana, O. Reiter, C. Carrera, A. Barreiro, A. C. Halpern, S. Puig, et al., Bcn20000: Dermoscopic lesions in the wild, arXiv:1908.02288 (2019).
 - [19] V. Rotemberg, N. Kurtansky, B. Betz-Stablein, L. Caffery, E. Chousakos, N. Codella, M. Combalia, S. Dusza, P. Guitera, D. Gutman, et al., A patient-centric dataset of images and metadata for identifying melanomas using clinical context, *Scientific data* 8 (2021) 1–8.
 - [20] T. Mendonça, P. M. Ferreira, J. S. Marques, A. R. Marcal, J. Rozeira, Ph 2-a dermoscopic image database for research and benchmarking, in: 2013 35th annual international conference of the IEEE engineering in medicine and biology society (EMBC), IEEE, pp. 5437–5440.
 - [21] G. Argenziano, H. Soyer, V. De Giorgi, D. Piccolo, P. Carli, M. Delfino, et al., Dermoscopy: a tutorial, *EDRA, Medical Publishing & New Media* 16 (2002).
 - [22] N. Codella, J. Cai, M. Abedini, R. Garnavi, A. Halpern, J. R. Smith, Deep learning, sparse coding, and svm for melanoma recognition in dermoscopy images, in: *International workshop on machine learning in medical imaging*, Springer, pp. 118–126.
 - [23] R. Amelard, J. Glaister, A. Wong, D. A. Clausi, High-level intuitive features (hlifs) for intuitive skin lesion description, *IEEE Transactions on Biomedical Engineering* 62 (2014) 820–831.
 - [24] M. E. Celebi, S. Hwang, H. Iyatomi, G. Schaefer, Robust border detection in dermoscopy images using threshold fusion, in: 2010 IEEE International Conference on Image Processing, IEEE, pp. 2541–2544.
 - [25] M. K. Hasan, M. T. Jawad, K. N. I. Hasan, S. B. Partha, M. M. Al Masba, S. Saha, M. A. Moni,

- Covid-19 identification from volumetric chest ct scans using a progressively resized 3d-cnn incorporating segmentation, augmentation, and class-rebalancing, *Informatics in Medicine Unlocked* 26 (2021) 100709.
- [26] M. Osadebey, M. Pedersen, D. Waaler, Evaluation of color spaces for unsupervised and deep learning skin lesion segmentation, in: *Proceedings of the IADIS International Conference Computer Graphics, Visualization, Computer Vision and Image Processing*, IADIS Press.
- [27] E. Santos, R. Veras, H. Miguel, K. Aires, M. L. Claro, G. B. Junior, A skin lesion semi-supervised segmentation method, in: *2020 International Conference on Systems, Signals and Image Processing (IWSSIP)*, IEEE, pp. 33–38.
- [28] C. Huang, A. Yu, Y. Wang, H. He, Skin lesion segmentation based on mask r-cnn, in: *2020 International Conference on Virtual Reality and Visualization (ICVRV)*, IEEE, pp. 63–67.
- [29] Z. N. Khan, Frequency and spatial domain based saliency for pigmented skin lesion segmentation, *arXiv:2010.04022* (2020).
- [30] K. Sanjar, O. Bekhzod, J. Kim, J. Kim, A. Paul, J. Kim, Improved u-net: Fully convolutional network model for skin-lesion segmentation, *Applied Sciences* 10 (2020) 3658.
- [31] R. Wang, S. Chen, J. Fan, Y. Li, Cascaded context enhancement for automated skin lesion segmentation, *arXiv:2004.08107* (2020).
- [32] B. Hafhouf, A. Zitouni, A. C. Megherbi, S. Sbaa, A modified u-net for skin lesion segmentation, in: *2020 1st International Conference on Communications, Control Systems and Signal Processing (CCSSP)*, IEEE, pp. 225–228.
- [33] O. Salih, S. Viriri, Skin lesion segmentation using local binary convolution-deconvolution architecture, *Image Analysis & Stereology* 39 (2020) 169–185.
- [34] S. Nathan, P. Kansal, Lesion net—skin lesion segmentation using coordinate convolution and deep residual units, *arXiv:2012.14249* (2020).
- [35] G. Ramella, Automatic skin lesion segmentation based on saliency and color., in: *VISIGRAPP (4: VISAPP)*, pp. 452–459.
- [36] Y. Tang, Z. Fang, S. Yuan, Y. Xing, J. T. Zhou, F. Yang, et al., imscgnet: Iterative multi-scale context-guided segmentation of skin lesion in dermoscopic images, *IEEE Access* 8 (2020) 39700–39712.
- [37] K. Jayapriya, I. J. Jacob, Hybrid fully convolutional networks-based skin lesion segmentation and melanoma detection using deep feature, *International Journal of Imaging Systems and Technology* 30 (2020) 348–357.
- [38] A. R. Hawas, Y. Guo, C. Du, K. Polat, A. S. Ashour, Oce-ngc: A neutrosophic graph cut algorithm using optimized clustering estimation algorithm for dermoscopic skin lesion segmentation, *Applied*

Soft Computing 86 (2020) 105931.

- [39] V. Ribeiro, S. Avila, E. Valle, Less is more: Sample selection and label conditioning improve skin lesion segmentation, in: Proceedings of the IEEE/CVF Conference on Computer Vision and Pattern Recognition Workshops, pp. 738–739.
- [40] Z. Al Nazi, T. A. Abir, Automatic skin lesion segmentation and melanoma detection: Transfer learning approach with u-net and dcnn-svm, in: Proceedings of International Joint Conference on Computational Intelligence, Springer, pp. 371–381.
- [41] M. P. Pour, H. Seker, Transform domain representation-driven convolutional neural networks for skin lesion segmentation, Expert Systems with Applications 144 (2020) 113129.
- [42] F. Xie, J. Yang, J. Liu, Z. Jiang, Y. Zheng, Y. Wang, Skin lesion segmentation using high-resolution convolutional neural network, Computer Methods and Programs in Biomedicine 186 (2020) 105241.
- [43] R. Rout, P. Parida, Transition region based approach for skin lesion segmentation, Procedia Computer Science 171 (2020) 379–388.
- [44] Z. Deng, Y. Xin, X. Qiu, Y. Chen, Weakly and semi-supervised deep level set network for automated skin lesion segmentation, in: Innovation in Medicine and Healthcare, Springer, 2020, pp. 145–155.
- [45] K. Qin, D. Sun, S. Zhang, H. Zhao, Asymmetric encode-decode network with two decoding paths for skin lesion segmentation, in: 2020 5th International Conference on Biomedical Imaging, Signal Processing, pp. 22–27.
- [46] M. A. Anjum, J. Amin, M. Sharif, H. U. Khan, M. S. A. Malik, S. Kadry, Deep semantic segmentation and multi-class skin lesion classification based on convolutional neural network, IEEE Access 8 (2020) 129668–129678.
- [47] K. B. Nampalle, B. Raman, An efficient approach for skin lesion segmentation using dermoscopic images: A deep learning approach, in: International Conference on Computer Vision and Image Processing, Springer, pp. 430–439.
- [48] K. Abhishek, G. Hamarneh, M. S. Drew, Illumination-based transformations improve skin lesion segmentation in dermoscopic images, in: Proceedings of the IEEE/CVF Conference on Computer Vision and Pattern Recognition Workshops, pp. 728–729.
- [49] D. N. Thanh, N. N. Hien, V. Surya Prasath, U. Erkan, A. Khamparia, Adaptive thresholding skin lesion segmentation with gabor filters and principal component analysis, in: Intelligent Computing in Engineering, Springer, 2020, pp. 811–820.
- [50] Z. Wei, F. Shi, H. Song, W. Ji, G. Han, Attentive boundary aware network for multi-scale skin lesion segmentation with adversarial training, Multimedia Tools and Applications 79 (2020) 27115–27136.
- [51] Y. Jiang, S. Cao, S. Tao, H. Zhang, Skin lesion segmentation based on multi-scale attention convolutional neural network, IEEE Access 8 (2020) 122811–122825.

- [52] Y. Qiu, J. Cai, X. Qin, J. Zhang, Inferring skin lesion segmentation with fully connected crfs based on multiple deep convolutional neural networks, *IEEE Access* 8 (2020) 144246–144258.
- [53] R. Kaymak, C. Kaymak, A. Ucar, Skin lesion segmentation using fully convolutional networks: A comparative experimental study, *Expert Systems with Applications* 161 (2020) 113742.
- [54] H. Wu, J. Pan, Z. Li, Z. Wen, J. Qin, Automated skin lesion segmentation via an adaptive dual attention module, *IEEE Transactions on Medical Imaging* 40 (2020) 357–370.
- [55] R. Azad, M. Asadi-Aghbolaghi, M. Fathy, S. Escalera, Attention deeplabv3+: Multi-level context attention mechanism for skin lesion segmentation, in: *European Conference on Computer Vision*, Springer, pp. 251–266.
- [56] K. Zafar, S. O. Gilani, A. Waris, A. Ahmed, M. Jamil, M. N. Khan, A. Sohail Kashif, Skin lesion segmentation from dermoscopic images using convolutional neural network, *Sensors* 20 (2020) 1601.
- [57] Ş. Öztürk, U. Özkaya, Skin lesion segmentation with improved convolutional neural network, *Journal of digital imaging* 33 (2020) 958–970.
- [58] Y. Xie, J. Zhang, Y. Xia, C. Shen, A mutual bootstrapping model for automated skin lesion segmentation and classification, *IEEE transactions on medical imaging* 39 (2020) 2482–2493.
- [59] A. Mahbod, P. Tschandl, G. Langs, R. Ecker, I. Ellinger, The effects of skin lesion segmentation on the performance of dermoscopic image classification, *Computer Methods and Programs in Biomedicine* 197 (2020) 105725.
- [60] P. Shan, Y. Wang, C. Fu, W. Song, J. Chen, Automatic skin lesion segmentation based on fc-dpn, *Computers in Biology and Medicine* 123 (2020) 103762.
- [61] B. Lei, Z. Xia, F. Jiang, X. Jiang, Z. Ge, Y. Xu, J. Qin, S. Chen, T. Wang, S. Wang, Skin lesion segmentation via generative adversarial networks with dual discriminators, *Medical Image Analysis* 64 (2020) 101716.
- [62] A. W. Setiawan, Image segmentation metrics in skin lesion: Accuracy, sensitivity, specificity, dice coefficient, jaccard index, and matthews correlation coefficient, in: *2020 International Conference on Computer Engineering, Network, and Intelligent Multimedia (CENIM)*, IEEE, pp. 97–102.
- [63] A. Kamalakannan, S. S. Ganesan, G. Rajamanickam, Self-learning ai framework for skin lesion image segmentation and classification, *arXiv:2001.05838* (2020).
- [64] Y. Wang, Y. Wei, X. Qian, L. Zhu, Y. Yang, Donet: Dual objective networks for skin lesion segmentation, *arXiv:2008.08278* (2020).
- [65] A. Saha, P. Prasad, A. Thabit, Leveraging adaptive color augmentation in convolutional neural networks for deep skin lesion segmentation, in: *2020 IEEE 17th International Symposium on Biomedical Imaging (ISBI)*, IEEE, pp. 2014–2017.
- [66] L. Zhu, S. Feng, W. Zhu, X. Chen, Asnet: An adaptive scale network for skin lesion segmentation

- in dermoscopy images, in: *Medical Imaging 2020: Biomedical Applications in Molecular, Structural, and Functional Imaging*, volume 11317, International Society for Optics and Photonics, p. 113170W.
- [67] J. Zhang, C. Petitjean, S. Ainouz, Kappa loss for skin lesion segmentation in fully convolutional network, in: *2020 IEEE 17th International Symposium on Biomedical Imaging (ISBI)*, IEEE, pp. 2001–2004.
- [68] R. Iranpoor, A. S. Mahboob, S. Shahbandegan, N. Baniyasi, Skin lesion segmentation using convolutional neural networks with improved u-net architecture, in: *2020 6th Iranian Conference on Signal Processing and Intelligent Systems (ICSPIS)*, IEEE, pp. 1–5.
- [69] M. Hajabdollahi, R. Esfandiarpour, P. Khadivi, S. M. R. Soroushmehr, N. Karimi, S. Samavi, Simplification of neural networks for skin lesion image segmentation using color channel pruning, *Computerized Medical Imaging and Graphics* 82 (2020) 101729.
- [70] S. Justin, M. Pattnaik, Skin lesion segmentation by pixel by pixel approach using deep learning, *International Journal Of Advances In Signal And Image Sciences* 6 (2020) 12–20.
- [71] G. I. Sayed, G. Khoriba, M. H. Haggag, The novel multi-swarm coyote optimization algorithm for automatic skin lesion segmentation, *Evolutionary Intelligence* (2020) 1–33.
- [72] M. Rizzi, C. Guaragnella, Skin lesion segmentation using image bit-plane multilayer approach, *Applied Sciences* 10 (2020) 3045.
- [73] N. Bansal, S. Sridhar, P. D. Priya, Improved skin lesion detection and segmentation by fusing texture and geometric features, *International Journal of Applied Engineering Research* 15 (2020) 1116–1121.
- [74] P. Parida, R. Rout, Transition region based approach for skin lesion segmentation, *ELCVIA: Electronic Letters on Computer Vision and Image Analysis* 19 (2020) 0028–37.
- [75] V. Pillay, D. Hirasen, S. Viriri, M. V. Gwetu, Macroscopic skin lesion segmentation using grabcut, in: *International Conference on Computational Collective Intelligence*, Springer, pp. 528–539.
- [76] S. Sivaraj, R. Malmathanraj, P. Palanisamy, et al., Detecting anomalous growth of skin lesion using threshold-based segmentation algorithm and fuzzy k-nearest neighbor classifier, *Journal of cancer research and therapeutics* 16 (2020) 40.
- [77] P. Ganesan, B. Sathish, L. L. Joseph, Hsl color space based skin lesion segmentation using fuzzy-based techniques, in: *Advances in Electrical Control and Signal Systems*, Springer, 2020, pp. 903–911.
- [78] Z. Liu, H. Pan, C. Gong, Z. Fan, Y. Wen, T. Jiang, R. Xiong, H. Li, Y. Wang, Multi-class skin lesion segmentation for cutaneous t-cell lymphomas on high-resolution clinical images, in: *International Conference on Medical Image Computing and Computer-Assisted Intervention*, Springer, pp. 351–361.
- [79] M. Low, V. Huang, P. Raina, Automating vitiligo skin lesion segmentation using convolutional neural networks, in: *2020 IEEE 17th International Symposium on Biomedical Imaging (ISBI)*, IEEE, pp.

1–4.

- [80] L. Agilandeewari, M. Sagar, N. Keerthana, Skin lesion detection using texture based segmentation and classification by convolutional neural networks (cnn), *Art Int J Innov Technol Explor Eng (IJITEE)* 9 (2019).
- [81] R. Javed, T. Saba, M. Shafry, M. Rahim, An intelligent saliency segmentation technique and classification of low contrast skin lesion dermoscopic images based on histogram decision, in: *2019 12th International Conference on Developments in eSystems Engineering (DeSE)*, IEEE, pp. 164–169.
- [82] M. A. Khan, T. Akram, M. Sharif, T. Saba, K. Javed, I. U. Lali, U. J. Tanik, A. Rehman, Construction of saliency map and hybrid set of features for efficient segmentation and classification of skin lesion, *Microscopy research and technique* 82 (2019) 741–763.
- [83] Y. Tang, F. Yang, S. Yuan, et al., A multi-stage framework with context information fusion structure for skin lesion segmentation, in: *2019 IEEE 16th International Symposium on Biomedical Imaging (ISBI 2019)*, IEEE, pp. 1407–1410.
- [84] V. K. Singh, M. Abdel-Nasser, H. A. Rashwan, F. Akram, N. Pandey, A. Lalande, B. Presles, S. Romani, D. Puig, Fca-net: Adversarial learning for skin lesion segmentation based on multi-scale features and factorized channel attention, *IEEE Access* 7 (2019) 130552–130565.
- [85] X. Wang, X. Jiang, H. Ding, J. Liu, Bi-directional dermoscopic feature learning and multi-scale consistent decision fusion for skin lesion segmentation, *IEEE transactions on image processing* 29 (2019) 3039–3051.
- [86] L. Huang, Y.-g. Zhao, T.-j. Yang, Skin lesion segmentation using object scale-oriented fully convolutional neural networks, *Signal, Image and Video Processing* 13 (2019) 431–438.
- [87] R. Seeja, A. Suresh, Deep learning based skin lesion segmentation and classification of melanoma using support vector machine (svm), *Asian Pacific journal of cancer prevention: APJCP* 20 (2019) 1555.
- [88] M. A. Khan, M. I. Sharif, M. Raza, A. Anjum, T. Saba, S. A. Shad, Skin lesion segmentation and classification: A unified framework of deep neural network features fusion and selection, *Expert Systems* (2019) e12497.
- [89] L. Zhang, G. Yang, X. Ye, Automatic skin lesion segmentation by coupling deep fully convolutional networks and shallow network with textons, *Journal of Medical Imaging* 6 (2019) 024001.
- [90] S. Baghersalimi, B. Bozorgtabar, P. Schmid-Saugeon, H. K. Ekenel, J.-P. Thiran, Dermonet: densely linked convolutional neural network for efficient skin lesion segmentation, *EURASIP Journal on Image and Video Processing* 2019 (2019) 1–10.
- [91] P. Tang, Q. Liang, X. Yan, S. Xiang, W. Sun, D. Zhang, G. Coppola, Efficient skin lesion segmentation using separable-unet with stochastic weight averaging, *Computer methods and programs in*

- biomedicine 178 (2019) 289–301.
- [92] D. Thanh, L. Thanh, S. Dvoenko, V. Prasath, N. San, Adaptive thresholding segmentation method for skin lesion with normalized color channels of ntsc and ycbcr, in: International conference on pattern recognition and information processing (PRIP'2019), Minsk.
- [93] M. Hasan, B. Alyafi, F. I. Tushar, et al., Comparative analysis of automatic skin lesion segmentation with two different implementations, arXiv:1904.03075 (2019).
- [94] S. Saini, D. Gupta, A. K. Tiwari, Detector-segmentor network for skin lesion localization and segmentation, in: National Conference on Computer Vision, Pattern Recognition, Image Processing, and Graphics, Springer, pp. 589–599.
- [95] S. Rawas, A. El-Zaart, Hcet-g 2: dermoscopic skin lesion segmentation via hybrid cross entropy thresholding using gaussian and gamma distributions, in: 2019 Third International Conference on Intelligent Computing in Data Sciences (ICDS), IEEE, pp. 1–7.
- [96] E. Alfaro, X. B. Fonseca, E. M. Albornoz, C. E. Martínez, S. C. Ramrez, A brief analysis of u-net and mask r-cnn for skin lesion segmentation, in: 2019 IEEE International Work Conference on Bioinspired Intelligence (IWOBI), IEEE, pp. 000123–000126.
- [97] M. A. Al-Masni, M. A. Al-Antari, H. M. Park, N. H. Park, T.-S. Kim, A deep learning model integrating frcn and residual convolutional networks for skin lesion segmentation and classification, in: 2019 IEEE Eurasia Conference on Biomedical Engineering, Healthcare and Sustainability (ECBIOS), IEEE, pp. 95–98.
- [98] A. Soudani, W. Barhoumi, An image-based segmentation recommender using crowdsourcing and transfer learning for skin lesion extraction, *Expert Systems with Applications* 118 (2019) 400–410.
- [99] M. Goyal, J. Ng, A. Oakley, M. H. Yap, Skin lesion boundary segmentation with fully automated deep extreme cut methods, in: *Medical Imaging 2019: Biomedical Applications in Molecular, Structural, and Functional Imaging*, volume 10953, International Society for Optics and Photonics, p. 109530Q.
- [100] H. Wang, G. Wang, Z. Sheng, S. Zhang, Automated segmentation of skin lesion based on pyramid attention network, in: *International Workshop on Machine Learning in Medical Imaging*, Springer, pp. 435–443.
- [101] D. Ma, H. Wu, J. Sun, C. Yu, L. Liu, A light-weight context-aware self-attention model for skin lesion segmentation, in: *Pacific Rim International Conference on Artificial Intelligence*, Springer, pp. 501–505.
- [102] X. Liu, G. Hu, X. Ma, H. Kuang, An enhanced neural network based on deep metric learning for skin lesion segmentation, in: 2019 Chinese Control And Decision Conference (CCDC), IEEE, pp. 1633–1638.
- [103] G. G. De Angelo, A. G. Pacheco, R. A. Krohling, Skin lesion segmentation using deep learning for

- images acquired from smartphones, in: 2019 International Joint Conference on Neural Networks (IJCNN), IEEE, pp. 1–8.
- [104] L. Song, J. Lin, Z. J. Wang, H. Wang, Dense-residual attention network for skin lesion segmentation, in: International Workshop on Machine Learning in Medical Imaging, Springer, pp. 319–327.
- [105] F. Jiang, F. Zhou, J. Qin, T. Wang, B. Lei, Decision-augmented generative adversarial network for skin lesion segmentation, in: 2019 IEEE 16th International Symposium on Biomedical Imaging (ISBI 2019), IEEE, pp. 447–450.
- [106] A. Adegun, S. Viriri, Deep learning model for skin lesion segmentation: Fully convolutional network, in: International Conference on Image Analysis and Recognition, Springer, pp. 232–242.
- [107] M. M. K. Sarker, H. A. Rashwan, F. Akram, V. K. Singh, S. F. Banu, F. U. Chowdhury, K. A. Choudhury, S. Chambon, P. Radeva, D. Puig, et al., Slsnet: Skin lesion segmentation using a lightweight generative adversarial network, *Expert Systems with Applications* (2021) 115433.
- [108] L. Bi, D. Feng, M. Fulham, J. Kim, Improving skin lesion segmentation via stacked adversarial learning, in: 2019 IEEE 16th International Symposium on Biomedical Imaging (ISBI 2019), IEEE, pp. 1100–1103.
- [109] Q. C. Ninh, T.-T. Tran, T. T. Tran, T. A. X. Tran, V.-T. Pham, Skin lesion segmentation based on modification of segnet neural networks, in: 2019 6th NAFOSTED Conference on Information and Computer Science (NICS), IEEE, pp. 575–578.
- [110] V. Ribeiro, S. Avila, E. Valle, Handling inter-annotator agreement for automated skin lesion segmentation, *arXiv:1906.02415* (2019).
- [111] L. Liu, L. Mou, X. X. Zhu, M. Mandal, Skin lesion segmentation based on improved u-net, in: 2019 IEEE Canadian Conference of Electrical and Computer Engineering (CCECE), IEEE, pp. 1–4.
- [112] D. N. Thanh, U. Erkan, V. S. Prasath, V. Kumar, N. N. Hien, A skin lesion segmentation method for dermoscopic images based on adaptive thresholding with normalization of color models, in: 2019 6th International Conference on Electrical and Electronics Engineering (ICEEE), IEEE, pp. 116–120.
- [113] W. Tu, X. Liu, W. Hu, Z. Pan, Dense-residual network with adversarial learning for skin lesion segmentation, *IEEE Access* 7 (2019) 77037–77051.
- [114] H. M. Ünver, E. Ayan, Skin lesion segmentation in dermoscopic images with combination of yolo and grabcut algorithm, *Diagnostics* 9 (2019) 72.
- [115] D. Bisla, A. Choromanska, J. A. Stein, D. Polsky, R. Berman, Skin lesion segmentation and classification with deep learning system, *arXiv:1902.06061* (2019) 1–6.
- [116] P. Tschandl, C. Sinz, H. Kittler, Domain-specific classification-pretrained fully convolutional network encoders for skin lesion segmentation, *Computers in biology and medicine* 104 (2019) 111–116.
- [117] Z. Wei, H. Song, L. Chen, Q. Li, G. Han, Attention-based denseunet network with adversarial training

- for skin lesion segmentation, *IEEE Access* 7 (2019) 136616–136629.
- [118] P.-f. Shan, Y.-d. Wang, C. Fu, Improving skin lesion segmentation with deep convolutional generative adversarial networks, in: *International Conference on Frontier Computing*, Springer, pp. 138–147.
- [119] O. Salih, S. Viriri, Skin lesion segmentation techniques based on markov random field, in: *International Conference on Mining Intelligence and Knowledge Exploration*, Springer, pp. 210–220.
- [120] Z. Cui, L. Wu, R. Wang, W.-S. Zheng, Ensemble transductive learning for skin lesion segmentation, in: *Chinese Conference on Pattern Recognition and Computer Vision (PRCV)*, Springer, pp. 572–581.
- [121] A. H. Shahin, K. Amer, M. A. Elattar, Deep convolutional encoder-decoders with aggregated multi-resolution skip connections for skin lesion segmentation, in: *2019 IEEE 16th International Symposium on Biomedical Imaging (ISBI 2019)*, IEEE, pp. 451–454.
- [122] A.-R. Ali, J. Li, T. Trappenberg, Supervised versus unsupervised deep learning based methods for skin lesion segmentation in dermoscopy images, in: *Canadian Conference on Artificial Intelligence*, Springer, pp. 373–379.
- [123] J. Wu, E. Z. Chen, R. Rong, X. Li, D. Xu, H. Jiang, Skin lesion segmentation with c-unet, in: *2019 41st Annual International Conference of the IEEE Engineering in Medicine and Biology Society (EMBC)*, IEEE, pp. 2785–2788.
- [124] R. Ali, R. C. Hardie, M. S. De Silva, T. M. Kebede, Skin lesion segmentation and classification for isic 2018 by combining deep cnn and handcrafted features, *arXiv:1908.05730* (2019).
- [125] J. Lameski, A. Jovanov, E. Zdravevski, P. Lameski, S. Gievska, Skin lesion segmentation with deep learning, in: *IEEE EUROCON 2019-18th International Conference on Smart Technologies*, IEEE, pp. 1–5.
- [126] S. N. Hasan, M. Gezer, R. A. Azeez, S. Gülseçen, Skin lesion segmentation by using deep learning techniques, in: *2019 Medical Technologies Congress (TIPTEKNO)*, IEEE, pp. 1–4.
- [127] L. Canalini, F. Pollastri, F. Bolelli, M. Cancilla, S. Allegretti, C. Grana, Skin lesion segmentation ensemble with diverse training strategies, in: *International Conference on Computer Analysis of Images and Patterns*, Springer, pp. 89–101.
- [128] M. H. Aljanabi, F. A. Jumaa, A. O. Aftan, M. S. S. Alkafaji, N. Alanı, Z. H. Al-Tameemi, D. H. Al-Mamoori, Various types of skin tumors lesion medical imaging (stlmi) of healthy and unhealthy moles a review and computational of: Segmentation, classification, methods and algorithms, in: *IOP Conference Series: Materials Science and Engineering*, volume 518, IOP Publishing, p. 052014.
- [129] W. S. Ooi, B. E. Khoo, C. P. Lim, An interactive evolutionary multi-objective approach to skin lesion segmentation, in: *10th International Conference on Robotics, Vision, Signal Processing and Power Applications*, Springer, Singapore, pp. 641–647.
- [130] O. Bingöl, S. Paçacı, U. Güvenç, Entropy-based skin lesion segmentation using stochastic fractal search

- algorithm, in: *The International Conference on Artificial Intelligence and Applied Mathematics in Engineering*, Springer, pp. 801–811.
- [131] P. Brahmabhatt, S. N. Rajan, Skin lesion segmentation using segnet with binary cross-entropy, in: *International Conference on Artificial Intelligence and Speech Technology (AIST2019)*, volume 14, p. 15th.
- [132] H. N. Abdullah, H. K. Abduljaleel, Deep cnn based skin lesion image denoising and segmentation using active contour method, *Engineering and Technology Journal* 37 (2019) 464–469.
- [133] T. Yang, Y. Chen, J. Lu, Z. Fan, Sampling with level set for pigmented skin lesion segmentation, *Signal, Image and Video Processing* 13 (2019) 813–821.
- [134] Y. Filali, S. Abdelouahed, A. Aarab, An improved segmentation approach for skin lesion classification, *Statistics, Optimization & Information Computing* 7 (2019) 456–467.
- [135] I. Filali, M. Belkadi, Multi-scale contrast based skin lesion segmentation in digital images, *Optik* 185 (2019) 794–811.
- [136] S. Sengupta, N. Mittal, M. Modi, Segmentation of skin lesion images using fudge factor based techniques, in: *Advances in Interdisciplinary Engineering*, Springer, 2019, pp. 837–846.
- [137] I. Bhakta, S. Phadikar, K. Majumder, A. Sau, S. Chowdhuri, Tsalli’s entropy-based segmentation method for accurate pigmented skin lesion identification, *IETE Journal of Research* (2019) 1–17.
- [138] M. Dash, N. D. Londhe, S. Ghosh, A. Semwal, R. S. Sonawane, Pslsnet: Automated psoriasis skin lesion segmentation using modified u-net-based fully convolutional network, *Biomedical Signal Processing and Control* 52 (2019) 226–237.
- [139] F. Riaz, S. Naeem, R. Nawaz, M. Coimbra, Active contours based segmentation and lesion periphery analysis for characterization of skin lesions in dermoscopy images, *IEEE journal of biomedical and health informatics* 23 (2018) 489–500.
- [140] J. Burdick, O. Marques, J. Weinthal, B. Furht, Rethinking skin lesion segmentation in a convolutional classifier, *Journal of digital imaging* 31 (2018) 435–440.
- [141] X. He, Z. Yu, T. Wang, B. Lei, Y. Shi, Dense deconvolution net: Multi path fusion and dense deconvolution for high resolution skin lesion segmentation, *Technology and Health Care* 26 (2018) 307–316.
- [142] S. S. Kolekar, P. G. Magdum, Skin lesion semantic segmentation using convolutional encoder decoder architecture, in: *2018 Fourth International Conference on Computing Communication Control and Automation (ICCUBEA)*, IEEE, pp. 1–3.
- [143] O. O. Olugbara, T. B. Taiwo, D. Heukelman, Segmentation of melanoma skin lesion using perceptual color difference saliency with morphological analysis, *Mathematical Problems in Engineering* 2018 (2018).

- [144] T. Akram, M. A. Khan, M. Sharif, M. Yasmin, Skin lesion segmentation and recognition using multichannel saliency estimation and m-svm on selected serially fused features, *Journal of Ambient Intelligence and Humanized Computing* (2018) 1–20.
- [145] M. A. Khan, T. Akram, M. Sharif, A. Shahzad, K. Aurangzeb, M. Alhussein, S. I. Haider, A. Altamrah, An implementation of normal distribution based segmentation and entropy controlled features selection for skin lesion detection and classification, *BMC cancer* 18 (2018) 1–20.
- [146] H. Li, X. He, F. Zhou, Z. Yu, D. Ni, S. Chen, T. Wang, B. Lei, Dense deconvolutional network for skin lesion segmentation, *IEEE journal of biomedical and health informatics* 23 (2018) 527–537.
- [147] M. Aljanabi, Y. E. Özok, J. Rahebi, A. S. Abdullah, Skin lesion segmentation method for dermoscopy images using artificial bee colony algorithm, *Symmetry* 10 (2018) 347.
- [148] H. Li, X. He, Z. Yu, F. Zhou, J.-Z. Cheng, L. Huang, T. Wang, B. Lei, Skin lesion segmentation via dense connected deconvolutional network, in: *2018 24th International Conference on Pattern Recognition (ICPR)*, IEEE, pp. 671–675.
- [149] S. Vesal, S. M. Patil, N. Ravikumar, A. K. Maier, A multi-task framework for skin lesion detection and segmentation, in: *OR 2.0 Context-Aware Operating Theaters, Computer Assisted Robotic Endoscopy, Clinical Image-Based Procedures, and Skin Image Analysis*, Springer, 2018, pp. 285–293.
- [150] X. Li, L. Yu, H. Chen, C.-W. Fu, P.-A. Heng, Semi-supervised skin lesion segmentation via transformation consistent self-ensembling model, *arXiv:1808.03887* (2018).
- [151] S. Vesal, N. Ravikumar, A. Maier, Skinnet: A deep learning framework for skin lesion segmentation, in: *2018 IEEE Nuclear Science Symposium and Medical Imaging Conference Proceedings (NSS/MIC)*, IEEE, pp. 1–3.
- [152] Z. Mirikharaji, S. Izadi, J. Kawahara, G. Hamarneh, Deep auto-context fully convolutional neural network for skin lesion segmentation, in: *2018 IEEE 15th International Symposium on Biomedical Imaging (ISBI 2018)*, IEEE, pp. 877–880.
- [153] G. Venkatesh, Y. Naresh, S. Little, N. E. O’Connor, A deep residual architecture for skin lesion segmentation, in: *OR 2.0 Context-Aware Operating Theaters, Computer Assisted Robotic Endoscopy, Clinical Image-Based Procedures, and Skin Image Analysis*, Springer, 2018, pp. 277–284.
- [154] Y. Yuan, Automatic skin lesion segmentation with fully convolutional-deconvolutional networks, *arXiv:1703.05165* (2017).
- [155] S. M. Jaisakthi, P. Mirunalini, C. Aravindan, Automated skin lesion segmentation of dermoscopic images using grabcut and k-means algorithms, *IET Computer Vision* 12 (2018) 1088–1095.
- [156] G. Zeng, G. Zheng, Multi-scale fully convolutional densenets for automated skin lesion segmentation in dermoscopy images, in: *International Conference Image Analysis and Recognition*, Springer, pp. 513–521.

- [157] S. Chen, Z. Wang, J. Shi, B. Liu, N. Yu, A multi-task framework with feature passing module for skin lesion classification and segmentation, in: 2018 IEEE 15th international symposium on biomedical imaging (ISBI 2018), IEEE, pp. 1126–1129.
- [158] N.-Q. Nguyen, Isic 2017 skin lesion segmentation using deep encoder-decoder network, arXiv:1807.09083 (2018).
- [159] M. Ammar, S. G. Khawaja, A. Atif, M. U. Akram, M. Sakeena, Learning based segmentation of skin lesion from dermoscopic images, in: 2018 IEEE 20th International Conference on e-Health Networking, Applications and Services (Healthcom), IEEE, pp. 1–6.
- [160] A. Youssef, D. D. Bloisi, M. Muscio, A. Pennisi, D. Nardi, A. Facchiano, Deep convolutional pixel-wise labeling for skin lesion image segmentation, in: 2018 IEEE International Symposium on Medical Measurements and Applications (MeMeA), IEEE, pp. 1–6.
- [161] S. Ross-Howe, H. R. Tizhoosh, The effects of image pre-and post-processing, wavelet decomposition, and local binary patterns on u-nets for skin lesion segmentation, in: 2018 International Joint Conference on Neural Networks (IJCNN), IEEE, pp. 1–8.
- [162] D. Patiño, J. Avendaño, J. W. Branch, Automatic skin lesion segmentation on dermoscopic images by the means of superpixel merging, in: International Conference on Medical Image Computing and Computer-Assisted Intervention, Springer, pp. 728–736.
- [163] F. Navarro, M. Escudero-Vinolo, J. Bescós, Accurate segmentation and registration of skin lesion images to evaluate lesion change, IEEE journal of biomedical and health informatics 23 (2018) 501–508.
- [164] H. Jiang, R. Rong, J. Wu, X. Li, X. Dong, E. Z. Chen, Skin lesion segmentation with improved c-unet networks, BioRxiv (2018) 382549.
- [165] F. Guth, T. E. deCampos, Skin lesion segmentation using u-net and good training strategies, arXiv:1811.11314 (2018).
- [166] H. Xu, T. H. Hwang, Automatic skin lesion segmentation using deep fully convolutional networks, arXiv:1807.06466 (2018).
- [167] Y. Wang, S. Sun, J. Yu, D. Yu, et al., Skin lesion segmentation using atrous convolution via deeplab v3, arXiv:1807.08891 (2018).
- [168] L. Bi, D. Feng, J. Kim, Improving automatic skin lesion segmentation using adversarial learning based data augmentation, arXiv:1807.08392 (2018).
- [169] C. Qian, T. Liu, H. Jiang, Z. Wang, P. Wang, M. Guan, B. Sun, A detection and segmentation architecture for skin lesion segmentation on dermoscopy images, arXiv:1809.03917 (2018).
- [170] A. Bissoto, F. Perez, V. Ribeiro, M. Fornaciali, S. Avila, E. Valle, Deep-learning ensembles for skin-lesion segmentation, analysis, classification: Recod titans at isic challenge 2018, arXiv:1808.08480

- (2018).
- [171] S. Louhichi, M. Gzara, H. B. Abdallah, Skin lesion segmentation using multiple density clustering algorithm mdcut and region growing, in: 2018 IEEE/ACIS 17th International Conference on Computer and Information Science (ICIS), IEEE, pp. 74–79.
 - [172] K. Hu, S. Liu, Y. Zhang, C. Cao, F. Xiao, W. Huang, X. Gao, A skin lesion segmentation method based on saliency and adaptive thresholding in wavelet domain, in: International Symposium on Artificial Intelligence and Robotics, Springer, pp. 445–453.
 - [173] M. Nasir, M. Attique Khan, M. Sharif, I. U. Lali, T. Saba, T. Iqbal, An improved strategy for skin lesion detection and classification using uniform segmentation and feature selection based approach, *Microscopy research and technique* 81 (2018) 528–543.
 - [174] A. P. Chakkaravarthy, A. Chandrasekar, An automatic segmentation of skin lesion from dermoscopy images using watershed segmentation, in: 2018 International Conference on Recent Trends in Electrical, Control and Communication (RTECC), IEEE, pp. 15–18.
 - [175] W. Luo, M. Yang, Fast skin lesion segmentation via fully convolutional network with residual architecture and crf, in: 2018 24th International Conference on Pattern Recognition (ICPR), IEEE, pp. 1438–1443.
 - [176] I. Ahmed, Q. N. u. Rehman, G. Masood, A. Adnan, A. Ahmad, S. Rho, Segmentation of affected skin lesion with blind deconvolution and $l^* a^* b$ colour space, in: Proceedings of the 33rd Annual ACM Symposium on Applied Computing, pp. 634–639.
 - [177] O. Salih, S. Viriri, Skin lesion segmentation using enhanced unified markov random field, in: International Conference on Mining Intelligence and Knowledge Exploration, Springer, pp. 331–340.
 - [178] N. C. Lynn, Z. M. Kyu, Segmentation and classification of skin cancer melanoma from skin lesion images, in: 2017 18th International Conference on Parallel and Distributed Computing, Applications and Technologies (PDCAT), IEEE, pp. 117–122.
 - [179] M. P. Pour, H. Seker, L. Shao, Automated lesion segmentation and dermoscopic feature segmentation for skin cancer analysis, in: 2017 39th Annual International Conference of the IEEE Engineering in Medicine and Biology Society (EMBC), IEEE, pp. 640–643.
 - [180] B. Bozorgtabar, Z. Ge, R. Chakravorty, M. Abedini, S. Demyanov, R. Garnavi, Investigating deep side layers for skin lesion segmentation, in: 2017 IEEE 14th International Symposium on Biomedical Imaging (ISBI 2017), IEEE, pp. 256–260.
 - [181] X. He, Z. Yu, T. Wang, B. Lei, Skin lesion segmentation via deep refinenet, in: Deep Learning in Medical Image Analysis and Multimodal Learning for Clinical Decision Support, Springer, 2017, pp. 303–311.
 - [182] B. Bozorgtabar, S. Sedai, P. K. Roy, R. Garnavi, Skin lesion segmentation using deep convolution

- networks guided by local unsupervised learning, *IBM Journal of Research and Development* 61 (2017) 6–1.
- [183] L. Bi, J. Kim, E. Ahn, D. Feng, M. Fulham, Semi-automatic skin lesion segmentation via fully convolutional networks, in: *2017 IEEE 14th International Symposium on Biomedical Imaging (ISBI 2017)*, IEEE, pp. 561–564.
- [184] D. Ramachandram, G. W. Taylor, Skin lesion segmentation using deep hypercolumn descriptors, *Journal of Computational Vision and Imaging Systems* 3 (2017).
- [185] D. Alvarez, M. Iglesias, k-means clustering and ensemble of regressions: an algorithm for the isic 2017 skin lesion segmentation challenge, *arXiv:1702.07333* (2017).
- [186] J. Qi, M. Le, C. Li, P. Zhou, Global and local information based deep network for skin lesion segmentation, *arXiv:1703.05467* (2017).
- [187] S. Jaisakthi, A. Chandrabose, P. Mirunalini, Automatic skin lesion segmentation using semi-supervised learning technique, *arXiv:1703.04301* (2017).
- [188] R. Mishra, O. Daescu, Deep learning for skin lesion segmentation, in: *2017 IEEE International Conference on Bioinformatics and Biomedicine (BIBM)*, IEEE, pp. 1189–1194.
- [189] B. S. Lin, K. Michael, S. Kalra, H. R. Tizhoosh, Skin lesion segmentation: U-nets versus clustering, in: *2017 IEEE Symposium Series on Computational Intelligence (SSCI)*, IEEE, pp. 1–7.
- [190] A. Pardo, E. Real, G. Fernandez-Barreras, F. Madruga, J. López-Higuera, O. Conde, Automated skin lesion segmentation with kernel density estimation, in: *European Conference on Biomedical Optics*, Optical Society of America, p. 104110P.
- [191] E. Nasr-Esfahani, S. Rafiei, M. H. Jafari, N. Karimi, J. S. Wrobel, S. Soroushmehr, S. Samavi, K. Najarian, Dense fully convolutional network for skin lesion segmentation, *arXiv:1712.10207* (2017).
- [192] C. E. Martínez, E. M. Albornoz, Pigmented skin lesion segmentation based on sparse texture representations, in: *12th International Symposium on Medical Information Processing and Analysis*, volume 10160, International Society for Optics and Photonics, p. 101600N.
- [193] A. Gupta, A. Issac, M. K. Dutta, H.-H. Hsu, Adaptive thresholding for skin lesion segmentation using statistical parameters, in: *2017 31st International Conference on Advanced Information Networking and Applications Workshops (WAINA)*, IEEE, pp. 616–620.
- [194] A. Agarwal, A. Issac, M. K. Dutta, K. Riha, V. Uher, Automated skin lesion segmentation using k-means clustering from digital dermoscopic images, in: *2017 40th International Conference on Telecommunications and Signal Processing (TSP)*, IEEE, pp. 743–748.
- [195] Y. M. George, M. Aldeen, R. Garnavi, Automatic psoriasis lesion segmentation in two-dimensional skin images using multiscale superpixel clustering, *Journal of Medical Imaging* 4 (2017) 044004.
- [196] B. Bozorgtabar, M. Abedini, R. Garnavi, Sparse coding based skin lesion segmentation using dynamic

- rule-based refinement, in: international workshop on machine learning in medical imaging, Springer, pp. 254–261.
- [197] T. Majtner, K. Lidayova, S. Yildirim-Yayilgan, J. Y. Hardeberg, Improving skin lesion segmentation in dermoscopic images by thin artefacts removal methods, in: 2016 6th European Workshop on Visual Information Processing (EUVIP), IEEE, pp. 1–6.
- [198] M. Hassan, M. Hossny, S. Nahavandi, A. Yazdabadi, Skin lesion segmentation using gray level co-occurrence matrix, in: 2016 IEEE International Conference on Systems, Man, and Cybernetics (SMC), IEEE, pp. 000820–000825.
- [199] R. Kasmi, K. Mokrani, R. Rader, J. Cole, W. Stoecker, Biologically inspired skin lesion segmentation using a geodesic active contour technique, *Skin Research and Technology* 22 (2016) 208–222.
- [200] S. Khalid, U. Jamil, K. Saleem, M. U. Akram, W. Manzoor, W. Ahmed, A. Sohail, Segmentation of skin lesion using cohen–daubechies–feauveau biorthogonal wavelet, *SpringerPlus* 5 (2016) 1–17.
- [201] S. Joseph, J. R. Panicker, Skin lesion analysis system for melanoma detection with an effective hair segmentation method, in: 2016 International Conference on Information Science (ICIS), IEEE, pp. 91–96.
- [202] L. Bi, J. Kim, E. Ahn, D. Feng, M. Fulham, Automated skin lesion segmentation via image-wise supervised learning and multi-scale superpixel based cellular automata, in: 2016 IEEE 13th International Symposium on Biomedical Imaging (ISBI), IEEE, pp. 1059–1062.
- [203] A. Pennisi, D. D. Bloisi, D. Nardi, A. R. Giampetruzzi, C. Mondino, A. Facchiano, Skin lesion image segmentation using delaunay triangulation for melanoma detection, *Computerized Medical Imaging and Graphics* 52 (2016) 89–103.
- [204] C. Sagar, L. M. Saini, Color channel based segmentation of skin lesion from clinical images for the detection of melanoma, in: 2016 IEEE 1st international conference on power electronics, intelligent control and energy systems (ICPEICES), IEEE, pp. 1–5.
- [205] A. Ortega-Martinez, J. P. Padilla-Martinez, W. Franco, Statistical image segmentation for the detection of skin lesion borders in uv fluorescence excitation, in: *Imaging, Manipulation, and Analysis of Biomolecules, Cells, and Tissues IX*, volume 9711, International Society for Optics and Photonics, p. 97111B.
- [206] G. M. Azehoun-Pazou, K. M. Assogba, H. Adegbidi, A novel approach of black skin lesion images segmentation based on mlp neural network, in: 2016 International Conference on Bio-engineering for Smart Technologies (BioSMART), IEEE, pp. 1–4.
- [207] N. F. M. Azmi, H. M. Sarkan, Y. Yahya, S. Chuprat, Abcd rules segmentation on malignant tumor and benign skin lesion images, in: 2016 3rd International Conference on Computer and Information Sciences (ICCOINS), IEEE, pp. 66–70.

- [208] F. Torkashvand, M. Fartash, Automatic segmentation of skin lesion using markov random field, *Can. J. Basic Appl. Sci* 3 (2015) 93–107.
- [209] F. Rashid Sheykhahmad, N. Razmjoo, M. Ramezani, A novel method for skin lesion segmentation, *International Journal of Information, Security and Systems Management* 4 (2015) 458–466.
- [210] J. Pereira, A. Mendes, C. Nogueira, D. Baptista, R. Fonseca-Pinto, An adaptive approach for skin lesion segmentation in dermoscopy images using a multiscale local normalization, in: *Dynamics, Games and Science*, Springer, 2015, pp. 537–545.
- [211] O. Trabelsi, L. Tlig, M. Sayadi, F. Fnaiech, Skin lesion segmentation using the ds evidence theory based on the fcm using feature parameters, in: *2015 IEEE 12th International Multi-Conference on Systems, Signals & Devices (SSD15)*, IEEE, pp. 1–5.
- [212] J. Yasmin, M. Sathik, An improved iterative segmentation algorithm using canny edge detector for skin lesion border detection., *International Arab Journal of Information Technology (IAJIT)* 12 (2015).
- [213] S. S. Khattak, G. Saman, I. Khan, A. Salam, Maximum entropy based image segmentation of human skin lesion, *World Acad Sci Eng Technol Int J Comp Elect Autom Cont Info Eng* 9 (2015) 1094–1098.
- [214] A. A. Abbas, X. Guo, W.-H. Tan, H. Jalab, Combined spline and b-spline for an improved automatic skin lesion segmentation in dermoscopic images using optimal color channel, *Journal of medical systems* 38 (2014) 1–8.
- [215] A. A. A. Al-abayechia, X. Guoa, W.-H. Tana, H. A. Jalabc, Automatic skin lesion segmentation with optimal colour channel from dermoscopic images, *Science Asia* 40 (2014) 1–7.
- [216] O. Lézoray, M. Revenu, M. Desvignes, Graph-based skin lesion segmentation of multispectral dermoscopic images, in: *2014 IEEE International Conference on Image Processing (ICIP)*, IEEE, pp. 897–901.
- [217] Y. K. Ch'ng, H. Nisar, V. V. Yap, J. J. Tang, A two level k-means segmentation technique for eczema skin lesion segmentation using class specific criteria, in: *2014 IEEE Conference on Biomedical Engineering and Sciences (IECBES)*, IEEE, pp. 985–990.
- [218] K. Jyothilakshmi, J. Jeeva, Detection of malignant skin diseases based on the lesion segmentation, in: *Proc. International Conference on Communications and Signal Processing (ICCSP)*, pp. 382–386.
- [219] A. Masood, A. A. Al-Jumaily, Integrating soft and hard threshold selection algorithms for accurate segmentation of skin lesion, in: *2nd Middle East Conference on Biomedical Engineering*, IEEE, pp. 83–86.
- [220] A. Amelio, C. Pizzuti, Skin lesion image segmentation using a color genetic algorithm, in: *Proceedings of the 15th annual conference companion on Genetic and evolutionary computation*, pp. 1471–1478.
- [221] H. Nisar, Y. K. Ch'ng, T. Y. Chew, V. V. Yap, K. H. Yeap, J. J. Tang, A color space study for skin lesion segmentation, in: *2013 IEEE International Conference on Circuits and Systems (ICCAS)*,

- IEEE, pp. 172–176.
- [222] Y. Wu, F. Xie, Z. Jiang, R. Meng, Automatic skin lesion segmentation based on supervised learning, in: 2013 Seventh International Conference on Image and Graphics, IEEE, pp. 164–169.
- [223] A. A. Abbas, W.-H. Tan, An improved automatic segmentation skin lesion from dermoscopic images using optimal rgb channel, in: Conference on Computer Science & Computational Mathematics (ICCSCM 2013), volume 39.
- [224] S. Khakabi, P. Wighton, T. K. Lee, M. S. Atkins, Multi-level feature extraction for skin lesion segmentation in dermoscopic images, in: Medical Imaging 2012: Computer-Aided Diagnosis, volume 8315, International Society for Optics and Photonics, p. 83150E.
- [225] A. Madooei, M. S. Drew, M. Sadeghi, M. S. Atkins, Automated pre-processing method for dermoscopic images and its application to pigmented skin lesion segmentation, in: Color and Imaging Conference, volume 2012, Society for Imaging Science and Technology, pp. 158–163.
- [226] M. Ivanovici, D. Stoica, Color diffusion model for active contours-an application to skin lesion segmentation, in: 2012 Annual International Conference of the IEEE Engineering in Medicine and Biology Society, IEEE, pp. 5347–5350.
- [227] Y. He, F. Xie, Automatic skin lesion segmentation based on texture analysis and supervised learning, in: Asian Conference on Computer Vision, Springer, pp. 330–341.
- [228] G. Schaefer, M. I. Rajab, M. E. Celebi, H. Iyatomi, Colour and contrast enhancement for improved skin lesion segmentation, *Computerized Medical Imaging and Graphics* 35 (2011) 99–104.
- [229] H. Zhou, G. Schaefer, M. E. Celebi, F. Lin, T. Liu, Gradient vector flow with mean shift for skin lesion segmentation, *Computerized Medical Imaging and Graphics* 35 (2011) 121–127.
- [230] A. Wong, J. Scharcanski, P. Fieguth, Automatic skin lesion segmentation via iterative stochastic region merging, *IEEE Transactions on Information Technology in Biomedicine* 15 (2011) 929–936.
- [231] X. Li, B. Aldridge, R. Fisher, J. Rees, Estimating the ground truth from multiple individual segmentations incorporating prior pattern analysis with application to skin lesion segmentation, in: 2011 IEEE International Symposium on Biomedical Imaging: From Nano to Macro, IEEE, pp. 1438–1441.
- [232] M. A. Al-Masni, M. A. Al-Antari, M.-T. Choi, S.-M. Han, T.-S. Kim, Skin lesion segmentation in dermoscopy images via deep full resolution convolutional networks, *Computer methods and programs in biomedicine* 162 (2018) 221–231.
- [233] J. Wu, W. Hu, Y. Wen, W. Tu, X. Liu, Skin lesion classification using densely connected convolutional networks with attention residual learning, *Sensors* 20 (2020) 7080.
- [234] E. Yilmaz, M. Trocan, Benign and malignant skin lesion classification comparison for three deep-learning architectures, in: Asian conference on intelligent information and database systems, Springer, pp. 514–524.

- [235] D. d. A. Rodrigues, R. F. Ivo, S. C. Satapathy, S. Wang, J. Hemanth, P. P. Reboucas Filho, A new approach for classification skin lesion based on transfer learning, deep learning, and iot system, *Pattern Recognition Letters* 136 (2020) 8–15.
- [236] A. Kwasigroch, M. Grochowski, A. Mikołajczyk, Neural architecture search for skin lesion classification, *IEEE Access* 8 (2020) 9061–9071.
- [237] C. Dhivyaa, K. Sangeetha, M. Balamurugan, S. Amaran, T. Vetriselvi, P. Johnpaul, Skin lesion classification using decision trees and random forest algorithms, *Journal of Ambient Intelligence and Humanized Computing* (2020) 1–13.
- [238] A. Kwasigroch, M. Grochowski, A. Mikołajczyk, Self-supervised learning to increase the performance of skin lesion classification, *Electronics* 9 (2020) 1930.
- [239] F. Afza, M. A. Khan, M. Sharif, T. Saba, A. Rehman, M. Y. Javed, Skin lesion classification: An optimized framework of optimal color features selection, in: *2020 2nd International Conference on Computer and Information Sciences (ICCIS)*, IEEE, pp. 1–6.
- [240] T. Akram, H. M. J. Lodhi, S. R. Naqvi, S. Naeem, M. Alhaisoni, M. Ali, S. A. Haider, N. N. Qadri, A multilevel features selection framework for skin lesion classification, *Human-centric Computing and Information Sciences* 10 (2020) 1–26.
- [241] S. Yildirim-Yayilgan, B. Arifaj, M. Rahimpour, J. Y. Hardeberg, L. Ahmedi, Pre-trained cnn based deep features with hand-crafted features and patient data for skin lesion classification, in: *International Conference on Intelligent Technologies and Applications*, Springer, pp. 151–162.
- [242] L. Liu, L. Mou, X. X. Zhu, M. Mandal, Automatic skin lesion classification based on mid-level feature learning, *Computerized Medical Imaging and Graphics* 84 (2020) 101765.
- [243] J. Wu, W. Hu, Y. Wang, Y. Wen, A multi-input cnns with attention for skin lesion classification, in: *2020 IEEE International Conference on Smart Cloud (SmartCloud)*, IEEE, pp. 78–83.
- [244] I. Mporas, I. Perikos, M. Paraskevas, Color models for skin lesion classification from dermatoscopic images, in: *Advances in Integrations of Intelligent Methods*, Springer, 2020, pp. 85–98.
- [245] J. Sun, T. Chakraborti, J. A. Noble, A comparative study of explainer modules applied to automated skin lesion classification., in: *XI-ML@ KI*.
- [246] A. C. Salian, S. Vaze, P. Singh, G. N. Shaikh, S. Chapaneri, D. Jayaswal, Skin lesion classification using deep learning architectures, in: *2020 3rd International conference on communication system, computing and IT applications (CSCITA)*, IEEE, pp. 168–173.
- [247] S. S. Chaturvedi, K. Gupta, P. S. Prasad, Skin lesion analyser: An efficient seven-way multi-class skin cancer classification using mobilenet, in: *International Conference on Advanced Machine Learning Technologies and Applications*, Springer, pp. 165–176.
- [248] V. Miglani, M. Bhatia, Skin lesion classification: A transfer learning approach using efficientnets, in:

- International Conference on Advanced Machine Learning Technologies and Applications, Springer, pp. 315–324.
- [249] A. Mahbod, G. Schaefer, C. Wang, G. Dorffner, R. Ecker, I. Ellinger, Transfer learning using a multi-scale and multi-network ensemble for skin lesion classification, *Computer methods and programs in biomedicine* 193 (2020) 105475.
- [250] Z. Rahman, A. M. Ami, A transfer learning based approach for skin lesion classification from imbalanced data, in: 2020 11th International Conference on Electrical and Computer Engineering (ICECE), IEEE, pp. 65–68.
- [251] Z. Qin, Z. Liu, P. Zhu, Y. Xue, A gan-based image synthesis method for skin lesion classification, *Computer Methods and Programs in Biomedicine* 195 (2020) 105568.
- [252] S. R. Guha, S. Rafizul Haque, Performance comparison of machine learning-based classification of skin diseases from skin lesion images, in: *International conference on communication, computing and electronics systems*, Springer, pp. 15–25.
- [253] B. Harangi, A. Baran, A. Hajdu, Assisted deep learning framework for multi-class skin lesion classification considering a binary classification support, *Biomedical Signal Processing and Control* 62 (2020) 102041.
- [254] S. R. Hassan, S. Afroge, M. B. Mizan, Skin lesion classification using densely connected convolutional network, in: 2020 IEEE Region 10 Symposium (TENSYP), IEEE, pp. 750–753.
- [255] A. Jibhakate, P. Parnerkar, S. Mondal, V. Bharambe, S. Mantri, Skin lesion classification using deep learning and image processing, in: 2020 3rd International Conference on Intelligent Sustainable Systems (ICISS), IEEE, pp. 333–340.
- [256] J.-A. Almaraz-Damian, V. Ponomaryov, S. Sadovnychiy, H. Castillejos-Fernandez, Melanoma and nevus skin lesion classification using handcraft and deep learning feature fusion via mutual information measures, *Entropy* 22 (2020) 484.
- [257] D. Zhuang, K. Chen, J. M. Chang, Cs-af: A cost-sensitive multi-classifier active fusion framework for skin lesion classification, *arXiv:2004.12064* (2020).
- [258] E. O. Molina-Molina, S. Solorza-Calderón, J. Álvarez-Borrogo, Classification of dermoscopy skin lesion color-images using fractal-deep learning features, *Applied Sciences* 10 (2020) 5954.
- [259] S. A. A. Ahmed, B. Yanikoğlu, Ö. Göksu, E. Aptoula, Skin lesion classification with deep cnn ensembles, in: 2020 28th Signal Processing and Communications Applications Conference (SIU), IEEE, pp. 1–4.
- [260] S. Muckatira, Properties of winning tickets on skin lesion classification, *arXiv:2008.12141* (2020).
- [261] F. Nunnari, C. Bhuvaneshwara, A. O. Ezema, D. Sonntag, A study on the fusion of pixels and patient metadata in cnn-based classification of skin lesion images, in: *International Cross-Domain Conference*

- for Machine Learning and Knowledge Extraction, Springer, pp. 191–208.
- [262] S. Bagchi, A. Banerjee, D. R. Bathula, Learning a meta-ensemble technique for skin lesion classification and novel class detection, in: Proceedings of the IEEE/CVF Conference on Computer Vision and Pattern Recognition Workshops, pp. 746–747.
- [263] N. Gessert, M. Nielsen, M. Shaikh, R. Werner, A. Schlaefer, Skin lesion classification using ensembles of multi-resolution efficientnets with meta data, *MethodsX* 7 (2020) 100864.
- [264] G. S. Ghalejoogh, H. M. Kordy, F. Ebrahimi, A hierarchical structure based on stacking approach for skin lesion classification, *Expert Systems with Applications* 145 (2020) 113127.
- [265] L. Bi, D. D. Feng, M. Fulham, J. Kim, Multi-label classification of multi-modality skin lesion via hyper-connected convolutional neural network, *Pattern Recognition* 107 (2020) 107502.
- [266] P. M. Pereira, R. Fonseca-Pinto, R. P. Paiva, P. A. Assuncao, L. M. Tavora, L. A. Thomaz, S. M. Faria, Skin lesion classification enhancement using border-line features—the melanoma vs nevus problem, *Biomedical Signal Processing and Control* 57 (2020) 101765.
- [267] F. A. Damian, S. Moldovanu, N. Dey, A. S. Ashour, L. Moraru, Feature selection of non-dermoscopic skin lesion images for nevus and melanoma classification, *Computation* 8 (2020) 41.
- [268] K. Thomsen, A. L. Christensen, L. Iversen, H. B. Lomholt, O. Winther, Deep learning for diagnostic binary classification of multiple-lesion skin diseases, *Frontiers in medicine* 7 (2020) 604.
- [269] E. Goceri, A. A. Karakas, Comparative evaluations of cnn based networks for skin lesion classification, in: 14th International Conference on Computer Graphics, Visualization, Computer Vision and Image Processing (CGVCVIP), Zagreb, Croatia, pp. 1–6.
- [270] J. Yan, F. Liu, W. Wang, Scalable skin lesion multi-classification recognition system, *Computers, Materials & Continua* 62 (2020) 801–816.
- [271] Y. Filali, H. El Khoukhi, M. A. Sabri, A. Yahyaouy, A. Aarab, Texture classification of skin lesion using convolutional neural network, in: 2019 International Conference on Wireless Technologies, Embedded and Intelligent Systems (WITS), IEEE, pp. 1–5.
- [272] Y. Wang, H. Pan, B. Yang, X. Bian, Q. Cui, Mutual learning model for skin lesion classification, in: International Conference of Pioneering Computer Scientists, Engineers and Educators, Springer, pp. 214–222.
- [273] M. A. Khan, M. Y. Javed, M. Sharif, T. Saba, A. Rehman, Multi-model deep neural network based features extraction and optimal selection approach for skin lesion classification, in: 2019 international conference on computer and information sciences (ICCIS), IEEE, pp. 1–7.
- [274] E. Veltmeijer, S. Karaoglu, T. Gevers, et al., Integrating clinically-relevant features into skin lesion classification., in: BNAIC/BENELEARN.
- [275] C. Xue, Q. Dou, X. Shi, H. Chen, P.-A. Heng, Robust learning at noisy labeled medical images:

- Applied to skin lesion classification, in: 2019 IEEE 16th International Symposium on Biomedical Imaging (ISBI 2019), IEEE, pp. 1280–1283.
- [276] W. Zheng, C. Gou, L. Yan, A relation hashing network embedded with prior features for skin lesion classification, in: International Workshop on Machine Learning in Medical Imaging, Springer, pp. 115–123.
- [277] A. Mahbod, G. Schaefer, C. Wang, R. Ecker, I. Ellinge, Skin lesion classification using hybrid deep neural networks, in: ICASSP 2019-2019 IEEE International Conference on Acoustics, Speech and Signal Processing (ICASSP), IEEE, pp. 1229–1233.
- [278] A. Mahbod, G. Schaefer, I. Ellinger, R. Ecker, A. Pitiot, C. Wang, Fusing fine-tuned deep features for skin lesion classification, *Computerized Medical Imaging and Graphics* 71 (2019) 19–29.
- [279] R. Kulhalli, C. Savadikar, B. Garware, A hierarchical approach to skin lesion classification, in: Proceedings of the ACM India Joint International Conference on Data Science and Management of Data, pp. 245–250.
- [280] S. Serte, H. Demirel, Wavelet-based deep learning for skin lesion classification, *IET Image Processing* 14 (2019) 720–726.
- [281] S. Serte, H. Demirel, Gabor wavelet-based deep learning for skin lesion classification, *Computers in biology and medicine* 113 (2019) 103423.
- [282] M. A. Albahar, Skin lesion classification using convolutional neural network with novel regularizer, *IEEE Access* 7 (2019) 38306–38313.
- [283] N. Gessert, T. Sentker, F. Madesta, R. Schmitz, H. Kniep, I. Baltruschat, R. Werner, A. Schlaefer, Skin lesion classification using cnns with patch-based attention and diagnosis-guided loss weighting, *IEEE Transactions on Biomedical Engineering* 67 (2019) 495–503.
- [284] M. A. A. Milton, Automated skin lesion classification using ensemble of deep neural networks in isic 2018: Skin lesion analysis towards melanoma detection challenge, *arXiv:1901.10802* (2019).
- [285] H. Rashid, M. A. Tanveer, H. A. Khan, Skin lesion classification using gan based data augmentation, in: 2019 41st Annual International Conference of the IEEE Engineering in Medicine and Biology Society (EMBC), IEEE, pp. 916–919.
- [286] C. Yoon, G. Hamarneh, R. Garbi, Generalizable feature learning in the presence of data bias and domain class imbalance with application to skin lesion classification, in: International Conference on Medical Image Computing and Computer-Assisted Intervention, Springer, pp. 365–373.
- [287] Y.-M. Chung, C.-S. Hu, A. Lawson, C. Smyth, Toporesnet: A hybrid deep learning architecture and its application to skin lesion classification, *arXiv:1905.08607* (2019).
- [288] P. Van Molle, T. Verbelen, C. De Boom, B. Vankeirsbilck, J. De Vylder, B. Diricx, T. Kimpe, P. Simoens, B. Dhoedt, Quantifying uncertainty of deep neural networks in skin lesion classification,

- in: *Uncertainty for Safe Utilization of Machine Learning in Medical Imaging and Clinical Image-Based Procedures*, Springer, 2019, pp. 52–61.
- [289] S. H. Kassani, P. H. Kassani, M. J. Wesolowski, K. A. Schneider, R. Deters, Depthwise separable convolutional neural network for skin lesion classification, in: *2019 IEEE International Symposium on Signal Processing and Information Technology (ISSPIT)*, IEEE, pp. 1–6.
- [290] A. Aldwgeri, N. F. Abubacker, Ensemble of deep convolutional neural network for skin lesion classification in dermoscopy images, in: *International Visual Informatics Conference*, Springer, pp. 214–226.
- [291] A. Eddine Guissous, Skin lesion classification using deep neural network, *arXiv e-prints* (2019) arXiv:1911.
- [292] A. E. Guissous, Skin lesion classification using deep neural network, *arXiv:1911.07817* (2019).
- [293] R. B. Fisher, J. Rees, A. Bertrand, Classification of ten skin lesion classes: Hierarchical knn versus deep net, in: *Annual Conference on Medical Image Understanding and Analysis*, Springer, pp. 86–98.
- [294] M. Monisha, A. Suresh, B. T. Bapu, M. Rashmi, Classification of malignant melanoma and benign skin lesion by using back propagation neural network and abcd rule, *Cluster Computing* 22 (2019) 12897–12907.
- [295] J. Zhang, Y. Xie, Q. Wu, Y. Xia, Skin lesion classification in dermoscopy images using synergic deep learning, in: *International Conference on Medical Image Computing and Computer-Assisted Intervention*, Springer, pp. 12–20.
- [296] M. ur Rehman, S. H. Khan, S. D. Rizvi, Z. Abbas, A. Zafar, Classification of skin lesion by interference of segmentation and convolution neural network, in: *2018 2nd International Conference on Engineering Innovation (ICEI)*, IEEE, pp. 81–85.
- [297] M. A. Wahba, A. S. Ashour, Y. Guo, S. A. Napoleon, M. M. Abd Elnaby, A novel cumulative level difference mean based gldm and modified abcd features ranked using eigenvector centrality approach for four skin lesion types classification, *Computer methods and programs in biomedicine* 165 (2018) 163–174.
- [298] T.-C. Pham, C.-M. Luong, M. Visani, V.-D. Hoang, Deep cnn and data augmentation for skin lesion classification, in: *Asian Conference on Intelligent Information and Database Systems*, Springer, pp. 573–582.
- [299] K. Thandiackal, O. Goksel, A structure-aware convolutional neural network for skin lesion classification, in: *OR 2.0 Context-Aware Operating Theaters, Computer Assisted Robotic Endoscopy, Clinical Image-Based Procedures, and Skin Image Analysis*, Springer, 2018, pp. 312–319.
- [300] B. Harangi, Skin lesion classification with ensembles of deep convolutional neural networks, *Journal of biomedical informatics* 86 (2018) 25–32.
- [301] Y. Filali, A. Ennoui, M. A. Sabri, A. Aarab, A study of lesion skin segmentation, features selection

- and classification approaches, in: 2018 International Conference on Intelligent Systems and Computer Vision (ISCV), IEEE, pp. 1–7.
- [302] Y. Xie, J. Zhang, Y. Xia, A multi-level deep ensemble model for skin lesion classification in dermoscopy images, arXiv:1807.08488 (2018).
- [303] X. Li, J. Wu, H. Jiang, E. Z. Chen, X. Dong, R. Rong, Skin lesion classification via combining deep learning features and clinical criteria representations, bioRxiv (2018) 382010.
- [304] Y. C. Lee, S.-H. Jung, H.-H. Won, Wonderm: Skin lesion classification with fine-tuned neural networks, arXiv:1808.03426 (2018).
- [305] S. Kitada, H. Iyatomi, Skin lesion classification with ensemble of squeeze-and-excitation networks and semi-supervised learning, arXiv:1809.02568 (2018).
- [306] A. Namozov, D. Ergashev, Y. Im Cho, Adaptive activation functions for skin lesion classification using deep neural networks, in: 2018 Joint 10th International Conference on Soft Computing and Intelligent Systems (SCIS) and 19th International Symposium on Advanced Intelligent Systems (ISIS), IEEE, pp. 232–235.
- [307] Y. Pan, Y. Xia, Residual network based aggregation model for skin lesion classification, arXiv:1807.09150 (2018).
- [308] F. P. dos Santos, M. A. Ponti, Robust feature spaces from pre-trained deep network layers for skin lesion classification, in: 2018 31st SIBGRAPI Conference on Graphics, Patterns and Images (SIBGRAPI), IEEE, pp. 189–196.
- [309] H. Liao, J. Luo, A deep multi-task learning approach to skin lesion classification, arXiv:1812.03527 (2018).
- [310] W. Songpan, Improved skin lesion image classification using clustering with local-g lcm normalization, in: 2018 2nd European Conference on Electrical Engineering and Computer Science (EECS), IEEE, pp. 206–210.
- [311] J. Yap, W. Yolland, P. Tschandl, Multimodal skin lesion classification using deep learning, *Experimental dermatology* 27 (2018) 1261–1267.
- [312] P. Van Molle, M. De Strooper, T. Verbelen, B. Vankeirsbilck, P. Simoens, B. Dhoedt, Visualizing convolutional neural networks to improve decision support for skin lesion classification, in: *Understanding and Interpreting Machine Learning in Medical Image Computing Applications*, Springer, 2018, pp. 115–123.
- [313] F. Navarro, S. Conjeti, F. Tombari, N. Navab, Webly supervised learning for skin lesion classification, in: *International Conference on Medical Image Computing and Computer-Assisted Intervention*, Springer, pp. 398–406.
- [314] M. A. Wahba, A. S. Ashour, S. A. Napoleon, M. M. Abd Elnaby, Y. Guo, Combined empirical

- mode decomposition and texture features for skin lesion classification using quadratic support vector machine, *Health information science and systems* 5 (2017) 1–13.
- [315] T. Satheesha, D. Satyanarayana, M. G. Prasad, K. D. Dhruve, Melanoma is skin deep: a 3d reconstruction technique for computerized dermoscopic skin lesion classification, *IEEE journal of translational engineering in health and medicine* 5 (2017) 1–17.
- [316] A. R. Lopez, X. Giro-i Nieto, J. Burdick, O. Marques, Skin lesion classification from dermoscopic images using deep learning techniques, in: 2017 13th IASTED international conference on biomedical engineering (BioMed), IEEE, pp. 49–54.
- [317] D. H. Murphree, C. Ngufor, Transfer learning for melanoma detection: Participation in isic 2017 skin lesion classification challenge, *arXiv:1703.05235* (2017).
- [318] P. Mirunalini, A. Chandrabose, V. Gokul, S. Jaisakthi, Deep learning for skin lesion classification, *arXiv:1703.04364* (2017).
- [319] X. Jia, L. Shen, Skin lesion classification using class activation map, *arXiv:1703.01053* (2017).
- [320] T. DeVries, D. Ramachandram, Skin lesion classification using deep multi-scale convolutional neural networks, *arXiv:1703.01402* (2017).
- [321] N. Danpakdee, W. Songpan, Classification model for skin lesion image, in: *International Conference on Information Science and Applications*, Springer, pp. 553–561.
- [322] S. A. Mahdiraji, Y. Baleghi, S. M. Sakhaei, Skin lesion images classification using new color pigmented boundary descriptors, in: 2017 3rd International Conference on Pattern Recognition and Image Analysis (IPRIA), IEEE, pp. 102–107.
- [323] L. Haofu, J. Luo, A deep multi-task learning approach to skin lesion classification, in: *Workshops at the Thirty-First AAAI Conference on Artificial Intelligence*.
- [324] Y. Filali, A. Ennoui, M. A. Sabri, A. Aarab, Multiscale approach for skin lesion analysis and classification, in: 2017 International Conference on Advanced Technologies for Signal and Image Processing (ATSIP), IEEE, pp. 1–6.
- [325] A. A. A. Al-abayechi, H. A. Jalab, R. W. Ibrahim, A classification of skin lesion using fractional poisson for texture feature extraction, in: *Proceedings of the Second International Conference on Internet of things, Data and Cloud Computing*, pp. 1–7.
- [326] T. Majtner, S. Yildirim-Yayilgan, J. Y. Hardeberg, Combining deep learning and hand-crafted features for skin lesion classification, in: 2016 Sixth International Conference on Image Processing Theory, Tools and Applications (IPTA), IEEE, pp. 1–6.
- [327] R. Chakravorty, S. Liang, M. Abedini, R. Garnavi, Dermatologist-like feature extraction from skin lesion for improved asymmetry classification in ph 2 database, in: 2016 38th Annual International Conference of the IEEE Engineering in Medicine and Biology Society (EMBC), IEEE, pp. 3855–3858.

- [328] H. Liao, Y. Li, J. Luo, Skin disease classification versus skin lesion characterization: Achieving robust diagnosis using multi-label deep neural networks, in: 2016 23rd International Conference on Pattern Recognition (ICPR), IEEE, pp. 355–360.
- [329] V. Pomponiu, H. Nejati, N.-M. Cheung, Deepmole: Deep neural networks for skin mole lesion classification, in: 2016 IEEE International Conference on Image Processing (ICIP), IEEE, pp. 2623–2627.
- [330] M. A. Farooq, M. A. M. Azhar, R. H. Raza, Automatic lesion detection system (alds) for skin cancer classification using svm and neural classifiers, in: 2016 IEEE 16th International Conference on Bioinformatics and Bioengineering (BIBE), IEEE, pp. 301–308.
- [331] C. Di Leo, V. Bevilacqua, L. Ballerini, R. Fisher, B. Aldridge, J. Rees, Hierarchical classification of ten skin lesion classes, in: Proc. SICSA Dundee Medical Image Analysis Workshop.
- [332] M. K. A. Mahmoud, A. Al-Jumaily, A hybrid system for skin lesion detection: Based on gabor wavelet and support vector machine, in: Information Technology: Proceedings of the 2014 International Symposium on Information Technology (ISIT 2014), Dalian, China, p. 39.
- [333] N. M. Sirakov, Y.-L. Ou, M. Mete, Skin lesion feature vectors classification in models of a riemannian manifold, *Annals of Mathematics and Artificial Intelligence* 75 (2015) 217–229.
- [334] M. E. Celebi, A. Zornberg, Automated quantification of clinically significant colors in dermoscopy images and its application to skin lesion classification, *IEEE systems journal* 8 (2014) 980–984.
- [335] U. Jamil, S. Khalid, Comparative study of classification techniques used in skin lesion detection systems, in: 17th IEEE International Multi Topic Conference 2014, IEEE, pp. 266–271.
- [336] G. Surówka, M. Ogorzałek, On optimal wavelet bases for classification of skin lesion images through ensemble learning, in: 2014 International Joint Conference on Neural Networks (IJCNN), IEEE, pp. 165–170.
- [337] Z. She, P. Excell, Lesion classification using 3d skin surface tilt orientation, *Skin Research and Technology* 19 (2013) e305–e311.
- [338] L. Rosado, M. Ferreira, A prototype for a mobile-based system of skin lesion analysis using supervised classification, in: 2013 2nd Experiment@ International Conference (exp. at'13), IEEE, pp. 156–157.
- [339] P. G. Cavalcanti, J. Scharcanski, Macroscopic pigmented skin lesion segmentation and its influence on lesion classification and diagnosis, in: *Color medical image analysis*, Springer, 2013, pp. 15–39.
- [340] M. Mete, Y.-L. Ou, N. M. Sirakov, Skin lesion feature vector space with a metric to model geometric structures of malignancy for classification, in: *International Workshop on Combinatorial Image Analysis*, Springer, pp. 285–297.
- [341] R. Amelard, A. Wong, D. A. Clausi, Extracting morphological high-level intuitive features (hlif) for enhancing skin lesion classification, in: 2012 Annual International Conference of the IEEE Engineering in Medicine and Biology Society, IEEE, pp. 4458–4461.

- [342] L. Ballerini, R. B. Fisher, B. Aldridge, J. Rees, Non-melanoma skin lesion classification using colour image data in a hierarchical k-nn classifier, in: 2012 9th IEEE International Symposium on Biomedical Imaging (ISBI), IEEE, pp. 358–361.
- [343] Z. She, P. S. Excell, Skin pattern analysis for lesion classification using local isotropy, *Skin Research and Technology* 17 (2011) 206–212.
- [344] K. Ramlakhan, Y. Shang, A mobile automated skin lesion classification system, in: 2011 IEEE 23rd International Conference on Tools with Artificial Intelligence, IEEE, pp. 138–141.
- [345] F. I. Tushar, B. Alyafi, M. K. Hasan, L. Dahal, Brain tissue segmentation using neuronet with different pre-processing techniques, in: 2019 Joint 8th International Conference on Informatics, Electronics & Vision (ICIEV) and 2019 3rd International Conference on Imaging, Vision & Pattern Recognition (icIVPR), IEEE, pp. 223–227.
- [346] Q. Abbas, M. E. Celebi, I. F. García, Hair removal methods: A comparative study for dermoscopy images, *Biomedical Signal Processing and Control* 6 (2011) 395–404.
- [347] A. Mikołajczyk, M. Grochowski, Data augmentation for improving deep learning in image classification problem, in: 2018 international interdisciplinary PhD workshop (IIPhDW), IEEE, pp. 117–122.
- [348] Y. LeCun, Y. Bengio, G. Hinton, Deep learning, *nature* 521 (2015) 436–444.
- [349] A. Krizhevsky, I. Sutskever, G. E. Hinton, Imagenet classification with deep convolutional neural networks, in: *Advances in neural information processing systems*, pp. 1097–1105.
- [350] Ö. Yildirim, P. Pławiak, R.-S. Tan, U. R. Acharya, Arrhythmia detection using deep convolutional neural network with long duration ecg signals, *Computers in biology and medicine* 102 (2018) 411–420.
- [351] A. Y. Hannun, P. Rajpurkar, M. Haghpanahi, G. H. Tison, C. Bourn, M. P. Turakhia, A. Y. Ng, Cardiologist-level arrhythmia detection and classification in ambulatory electrocardiograms using a deep neural network, *Nature medicine* 25 (2019) 65.
- [352] U. R. Acharya, S. L. Oh, Y. Hagiwara, J. H. Tan, M. Adam, A. Gertych, R. San Tan, A deep convolutional neural network model to classify heartbeats, *Computers in biology and medicine* 89 (2017) 389–396.
- [353] A. Esteva, B. Kuprel, R. A. Novoa, J. Ko, S. M. Swetter, H. M. Blau, S. Thrun, Dermatologist-level classification of skin cancer with deep neural networks, *nature* 542 (2017) 115–118.
- [354] N. C. Codella, Q.-B. Nguyen, S. Pankanti, D. A. Gutman, B. Helba, A. C. Halpern, J. R. Smith, Deep learning ensembles for melanoma recognition in dermoscopy images, *IBM Journal of Research and Development* 61 (2017) 5–1.
- [355] Y. Celik, M. Talo, O. Yildirim, M. Karabatak, U. R. Acharya, Automated invasive ductal carcinoma detection based using deep transfer learning with whole-slide images, *Pattern Recognition Letters* (2020).

- [356] A. Cruz-Roa, A. Basavanthally, F. González, H. Gilmore, M. Feldman, S. Ganesan, N. Shih, J. Tomaszewski, A. Madabhushi, Automatic detection of invasive ductal carcinoma in whole slide images with convolutional neural networks, in: *Medical Imaging 2014: Digital Pathology*, volume 9041, International Society for Optics and Photonics, p. 904103.
- [357] M. K. Hasan, T. A. Aleef, S. Roy, Automatic mass classification in breast using transfer learning of deep convolutional neural network and support vector machine, in: *2020 IEEE Region 10 Symposium (TENSYP)*, IEEE, pp. 110–113.
- [358] M. Talo, O. Yildirim, U. B. Baloglu, G. Aydin, U. R. Acharya, Convolutional neural networks for multi-class brain disease detection using mri images, *Computerized Medical Imaging and Graphics* 78 (2019) 101673.
- [359] P. Rajpurkar, J. Irvin, K. Zhu, B. Yang, H. Mehta, T. Duan, D. Ding, A. Bagul, C. Langlotz, K. Shpanskaya, et al., Chexnet: Radiologist-level pneumonia detection on chest x-rays with deep learning, *arXiv:1711.05225* (2017).
- [360] J. H. Tan, H. Fujita, S. Sivaprasad, S. V. Bhandary, A. K. Rao, K. C. Chua, U. R. Acharya, Automated segmentation of exudates, haemorrhages, microaneurysms using single convolutional neural network, *Information sciences* 420 (2017) 66–76.
- [361] M. K. Hasan, M. A. Alam, M. T. E. Elahi, S. Roy, R. Martí, Drnet: Segmentation and localization of optic disc and fovea from diabetic retinopathy image, *Artificial Intelligence in Medicine* 111 (2021) 102001.
- [362] M. K. Hasan, L. Calvet, N. Rabbani, A. Bartoli, Detection, segmentation, and 3d pose estimation of surgical tools using convolutional neural networks and algebraic geometry, *Medical Image Analysis* 70 (2021) 101994.
- [363] G. Gaál, B. Maga, A. Lukács, Attention u-net based adversarial architectures for chest x-ray lung segmentation, *arXiv:2003.10304* (2020).
- [364] O. Ronneberger, P. Fischer, T. Brox, U-net: Convolutional networks for biomedical image segmentation, in: *International Conference on Medical image computing and computer-assisted intervention*, Springer, pp. 234–241.
- [365] J. Long, E. Shelhamer, T. Darrell, Fully convolutional networks for semantic segmentation, in: *Proceedings of the IEEE conference on computer vision and pattern recognition*, pp. 3431–3440.
- [366] A. Odena, V. Dumoulin, C. Olah, Deconvolution and checkerboard artifacts, *Distill* 1 (2016) e3.
- [367] Z. Mirikharaji, C. Barata, K. Abhishek, A. Bissoto, S. Avila, E. Valle, M. E. Celebi, G. Hamarneh, A survey on deep learning for skin lesion segmentation, *arXiv:2206.00356* (2022).
- [368] C. Barata, M. E. Celebi, J. S. Marques, Melanoma detection algorithm based on feature fusion, in: *2015 37th Annual International Conference of the IEEE Engineering in Medicine and Biology Society*

- (EMBC), IEEE, pp. 2653–2656.
- [369] M. Rastgoo, R. Garcia, O. Morel, F. Marzani, Automatic differentiation of melanoma from dysplastic nevi, *Computerized Medical Imaging and Graphics* 43 (2015) 44–52.
- [370] G. Schaefer, B. Krawczyk, M. E. Celebi, H. Iyatomi, An ensemble classification approach for melanoma diagnosis, *Memetic Computing* 6 (2014) 233–240.
- [371] Z. Abbas, M.-u. Rehman, S. Najam, S. D. Rizvi, An efficient gray-level co-occurrence matrix (glcm) based approach towards classification of skin lesion, in: *2019 Amity International Conference on Artificial Intelligence (AICAI)*, IEEE, pp. 317–320.
- [372] I. Giotis, N. Molders, S. Land, M. Biehl, M. F. Jonkman, N. Petkov, Med-node: A computer-assisted melanoma diagnosis system using non-dermoscopic images, *Expert systems with applications* 42 (2015) 6578–6585.
- [373] R. Garnavi, M. Aldeen, J. Bailey, Computer-aided diagnosis of melanoma using border-and wavelet-based texture analysis, *IEEE transactions on information technology in biomedicine* 16 (2012) 1239–1252.
- [374] I. Maglogiannis, K. K. Delibasis, Enhancing classification accuracy utilizing globules and dots features in digital dermoscopy, *Computer methods and programs in biomedicine* 118 (2015) 124–133.
- [375] Q. Abbas, M. E. Celebi, C. Serrano, I. F. Garcia, G. Ma, Pattern classification of dermoscopy images: A perceptually uniform model, *Pattern Recognition* 46 (2013) 86–97.
- [376] M. Sadeghi, T. K. Lee, D. McLean, H. Lui, M. S. Atkins, Global pattern analysis and classification of dermoscopic images using textons, in: *Medical Imaging 2012: Image Processing*, volume 8314, International Society for Optics and Photonics, p. 83144X.
- [377] M. K. Hasan, M. T. Jawad, A. Dutta, M. A. Awal, M. A. Islam, M. Masud, J. F. Al-Amri, Associating measles vaccine uptake classification and its underlying factors using an ensemble of machine learning models, *IEEE Access* 9 (2021) 119613–119628.
- [378] M. K. Hasan, M. A. Alam, D. Das, E. Hossain, M. Hasan, Diabetes prediction using ensembling of different machine learning classifiers, *IEEE Access* 8 (2020) 76516–76531.
- [379] H. Iyatomi, K.-A. Norton, M. E. Celebi, G. Schaefer, M. Tanaka, K. Ogawa, Classification of melanocytic skin lesions from non-melanocytic lesions, in: *2010 Annual International Conference of the IEEE Engineering in Medicine and Biology*, IEEE, pp. 5407–5410.
- [380] P. P. Patil, S. A. Patil, V. Udupi, Detection and classification of skin lesion in der-moscopy images, *International Journal of Applied Engineering Research* 9 (2014) 27719–27731.
- [381] I. A. Ozkan, M. KOKLU, Skin lesion classification using machine learning algorithms, *International Journal of Intelligent Systems and Applications in Engineering* 5 (2017) 285–289.
- [382] R. C. Hardie, R. Ali, M. S. De Silva, T. M. Kebede, Skin lesion segmentation and classification for

- isic 2018 using traditional classifiers with hand-crafted features, arXiv:1807.07001 (2018).
- [383] P. Jayapal, R. Manikandan, M. Ramanan, R. S. Sundar, T. U. Suriya, Skin lesion classification using hybrid spatial features and radial basis network, *Skin* 3 (2014).
- [384] Q. Ha, B. Liu, F. Liu, Identifying melanoma images using efficientnet ensemble: Winning solution to the siim-isic melanoma classification challenge, arXiv:2010.05351 (2020).
- [385] A. G. Pacheco, A.-R. Ali, T. Trappenberg, Skin cancer detection based on deep learning and entropy to detect outlier samples, arXiv:1909.04525 (2019).
- [386] A. H. Shahin, A. Kamal, M. A. Elattar, Deep ensemble learning for skin lesion classification from dermoscopic images, in: 2018 9th Cairo International Biomedical Engineering Conference (CIBEC), IEEE, pp. 150–153.
- [387] I. Kandel, M. Castelli, The effect of batch size on the generalizability of the convolutional neural networks on a histopathology dataset, *ICT express* 6 (2020) 312–315.
- [388] J. Burdick, O. Marques, A. Romero-Lopez, X. Giró Nieto, J. Weinthal, The impact of segmentation on the accuracy and sensitivity of a melanoma classifier based on skin lesion images, in: SIIM 2017 scientific program: Pittsburgh, PA, June 1-June 3, 2017, David L. Lawrence Convention Center, pp. 1–6.
- [389] F. Bagheri, M. J. Tarokh, M. Ziaratban, Two-stage skin lesion segmentation from dermoscopic images by using deep neural networks, *Jorjani Biomedicine Journal* 8 (2020) 58–72.
- [390] R. T. Sousa, L. V. de Moraes, Araguaia medical vision lab at isic 2017 skin lesion classification challenge, arXiv:1703.00856 (2017).
- [391] S. Jeniva, C. Santhi, An efficient skin lesion segmentation analysis using statistical texture distinctiveness, *Int J Adv Res Trends Eng Technol* 3777 (2015) 111–116.
- [392] M. Yuvaraju, D. Divya, A. Poornima, Segmentation of skin lesion from digital images using morphological filter, *International research journal of Engineering and Technology* 3 (2016) 3223–3229.
- [393] A. A. Adeyinka, S. Viriri, Skin lesion images segmentation: A survey of the state-of-the-art, in: *International conference on mining intelligence and knowledge exploration*, Springer, pp. 321–330.
- [394] S. H. SALIH, S. AL-RAHEYM, Comparison of skin lesion image between segmentation algorithms, *Journal of Theoretical and Applied Information Technology* 96 (2018).
- [395] R. Javed, M. S. M. Rahim, T. Saba, M. Rashid, Region-based active contour jseg fusion technique for skin lesion segmentation from dermoscopic images, *Biomedical Research* 30 (2019) 1–10.
- [396] S. S. Devi, N. H. Singh, R. H. Laskar, Fuzzy c-means clustering with histogram based cluster selection for skin lesion segmentation using non-dermoscopic images., *International Journal of Interactive Multimedia & Artificial Intelligence* 6 (2020).
- [397] S. Jabbari, Y. Baleghi, Segmentation of skin lesion images using a combination of texture and color

- information, *Journal of Soft Computing and Information Technology* 8 (2020) 87–97.
- [398] A. Dutta, M. K. Hasan, M. Ahmad, Skin lesion classification using convolutional neural network for melanoma recognition, in: *Proceedings of International Joint Conference on Advances in Computational Intelligence*, Springer, pp. 55–66.
- [399] P. M. Pereira, L. M. Tavora, R. Fonseca-Pinto, R. P. Paiva, P. A. A. Assunção, S. M. de Faria, Image segmentation using gradient-based histogram thresholding for skin lesion delineation., in: *Bioimaging*, pp. 84–91.
- [400] A. Huang, S.-Y. Kwan, W.-Y. Chang, M.-Y. Liu, M.-H. Chi, G.-S. Chen, A robust hair segmentation and removal approach for clinical images of skin lesions, in: *2013 35th Annual International Conference of the IEEE Engineering in Medicine and Biology Society (EMBC)*, IEEE, pp. 3315–3318.
- [401] C. K. Rekha, K. Manjunathachari, B. Prakash, Log-gaussian fuzzy c-means clustering algorithm for skin lesion segmentation, *Journal of Science and Technology (JST)* 3 (2018) 18–27.
- [402] M. H. Hamd, L. M. Mohamad, Skin cancer prognosis based on color matching and segmentation of pigmented skin lesion, *Engineering and Technology Journal* 31 (2013).